Program #1363

RETINAL HISTOPATHOLOGY IN EYES FROM A PATIENT WITH STARGARDT DISEASE CAUSED BY COMPOUND HETEROZYGOUS *ABCA4* MUTATIONS

Cleveland Clinic

J. G. Hollyfield[1], V. L. Bonilha[1], M. E. Rayborn[1], B. A. Bell[1], M. J. Marino[1], and G.A. Fishman[2].

1- The Cole Eye Institute, Cleveland Clinic Lerner College of Medicine, Cleveland, OH; 2- Chicago Lighthouse for People Who Are Blind or Visually Impaired, Chicago, IL.

Supported by Research to Prevent Blindness

Foundation Fighting Blindness

Abstract

Purpose: To evaluate the histopathology of the retina in donor eyes from a patient with Stargardt disease caused by *ABCA4* mutations.

Methods: Eyes from a 66 year-old female were fixed in 4% paraformaldehyde and 0.5% glutaraldehyde in PBS within 18 hours postmortem. Globes were evaluated with macroscopic, SLO and OCT imaging. Perifovea and peripheral regions were processed for electron microscopy and immunocytochemistry. Three age-similar normal eyes were used as controls. Genetic testing was done by both SSCP and direct sequencing of the *ABCA4* gene.

Results: Donor ABCA4 gene analysis revealed three heterozygous mutations in exon 42, namely Gly1961Glu, IVS41-43 C>A, and IVS41-11 G>A, and a heterozygous IVS46+2 C>G mutation in exon 46. All imaging modalities showed peripheral areas with few bone spicules. The area surrounding the optic nerve showed evidence of RPE atrophy as visualized by SLO autofluorescence. The fovea and optic nerve were clearly identified in OCT. Histology showed a degenerated retina with only a few disorganized photoreceptors and the absence of RPE in the perifovea. The macula was severely degenerated, with little evidence of any retinal cell layer including the RPE. In contrast, stratified nuclear layers were observed in the retinal periphery. In the periphery, the RPE was present and thicker than normal, but lacked melanin pigment. Cones were present in small areas in the perifovea that labeled with opsin and arrestin antibodies. Disorganized rhodopsin labeled rods were detected in the perifovea and in the periphery. Calbindin labeled second order neurons were sparse in the perifovea but were more abundant in the periphery. No labeling with any of the markers used was evident in the macula due to extensive neuronal loss. Reactive glia labeled with GFAP was increased in the perifovea and periphery of the donor tissue. Autofluorescent material in the perifovea was significantly reduced in areas where the RPE remained. In the periphery, the RPE was hypertrophied and the autofluorescence was more intense.

Conclusions: The histopathology of the retina in a patient with Stargardt disease due to compound heterozygous *ABCA4* mutations displayed a highly degenerated perifovea and preservation of some cone and rod photoreceptors in the perifovea and periphery.

Introduction

Stargardt disease is an autosomal-recessive macular disease with estimated frequency between 1 in 8,000 and 1 in 10,000 (Blacharski, 1988). Over 600 disease-causing mutations in the *ABCA4* gene have been reported, with the three most common mutations accounting for less than 10% of the disease phenotypes (Allikmets et al., 2007).

Stargardt disease is characterized by excessive accumulation of lipofuscin in the RPE (Cideciyan et al., 2004). The general course of the disease is a slow progressive loss of central vision due to macular atrophy (Fishman et al., 1987, Rotenstreich et al., 2003). The *ABCA4* gene, encodes a transport protein located in the rim of photoreceptor discs and is involved in the transport of all-trans retinal through the disc membrane. *ABCA4* protein dysfunction determines accumulation of all-trans retinal in the photoreceptors and in the RPE, due to the phagocytosis of the photoreceptor outer segments by RPE. All-trans retinal is converted to A2-E, a major component of lipofuscin, which leads to RPE and photoreceptors toxicity (Allikmets et al., 97, Sun et al., 2001).

(1) Fundus Macrography of Donor Eyes

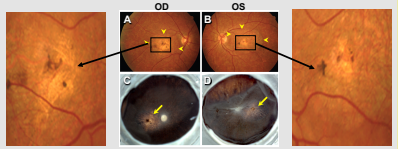

Fundus image of eyes from a Stargardt disease (SD) donor due to compound heterozygous *ABCA4* mutations. Fundus photograph of both the right (A) and left (B) eyes of a Stargardt disease patient at age 55, when last seen for examination showing a normal-appearing optic disc and RPE atrophy with hyperpigmented areas adjacent to the fovea (arrowhead). Images of 66 year-old donor eyes (C, D) also display RPE atrophy (arrows) in the perifovea.

(2) Fundus Images of Donor Eyes

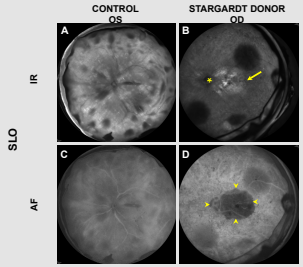

***Ex vivo* imaging of Stargardt donor and age-similar control eyes.** SLO images were collected by using a model HRA2 confocal scanning laser ophthalmoscope (Heidelberg Engineering, Inc.). Prior to imaging, the cornea and lens were removed leaving only the posterior pole. Remaining eye cups were filled with PBS to eliminate specular reflections and improve contrast and image quality. To accomplish SLO imaging, the entire instrument was rotated 90º so that the scan is perpendicular to the table surface for optimal imaging of the PBS filled eye cups. SLO-IR imaging of the Stargardt donor eye (B) identified the optic disk (*) and the hypopigmented macula identified also by fundus image (arrow). SLO-AF imaging of Stargardt eye (D) revealed that the area surrounding the optic nerve and fovea displayed evidence of RPE atrophy (arrowheads) compared to the control (C), which clearly showed the retinal vasculature. The area surrounding the optic nerve showed evidence of RPE atrophy as choroidal vasculature could be visualized.

(3) OCT Images of Donor Eyes

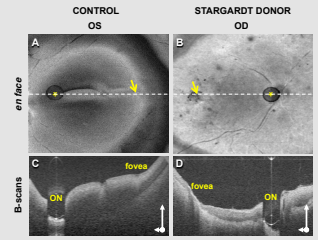

***Ex Vivo* imaging of the Stargardt donor and age-similar control eyes using SD-OCT.** Spectral Domain Optical Coherence Tomography images were collected using the SD-OCT system (Bioptigen, Inc.) with ~7x7mm field of view. SD-OCT *en face* view displayed several degenerated areas around the fovea and ON in the retina of the Stargardt donor eye (B) when compared to the age-similar control eye (A). The fovea and optic nerve could be clearly identified. SD-OCT B-scans revealed structural differences in the retina that suggested disorganization of the Stargardt donor retina (B), absence of a photoreceptor layer when compared to the control eye (C). Arrows point to the in-depth, B-scan plane shown in the OCT images; (*) 1mm ruby sphere positioned on top of the ON to serve as reference. B-scan scale bar is 0.5mm

(4) Histology

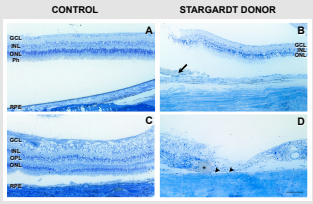

Degeneration in the retina of a Stargardt donor eye. Representative photomicrographs of toluidine blue stained plastic sections (1µm) from the Stargardt donor and matched control. Morphology of control retina in the periphery (A) and perifovea (C) displayed typical characteristics of a healthy retina including structural lamina consisting of retinal cells. In the periphery of the Stargardt donor retina all the retinal layers were present (B). However, a decrease in this retinal thickness could be observed due mostly to degeneration in the OPL. The RPE was increased from its normal thickness and displayed lack of pigment (arrow). In contrast, in the perifovea of the Stargardt donor (D) displayed absence of the outer nuclear layer (ONL) and photoreceptors (Ph). The nuclei in the inner nuclear layer (INL) were significantly decreased. Although the RPE was mostly absent from this area, Bruch's membrane was still present (arrowheads). The perifovea revealed a highly degenerate retina with little evidence of stratified nuclear layers and the presence of a giant lipophilic drop in the choroid (D, *). The choroid (Ch) was degenerated in the perifovea. GCL= ganglion cell layer; INL= inner nuclear layer; OPL= outer plexiform layer; ONL= outer nuclear layer; RPE= retinal pigment epithelium. Bars =100µm.

(5) Immunocytochemistry

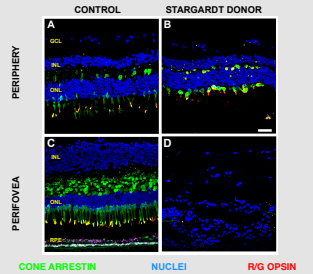

Decreased presence of cones in the perifovea of a Stargardt donor retina. Representative photomicrographs of cryosections obtained from the Stargardt donor (B, D) and the matched control (A, C). Sections were labeled with antibodies specific to cone arrestin (Alexa488, green) and red/green cone opsin (Alexa594, red) while cell nuclei have been labeled with TO-PRO-3 (blue). Observation of control retinas (A, B) showed that cone arrestin was distributed along the entire plasma membrane of this cone type, from the tip of the outer segment to the synaptic base while the red/green opsin was restricted to the cone outer segments both in the periphery (A) and perifovea (C). The presence of stubby cones could be observed in the periphery of the Stargardt donor retina (B). In contrast, a few cones were present in the perifovea of the Stargardt donor (D). GCL=ganglion cell layer, INL=inner nuclear layer, ONL=outer nuclear layer, RPE=retinal pigment epithelium. Bar = 40µm.

(6) Immunocytochemistry

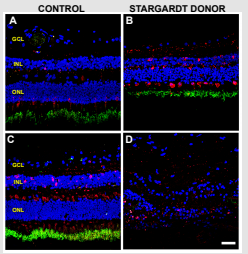

Significant decrease in rods in the perifovea of the Stargardt donor. Representative photomicrographs of cryosections collected from the age-similar control (A, C) and the Stargardt donor (B, D). Sections are shown labeled with antibodies specific to rhodopsin (Alexa488, green) while cell nuclei were labeled with TO-PRO-3 (blue). Rhodopsin labeling revealed the presence of rods in the periphery (B) of the Stargardt donor and complete absence of rods in the perifovea (D) of this donor when compared to the control retinas in the periphery (A) and perifovea (C). Calbindin labeling in the control retina was present in the amacrine, bipolar and cones both in the periphery (A) and in the perifovea (C). Interestingly, calbindin positive cells were increased and revealed the presence of stubby cones in the Stargardt donor retina in the periphery (B). However, in the perifovea calbindin positive cells were significantly decreased and were observed scattered throughout the entire retina (B). GCL=ganglion cell layer, INL=inner nuclear layer, OPL=outer plexiform layer, ONL=outer nuclear layer. Bar = 40µm..

(7) Immunocytochemistry

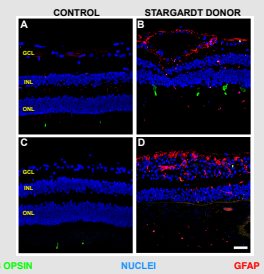

Increased presence of Müller cells which have undergone reactive gliosis in the eyes of a Stargard donor. Representative photomicrographs of cryosections obtained from the Stargardt donor and age-similar control. Sections were labeled with antibodies specific to blue cone opsin (Alexa488, green) and GFAP (Alexa594, red) while cell nuclei were labeled with TO-PRO-3 (blue). While blue cone opsin is restricted to the outer segments of the cones in the control (A) it is not in the Stargardt donor retina in the periphery (B). The Muller cells had undergone reactive gliosis throughout the retina and their hypertrophic processes were GFAP positive in the of the Stargardt donor (B) but not in the control retina (A). A decrease in the presence of blue cones was detected in the Stargardt donor in the perifovea (D) when compared to the control perifovea (C). The Muller cells had undergone reactive gliosis mostly in the inner retina of the perifovea (D). GCL=ganglion cell layer, INL=innerretinal nuclear layer, OPL=outer plexiform layer, ONL=outer nuclear layer. Bar = 40µm.

(8) Immunocytochemistry

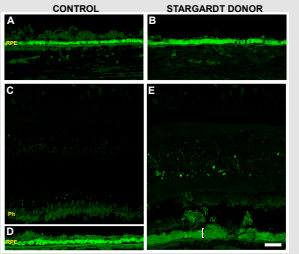

Significant accumulation of autofluorescent material in the RPE in the periphery of the Stargardt donor retina. Representative epifluorescence photomicrographs of cryosections obtained from the Stargardt donor (B, E) and matched control (A, C, D). Sections were observed using the green channel (FITC filter: excitation 495nm/ emission 519nm). Hypertrophic RPE from the Stargardt donor retina displayed significantly increased autofluorescent granules (B) when compared to the control RPE (A) in the periphery. In contrast, hypertrophic RPE from the Stargardt donor displayed significantly decreased autofluorescent granules in the perifovea (E, bracket) when compared to the control RPE (D) Autofluorescence was also observed in the photoreceptor inner and outer segments detached from the top of the RPE (C, Ph), due to the presence of glutaraldehyde in the fixation solution. Bar = 40µm.

Conclusions

The retina of a Stargardt disease donor displays:

- In the periphery all the retinal layers were present, with lower degree of degeneration in the OPL. The RPE was increased from its normal thickness and displayed lack of pigment;
- The perifovea displayed absence of the outer nuclear layer and photoreceptors. The nuclei in the inner nuclear layer were significantly decreased. Although the RPE was mostly absent from this area, Bruch's membrane was still present;
- The macula revealed a highly degenerated retina with little evidence of stratified nuclear layers and the presence of a giant lipophilic drop in the choroid ;
- Presence of stubby, disorganized cones in the periphery and absence of cones in the perifovea;
- Presence of rods in the periphery and absent in the perifovea;
- Increased distribution of calbindin positive cells in the periphery and decreased in the perifovea;
- Increased Müller cells which have undergone reactive gliosis both in the periphery and perifovea;
- In the periphery, blue cone opsin is distributed in the inner and outer segments, but blue cones were significantly decreased in the perifovea;
- Significant increase of autofluorescent material in the RPE in the periphery but decrease of autofluorescent material in the RPE in the perifovea.

References

- Allikmets R, Singh N, Sun H, et al. *Nat Genet*. 1997;15:236–246.
- Allikmets R. In: Tombran-Tink J, Barnstable CJ, eds. Retinal Degenerations: Biology, Diagnostics and Therapeutics. Totowa, NJ: Humana Press, 2007;105–118.
- Blacharski PA. In: Newsome DA, ed. Retinal Dystrophies and Degenerations. New York: Raven Press, 1988;135–159.
- Cideciyan AV, Aleman TS, Swider M, et al. *Hum Mol Genet*. 2004;13:525–534.
- Fishman GA, Stone EM, Grover S, et al. *Arch Ophthalmol*. 1999;117:504–510.
- Jaakson K, Zernant J, Külm M, et al. *Hum Mutat*. 2003;22(5):395–403.
- Rotenstreich Y, Fishman, GA, Anderson RJ. *Ophthalmology*. 2003;110:1151–1158.
- Sun H, Nathans J. *J Bioenerg Biomembr*. 2001;33:523–530.
- Yatsenko AN, Shroyer NF, Lewis RA, et al. *Hum Genet*. 2001;108:346–355.

RETINAL HISTOPATHOLOGY IN EYES FROM PATIENTS WITH AUTOSOMAL RECESSIVE RETINITIS PIGMENTOSA CAUSED BY *EYS* MUTATIONS

G. J. Pauer[1], V. L. Bonilha[1], M. E. Rayborn[1], B. A. Bell[1], M. J. Marino[1], C. D. Beight[1], J. Chiang[2], E. I. Traboulsi[1], S. A. Hagstrom[1] and J. G. Hollyfield[1]

Program #1362

[1] The Cole Eye Institute, Cleveland Clinic Lerner College of Medicine, Cleveland, OH; [2] Casey Eye Institute Molecular Lab, Portland, OR.

Cleveland Clinic

Abstract

Purpose: To evaluate the histopathology in donor eyes from patients with autosomal recessive retinitis pigmentosa (arRP) caused by *EYS* mutations.

Methods: Eyes were obtained from a 72 year-old female (donor 1), a 91 year-old female (donor 2), and her 97 year-old sister (donor 3). Eyes were fixed in 4% paraformaldehyde and 0.5% glutaraldehyde in PBS within 6 to 11 hours postmortem. Globes were evaluated with macroscopic, SLO and OCT imaging. Macular and peripheral regions were processed for immunocytochemistry. Three age-matched normal eyes and an eye donated by donor 1's asymptomatic mother were used as controls. DNA was obtained from blood samples of the donors for mutational analysis.

Results: DNA analysis of the affected brother of donor 1 revealed the *EYS* gene mutations, IVS11+1G→A and Q874X. DNA analysis of donors 2 and 3 led to the identification of a heterozygous 7 base pair deletion, L1451fs, in the *EYS* gene. The histopathological findings of the retina of donor 1 and her asymptomatic mother were reported previously and are compared to the findings in the retinas of donors 2 and 3. SLO of donor 3 showed hypofluorescence in one contiguous region involving the optic disk and macular region as opposed to the individually demarcated and isolated regions seen in donors 1 and 2. Histology of all three affected donors revealed a highly degenerate retina with little evidence of stratified nuclear layers in all peripheral areas studied. In contrast, the macular area displayed a prominent inner nuclear layer. Donor 2 and 3 revealed patchy areas of RPE in the macula whereas the RPE was thin in the macula and absent in the far periphery of donor 1. Rhodopsin-labeled rods were absent except in the far periphery of donor 1. However, rods were still present in the periphery of donors 2 and 3. Of interest, some rods were observed in the choroid of these eyes. In the perifovea, donor 2 displayed no rods while donor 3 displayed several disorganized rods. Cone-arrestin labeled cells were present in the perifovea but were mostly absent from the periphery of donor 1. Patches of cones were observed in the perimacula of both donors 2 and 3.

Conclusions: Advanced retinal degenerative changes with near-total absence of rods and preservation of macular cones characterized the retinal histopathology of arRP patients due to *EYS* mutations.

Support: Foundation Fighting Blindness, Research to Prevent Blindness, Wolf Family Foundation, National Eye Institute

Acknowledgements: Dr. Peter MacLeish (Morehouse School of Medicine, Atlanta, GA) for providing us with the antibody to cone arrestin (7G6) and Dr. Paul Hargrave (University of Florida, Gainesville, FL) for providing us with the antibody to rhodopsin (B630N).

Schematic Diagram of EYS

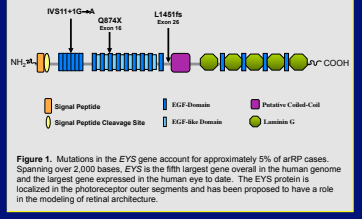

Figure 1. Mutations in the *EYS* gene account for approximately 5% of arRP cases. Spanning over 2,000 bases, *EYS* is the fifth largest gene overall in the human genome and the largest gene expressed in the human eye to date. The EYS protein is localized in the photoreceptor outer segments and has been proposed to have a role in the modeling of retinal architecture.

Sequence Changes Identified

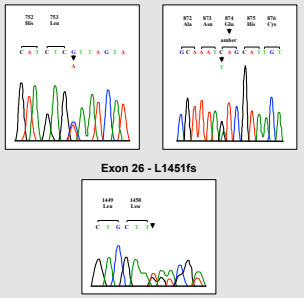

Figure 2. DNA analysis revealed *EYS* gene mutations, IVS11+1G →A and Q874X in donor 1 and a 7 base pair deletion, L1451fs, in donors 2 and 3.

Pedigrees of Families Studied

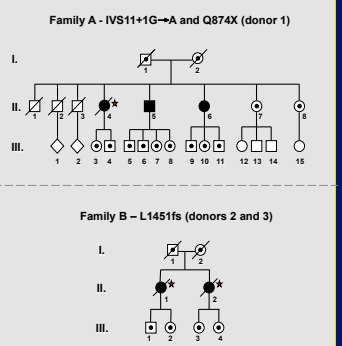

Figure 3. Pedigrees of families with arRP due to *EYS* mutations. Slashed symbols reflect deceased family members. Affected family members are with filled symbols, unaffected family members are shown with unfilled symbols and unaffected carrier family members are shown with unfilled symbols with a black dot inside.

DNA analysis of family A harboring the mutations IVS11+1G→A and Q874X was carried out in all three affected members (II-4, II-5 and II-6), in their two unaffected living sisters (II-7 and II-8), and in their mother (I-2). Postmortem analysis in family A was done on affected member II-4 now referred to as donor 1 (★).

DNA analysis of family B harboring the L1451fs mutation was carried out in II-1. Postmortem analysis in family B was done on affected members II-1 and II-2 now referred to as donors 2 (★) and 3 (★), respectively.

Fundus Images of Donor Eyes

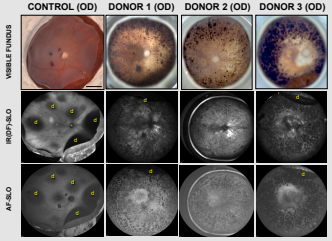

Figure 4. *Ex vivo* imaging of arRP donor eyes with *EYS* mutations. SLO and macroscopic fundus images were collected from donors and controls using an HRA2 SLO (Heidelberg Engineering, Inc.) and Zeiss AxioCam MRC5 macro imaging system, respectively. Prior to imaging, the anterior segment was removed leaving only the posterior pole. Remaining eye cups were filled with PBS for imaging. SLO imaging was performed by rotating the camera head 90°, from a horizontal to vertical viewing orientation.

In the control eye, detached retinas are apparent with all imaging modalities (d). In arRP eyes, all imaging modalities show bone spicules in peripheral areas to varying degree. SLO-IR imaging identified degeneration in the entire posterior pole region including the macula, perimacula and areas surrounding the optic nerve due to focal loss of RPE in donors 2 and 3. SLO-AF imaging identified hypofluorescence in one contiguous region involving the macula and area surrounding the optic disk of donor 3 as opposed to the individually demarcated and isolated regions seen with both donors 1 and 2. Scale bars in fundus image = 0.5 *cm*.

OCT Images of Donor Eyes

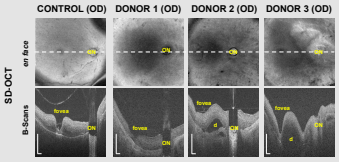

Figure 5. *Ex vivo* OCT imaging of arRP donor eyes with *EYS* mutations. OCT was performed with Envisu HR SD-OCT system (Bioptigen). Eye cups were filled with PBS and positioned directly below the SD-OCT objective for imaging. A 1mm ruby sphere positioned on top of the ON served as a calibration reference. Dashed-lines in the *en face* images indicate the location of the in-depth, B-scan images. The fovea and optic nerve could be identified in all samples.

In-depth B-scans from the control eye revealed a normal appearing retina with clearly defined fovea, some evidence of laminar architecture, and no appreciable evidence of retinal thinning and/or degeneration. Images from arRP donors revealed retinas of appreciable thickness but with less organized architecture and integrity in the macular region. In contrast, the peripheral regions showed some evidence of thinned retina relative to the control sample suggesting degeneration. Donor's 2 and 3 had macular detachments which are indicated by "d" in the B-scans. B-scan scale is 0.5mm.

Histology of Donor Eyes

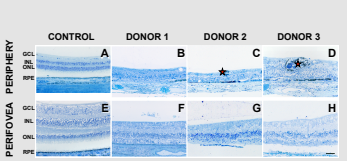

Figure 6. Degeneration in the retina of arRP donors due to *EYS* mutations. Representative photomicrographs from Toluidine blue stained plastic sections (1μm) of the arRP donors retinas and a matched control are shown for comparison. Morphology of control retina in the periphery (A) and perifovea (E) region displayed typical characteristics including structural lamina consisting of retinal cells. Histology of all three arRP donors revealed a highly degenerate retina with disorganization of the lamina and cellular layers and gliosis in all peripheral areas analyzed (B to D). Photoreceptor outer segments were also absent in all areas analyzed. Intraretinal bone spicules were visible in the retinas of donors 2 (C,★) and 3 (D,★). In contrast, the perifovea displayed a prominent inner nuclear layer. Donors 2 (G) and 3 (H) displayed patchy areas of RPE in the perifovea whereas the RPE was thin in the perifovea of donor 1 (F). Patchy, disorganized cones were observed on top of the RPE in the perifovea of donors 2 (G) and 3 (H). GCL= ganglion cell layer; INL= inner nuclear layer; ONL= outer nuclear layer; RPE= retinal pigment epithelium. Bars =50μm.

Immunocytochemistry of Donor Eyes

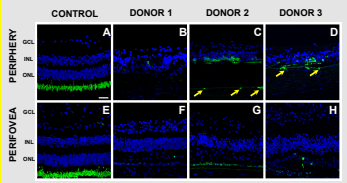

Figure 7. Significant decrease in rods both in the periphery and in the perifovea of arRP donors due to *EYS* mutations. Representative photomicrographs of cryosections collected from the matched control and arRP donors. Sections are shown labeled with antibodies specific to N-terminal domain of rhodopsin (green) while cell nuclei were labeled with TO-PRO-3 (blue). Comparison of the samples showed that rhodopsin was restricted to the rod outer segments in the control retina both in the periphery (A) and perifovea (E). Rhodopsin-labeled rods were mostly absent from the periphery of donor 1 (B). However, rods were still present in the periphery of donors 2 (C) and 3 (D). Of interest, some rods were observed in the choroid of these eyes (arrows). In the perifovea, donors 1 (F) and 2 (G) displayed no rods while donor 3 (H) displayed several disorganized rods. GCL= ganglion cell layer; INL= inner nuclear layer; ONL= outer nuclear layer. Bar = 40μm.

Immunocytochemistry of Donor Eyes

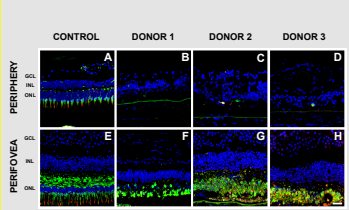

Figure 8. Significant decrease in the cones in the periphery of arRP donor retinas due to *EYS* mutations. Representative photomicrographs of cryosections obtained from the arRP donor and a matched control. Sections were labeled with antibodies specific to cone arrestin (green) and red/green cone opsin (red) while cell nuclei have been labeled with TO-PRO-3 (blue). In the control retina, cone arrestin was distributed along the entire plasma membrane of this cone type, from the tip of the outer segment to the synaptic base while the red/green opsin was restricted to the cone outer segments both in the periphery (A) and perifovea (E). Cones were mostly absent from the periphery of the all the arRP donor retinas (B to D). In contrast, cones were present but highly disorganized in the perifovea of the donor 1 (F), but synaptic terminals were not visualized. Interestingly, perifovea from both donor 2 (G) and 3 (H) displayed patchy, disorganized cones in areas that still have RPE. GCL= ganglion cell layer; INL= inner nuclear layer; ONL= outer nuclear layer. Bar = 40μm.

Conclusions

arRP donor retinas with *EYS* mutations display:

- atrophic retina with disorganization of the cellular layers and gliosis in the periphery of the retinas of all examined donors
- presence of intraretinal bone spicules in the periphery of donors 2 and 3
- prominent inner nuclear layer in the perifoveal region of all donors
- patchy areas of RPE in the perifovea of donors 2 and 3 and thin RPE in the perifovea of donor 1
- absence of cones in the periphery of all donors
- presence of disorganized cones in the perifovea of donor 1 and patchy disorganized cones in the perifovea of donors 2 and 3
- near-absence of rods both in the periphery and in the perifovea of all analyzed donors.

Foundation Fighting Blindness

SUPPORTED BY Research to Prevent Blindness

RETINAL HISTOPATHOLOGY IN EYES FROM PATIENTS WITH AUTOSOMAL DOMINANT RETINITIS PIGMENTOSA CAUSED BY RHODOPSIN MUTATIONS

Program #1364

M. E. Rayborn, V. L. Bonilha, B. A. Bell, X. Yang, M. J. Marino, G. J. Pauer, C. D. Beight, E. I. Traboulsi, S. A. Hagstrom, and J. G. Hollyfield

The Cole Eye Institute, Cleveland Clinic Lerner College of Medicine, Cleveland, OH

Cleveland Clinic

Supported by Research to Prevent Blindness

Foundation Fighting Blindness

Abstract

Purpose: To compare the histopathology in donor eyes from patients with autosomal dominant retinitis pigmentosa (adRP) caused by Pro23His, Pro347Thr and Pro347Leu rhodopsin mutations.

Methods: Eyes were obtained from 72, 80 and 83 year-old donors and fixed in 4% paraformaldehyde and 0.5% glutaraldehyde in PBS within 8 to 17.5 hours postmortem. Globes were evaluated with macroscopic, SLO and OCT imaging. Macula and peripheral regions were processed for microscopy and immunocytochemistry. Three age-matched normal eyes were used as controls. DNA was obtained from blood and buccal samples of the donor and family members. Direct genomic sequencing of the entire rhodopsin coding region and flanking intronic sequences was performed.

Results: DNA analysis of the donors and affected family members revealed rhodopsin Pro23His, Pro347Thr and Pro347Leu mutations. Histopathological findings in the retina of the donor carrying a Pro23His rhodopsin mutation were reported previously and are compared here to donors carrying the Pro347Thr and Pro347Leu mutations. The area surrounding the optic nerve showed evidence of RPE atrophy as choroidal vasculature could be visualized in the Pro23His and Pro347Thr eyes. A prominent inner nuclear layer was present in the perifoveal region in the Pro23His eye. In addition, the RPE was reduced from normal thickness in the macula in the Pro23His eye while it was discontinuous in the Pro347Thr and Pro347Leu eye in the macular region. Cones labeled with opsin and arrestin antibodies were present in the macula, but were mostly absent from the periphery in the Pro23His eye. Few cones were present in the Pro347Thr and Pro347Leu eyes. A few highly disorganized, rhodopsin labeled rods were detected in the macula but were absent in the periphery of the Pro23His eye. The retinas of the Pro347Thr and Pro347Leu eyes showed almost complete absence of rhodopsin labeled rods in both the perifovea and periphery.

Conclusions: The histopathology of the retina in patients with Pro23His rhodopsin mutation displayed highly degenerate peripheral retina and preservation of some cone and rod photoreceptors in the macula. The retina in patients with Pro347Thr and Pro347Leu rhodopsin mutations displayed near-complete loss of rods and the presence of few cones in the macula.

(1) Pedigrees of Families Studied

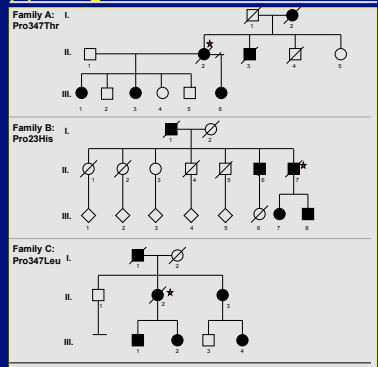

Pedigrees of families with adRP due to rhodopsin mutations. Slashed symbols reflect deceased family members. Affected family members are with filled symbols, unaffected family members are shown with unfilled symbols. (★) represents eye donor studied in each family.

(3) OCT Images of Donor Eyes

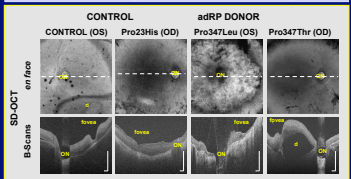

In situ imaging of adRP donor eyes due to rhodopsin mutations using SD-OCT.
Ex vivo OCT imaging of adRP donor eyes with *RHO* mutations. OCT was performed with Envisu HR SD-OCT system (Bioptigen). Eye cups were filled with PBS and positioned directly below the SD-OCT objective for imaging. A 1mm ruby sphere positioned on top of the ON served as a calibration reference. Dashed-lines in the *en face* images indicate the location of the in-depth, B-scan images. The fovea and optic nerve could be identified in all samples. SD-OCT B-scans revealed structural differences in the retina that suggests disorganization and degeneration of the affected retinas, especially Pro347Leu. Degeneration was not appreciable in Pro23His and Pro 347Thr samples as overall retinal thickness was similar to controls. All adRP donor eyes appeared to be absent of a photoreceptor layer when compared to the control eye. Dashed-lines in the en face images indicate the location of the in-depth, B-scan images. SD-OCT *en face* view displayed several bone spicules around the fovea and ON in the retina of the Pro23His rhodopsin RP donor eye. B-scan scale is 0.5mm.

(5) Immunocytochemistry

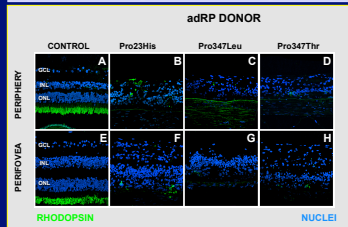

Significant decrease in rods both in the periphery and in the perifovea of adRP donor eyes due to rhodopsin mutations. Representative photomicrographs of cryosections collected from the matched control and the adRP donors. Sections are shown labeled with antibodies specific to C-terminal domain of rhodopsin (Alexa488, green) while cell nuclei were labeled with TO-PRO-3 (blue). In the control retina rhodopsin was restricted to the rods outer segment both in the periphery (A) and perifovea (E). A few highly disorganized rhodopsin-labeled rods were still present in the periphery of the donor carrying the Pro23His mutation (B) but were absent from the retinas from donors carrying Pro347Leu (C) and Pro347Thr (D) mutations. In the perifovea, donors carrying Pro23His (F) and Pro347Thr (H) mutations displayed a few disorganized rhodopsin-labeled rods. No rhodopsin labeled cells were detected in the perifovea of the donor carrying the Pro347Leu mutation. GCL= ganglion cell layer; INL= inner nuclear layer; ONL= outer nuclear layer. Bar = 40μm.

Conclusions

The retinas of adRP donors carrying rhodopsin mutations display:

- highly degenerate retina with disorganization of the lamina and cellular layers and gliosis in peripheral areas of all rhodopsin mutations;
- prominent inner nuclear layer in the perifovea in the donor carrying Pro23His mutation;
- RPE reduction from normal thickness in the perifovea in the donor carrying Pro23His mutation;
- severely atrophic retina and discontinuous RPE in the perifovea of donor carrying Pro347Leu mutation;
- prominent inner nuclear layer with the presence of patchy disorganized cones in the perifovea in the donor carrying the Pro347Thr mutation;
- near-absence of rods both in the periphery and in the perifovea in all adRP retinas;
- absence of cones in the periphery of all adRP donors carrying rhodopsin mutations;
- presence of disorganized cones in the perifovea of donors carrying both the Pro23His and Pro347Thr mutations;
- complete absence of cones in the perifovea of donor carrying Pro347Leu mutation.

Rhodopsin Gene Mutations

Approximately 15 - 35% of RP cases are autosomal dominant (adRP). According to RetNet, 23 different genes have been associated with adRP. The most common gene to cause adRP is the rhodopsin (*RHO*) gene—accounting for 20-30% of patients.

The most common mutation in *RHO* is the Pro23His mutation, which is found in about one third of patients. A few previous studies reported analysis of the retinal histology of eyes with the Pro23His mutation. Those studies all showed variable histological findings in the retina with a final common pathway leading to photoreceptor cell death (Kolb & Gouras, 1974; To et al., 2002; To et al., 2004).

Pro347 is a mutation hotspot in *RHO* with at least 4 mutations reported. It was previously reported that a human eye carrying the Pro347Leu mutation displayed focal, cone sparing (Marc et al., 2007). In addition, analysis of patients carrying this mutation showed that they displayed cone-mediated vision, extracentral retina showed loss of ONL, thickening of the inner retina, and demelanization of RPE (Aleman et al., 2008). Pro347Thr has also been previously reported in patients (Dryja et al., 2000).

According to Nathans and Hogness (1984), the 348-amino acid *RHO* protein has 7 transmembrane domains, with a luminal N terminus and a cytoplasmic C terminus. The cytoplasmic face of rhodopsin is made up of 3 loops. The C-terminal tail contains the catalytic site that promotes GTP-GDP exchange by transducin and several putative sites for light-dependent phosphorylation by rhodopsin kinase. Rhodopsin also has 2 sites for N-glycosylation, and lys296 is the site for 11-cis-retinal attachment (see scheme below).

Rhodopsin is essential for photoreceptor morphogenesis. Here we analyzed and reported for the first time the distribution of photoreceptors and other retinal cells in adults carrying point mutations in RP donors in the intradiscal (Pro23His) and cytoplasmic (Pro347Thr and Pro347Leu) region of the rod outer segments (see arrows in scheme below).

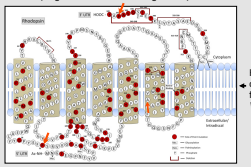

Human rhodopsin illustrating sites of known mutations or deletions. from: Rossmiller et al., *Molecular Vision*; 18:2479-2496 (2012).

(2) Fundus Images of Donor Eyes

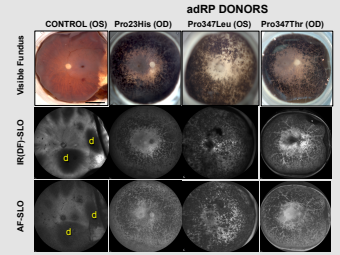

***In situ* imaging of whole adRP donor eyes due to rhodopsin mutations and age-matched control eyes.** *Ex vivo* imaging of adRP donor eyes with *RHO* mutations. SLO and macroscopic fundus images were collected from donors and controls using an HRA2 SLO (Heidelberg Engineering, Inc.) and Zeiss AxioCam MRC5 macro imaging system, respectively. Prior to imaging, the anterior segment was removed leaving only the posterior pole. Remaining eye cups were filled with PBS for imaging. SLO imaging was performed by rotating the camera head 90°, from a horizontal to vertical viewing orientation. All imaging modalities revealed peripheral areas of heavy bone spicules. SLO-IR imaging identified the optic disk and the hypopigmented macula identified by fundus image. AF-SLO imaging revealed some weak autofluorescence signal that was devoid of any structural detail compared to the control which clearly showed retinal vasculature and lipofuscin/RPE AF background. The area surrounding the optic nerve showed evidence of RPE atrophy as choroidal vasculature could be visualized. Scale bars in fundus image = 0.5 cm.

(4) Histology of Donor Eyes

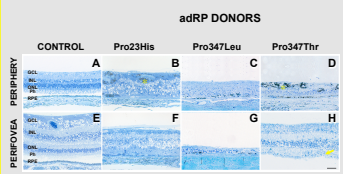

Degeneration in the retina of adRP donor eyes due to rhodopsin mutations. Representative photomicrographs from toluidine blue stained plastic sections (1μm) of both the adRP donor retinas and a matched control are shown for comparison. Morphology of control retina in the periphery (A) and perifovea (E) displayed typical characteristics including structural lamina consisting of retinal cells. Histology of all three adRP donor retinas revealed a highly degenerate retina with disorganization of the lamina and cellular layers and gliosis in all peripheral areas analyzed (B to D). Intraretinal bone spicules were visible in the retinas of donors carrying Pro23His (B, *) and Pro347Thr (D, *) mutations. A prominent inner nuclear layer was present in the perifovea in the donor carrying Pro23His mutation (F). In addition, the RPE was reduced from normal thickness in the perifovea in this eye. The retina of donor carrying Pro347Leu mutation was severely atrophic in the perifovea (G). The RPE was discontinuous in this region (G) in the perifovea. A prominent inner nuclear layer was present in the perifovea in the donor carrying the Pro347Thr mutation (H); a few disorganized photoreceptors can also be observed (arrows). GCL= ganglion cell layer; INL= inner nuclear layer; ONL= outer nuclear layer; Ph= photoreceptors; RPE= retinal pigment epithelium. Bars =50μm.

(6) Immunocytochemistry

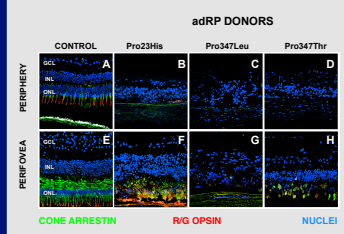

Significant reduction in the cones in the periphery of adRP donor eyes due to rhodopsin mutations. Representative photomicrographs of cryosections obtained from the adRP donor and a matched control. Sections were labeled with antibodies specific to cone arrestin (Alexa488, green) and red/green cone opsin (Alexa594, red) while cell nuclei have been labeled with TO-PRO-3 (blue). In the control retina cone arrestin was distributed along the entire plasma membrane of this cone type, from the tip of the outer segment to the synaptic base while the red/green opsin was restricted to the cone outer segments both in the periphery (A) and perifovea (E). Cones were mostly absent from the periphery of the all adRP donor retinas (B to D). In contrast, cones were present but highly disorganized in the perifovea of the donor carrying Pro23His (F) and Pro347Thr (H) mutations, but synaptic terminals were not visualized. The perifovea of donor carrying the Pro347Leu (G) mutation displayed to close to complete absence of cone arrestin labeled cells. GCL= ganglion cell layer; INL= inner nuclear layer; ONL= outer nuclear layer. Bar = 40μm.

References

- Aleman TS, Cideciyan AV, Sumaroka A, et al. *Invest Ophthalmol Vis Sci.* 2008; 49: 1580-1590.
- Berson EL, Rosner B, Sandberg MA, et al . *Arch Ophthalmol.* 1991; 109: 92-101.
- Dryja TP, Hahn LB, Cowley GS, et al. *Proc.Natl. Acad. Sci. USA.* 1991; 88: 9370- 9374.
- Dryja TP, McEvoy JA, McGee TL, et al. *Invest Ophthalmol Vis Sci.* 2000; 41: 3124- 3127.
- Kolb H & Gouras P. *Invest Ophthalmol Vis Sci.* 1974; 13: 487-498.
- Marc RE, Jones BW, Anderson JR, et al. *Invest Ophthalmol Vis Sci. 2007; 48: 3364- 3371.*
- To K, Adamian M, Dryja TP, et al. *Am J Ophthalmol.* 2002; 134: 290-293.
- To K, Adamian M & Berson EL. *Am J Ophthalmol.* 2004; 137: 946-948.

Acknowledgements

We thank Dr. Peter MacLeish (Morehouse School of Medicine, Atlanta, GA) for providing us with the antibody to cone arrestin (7G6). Pedigree courtesy of the Berman-Gund Lab (Massachusetts Eye and Ear Infirmary, Boston, MA).

Support

The Foundation Fighting Blindness
Research to Prevent Blindness
Wolf Family Foundation
National Eye Institute

Program # 6332

RETINAL HISTOPATHOLOGY IN EYES FROM PATIENTS WITH BEST DISEASE CAUSED BY *VMD2* MUTATIONS

Cleveland Clinic

Mary E. Rayborn[1], Vera L. Bonilha[1], Brent A. Bell[1], Xiaoping Yang[1], Meghan J. Marino[1], Gayle J.T. Pauer[1], Craig D. Beight [1], Elias I. Traboulsi[1], Stephanie A. Hagstrom[1], Gerald A. Fishman[2], and Joe G. Hollyfield[1]

[1]Cole Eye Institute, Department of Ophthalmology, CCLCM, Cleveland, OH; [2]Pangere Center at The Chicago Lighthouse for People Who Are Blind or Visually Impaired, Chicago, IL, USA.

Abstract

Purpose: To compare the histopathology in donor eyes from patients with Best disease (BD) caused by p.Asn296His and p.Ile201Thr *VMD2* mutations.

Methods: Eyes were obtained from 85 year-old (donor 1, female), and 65 year-old (donor 2, male) postmortem donors, and were fixed within 25 hrs postmortem. Globes were evaluated with macroscopic, SLO and OCT imaging. Perifoveal and peripheral retinal regions were processed for electron microscopy and immunocytochemistry using cell-specific antibodies. Four age-similar normal eyes were used as controls. DNA was obtained from donor blood samples. Sequence analysis of the entire *VMD2* coding region was performed.

Results: DNA analysis of donor 1 detected a p.Asn296His *VMD2* mutation. DNA analysis of donor 2 detected a p.Ile201Thr *VMD2* mutation. Fundus examination showed that donor 1 displayed a macular lesion with considerable scarring while donor 2 displayed close to normal macular morphology. Imaging modalities indicated considerable retinal atrophy in the perifoveal region of donor 1. In each BD donor, histology showed a distinct ganglion cell layer (GCL), inner nuclear layer (INL), outer nuclear layer (ONL), RPE and choriocapillaris (CC) in the periphery. In addition, donor 1 displayed edema of the interphotoreceptor matrix. Prominent GCL and INL were evident in the perifoveal region of donor 1. In addition, an extensive fibrovascular scar was present between Bruch's membrane and the retina; this area also displayed patchy thin RPE with no photoreceptors. In contrast, the perifoveal region of donor 2 had distinct GCL, INL, ONL and robust RPE and CC. Cells labeled with cone opsin and arrestin antibodies were evident in the macula, but mostly absent in the retina adjacent to the fibrovascular scar of donor 1. In the periphery of both BD donors, cells labeled with cone-specific antibodies were present. Cells labeled with rhodopsin were detected in the perifoveal region but not in the fibrovascular scar area of donor 1. Cells labeled with rhodopsin antibody were present in the periphery of both donors. Autofluorescent material in the perifoveal region was significantly reduced in areas where the RPE was still present in donor 1.

Conclusions: The histopathology of the retina from an individual with a *VMD2* p.Asn296His mutation displayed a highly degenerated perifoveal retina. The retina in the individual with a p.Ile201Thr *VMD2* mutation displayed normal perifoveal morphology with preservation of cones and rods in the periphery. **Support:** The Foundation Fighting Blindness, Research to Prevent Blindness, Wolf Family Foundation, National Eye Institute, and Llura and Gordon Gund Foundation

Fundus & SLO Images of Donor Eyes

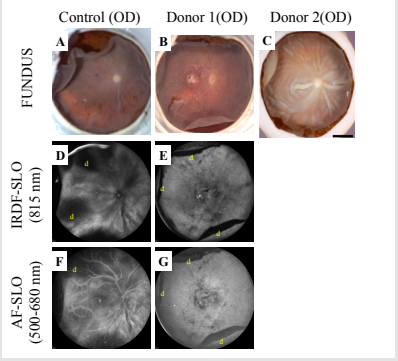

Figure 1. *Ex vivo* fundus imaging of donors and an age-similar control eye. Macroscopic fundus and SLO images were collected using an AxioCam MRC5 camera with video zoom lens (Zeiss) and a model HRA2 SLO (Heidelberg Engineering), respectively. All eyes showed areas of artifact (detached retina; d) due to fixation and processing. All imaging modalities indicated that the control eye (A, D, F) is free of retinal pathology. In contrast, all images from donor 1 (B,E,G) showed a macular lesion that was more noticeable by visible light fundus macroscopy (B) than either IRDF-SLO (E) or AF-SLO (G). AF-SLO (G) of donor 1 showed a bright, autofluorescent fundus which lacked typical detail (absence of a macula lutea) and appeared more homogeneous than the control eye (F). Donor 2 (C) was absent of any obvious retinal lesions but did have substantial fixation artifact (folds). No SLO or OCT images are available for donor 2. Scale bar - 2mm.

OCT Images of Donor Eyes

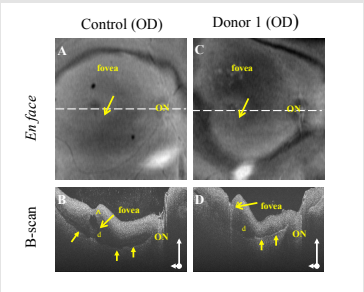

Figure 2. *Ex Vivo* OCT imaging of the donor (C,D) and an age-similar control eye (A,B). Spectral Domain-OCT images were collected using the Model SDOIS system (Bioptigen, Inc.) with ~7x7mm field of view. The control eyes had intact retinas that (1) were still adherent and congruent with the RPE-choroid complex and showed evidence of a photoreceptor layer (B - dark space above arrows). In contrast, the B-scan image from the donor eye (D) lacked a well-defined photoreceptor layer and exhibited a hyper-reflective RPE (arrows) compared to the control eye. Regions of minor retinal detachment (d) and elevated retina (^) were also observed due to fixation and processing. Dashed lines in *en face* image indicates B-scan location, optic nerve (ON), B-scan scale bar is 0.5mm.

Histology of Donor Eyes

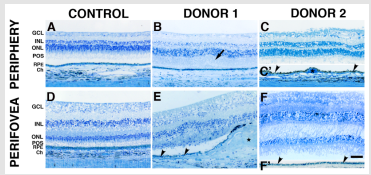

Figure 3. Degeneration in the retinas of donor eyes with *VMD2* mutations. Representative photomicrographs from toluidine blue stained plastic sections (1µm) of both the donor retinas and an age-similar control are shown for comparison. Morphology of control retina in the periphery (A) and perifovea (D) displayed typical characteristics including structural lamina consisting of retinal cells. In the periphery both donor 1 (B) and donor 2 (C) displayed a distinct ganglion cell layer (GCL), inner nuclear layer (INL), outer nuclear layer (ONL), RPE and choriocapillaris (CC). Donor 1 also displayed edema of the interphotoreceptor matrix (B, arrow). Both donor 1 and 2 displayed RPE thinning but donor 2 also displayed the presence of few drusen (C', asterisks) under the RPE in the periphery. In the perifoveal region of donor 1 prominent GCL and INL were evident. In addition, an extensive fibrovascular scar was present between Bruch's membrane and the retina (E, star); this area also displayed patchy thin RPE (arrowheads) with no photoreceptors. In contrast, the perifoveal region of donor 2 had distinct GCL, INL, ONL and robust thin RPE (F', arrowheads) and CC. GCL= ganglion cell layer; INL= inner nuclear layer; ONL= outer nuclear layer; POS= photoreceptor outer segments; RPE= retinal pigment epithelium. Bars =50µm.

Immunocytochemistry of Donor Eyes

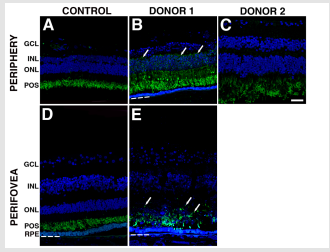

Figure 4. Significant decrease in rods in the perifovea of donor eyes with an Asn296His *VMD2* mutation. Representative photomicrographs of cryosections collected from the age-similar control and the donors. Sections are shown labeled with antibodies specific to rhodopsin (Alexa488, green) while cell nuclei were labeled with TO-PRO-3 (blue). In the control retina rhodopsin was restricted to the rods outer segment both in the periphery (A) and perifovea (D). In the periphery of the donor 1 (B) rhodopsin was also distributed throughout the whole photoreceptor cells (arrows). In the periphery of donor 2 (C) rhodopsin labeling was decreased but still restricted to the outer segments. In the perifovea of donor 1 (E) several very disorganized rhodopsin-labeled cells were detected opposed to the RPE cells and within the few photoreceptor nuclei still present (arrows). Bruch's membrane is indicated by hashed white line. GCL= ganglion cell layer; INL= inner nuclear layer; ONL= outer nuclear layer. Bar = 40µm.

Immunocytochemistry of Donor Eyes

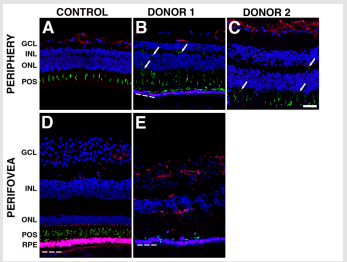

Figure 5. Significant decrease in cones in the perifovea of donor eyes with an Asn296His *VMD2* mutation. Representative photomicrographs of cryosections obtained from the donors and an age-similar control. Sections were labeled with antibodies specific to red/green cone opsin (Alexa488, green) and GFAP (Alexa594, red) while cell nuclei have been labeled with TO-PRO-3 (blue). In the control retina red/green cone opsin distribution was restricted to the cone outer segments both in the periphery (A) and perifovea (D). In the periphery of both donors 1 (B) and 2 (C) cells labeled with red/green cone opsin were present but red/green cone opsin was also distributed to the photoreceptor inner segments and synapses (B, C, arrows). In contrast, cells labeled with red/green cone opsin antibodies were mostly absent in the retina adjacent to the fibrovascular scar of donor 1 (E). The Muller cells had undergone reactive gliosis throughout the retina and their hypertrophic processes were GFAP positive in the periphery of donor 2 (C) and perifovea of donor 1 (E) when compared to the control retina (A, D). GCL= ganglion cell layer; INL= inner nuclear layer; ONL= outer nuclear layer. Bar = 40µm.

Immunocytochemistry of Donor Eyes

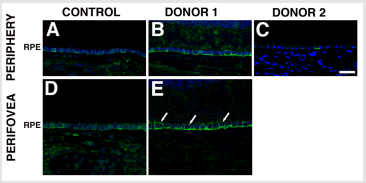

Figure 6. Changes in the distribution of monocarboxylate transporter 3 (MCT3) in the RPE of donor eyes with *VMD2* mutations. Representative photomicrographs of cryosections obtained from the donors and an age-similar control. Sections were labeled with antibodies specific to MCT3 (Alexa488, green) while cell nuclei have been labeled with TO-PRO-3 (blue). In the control retina MCT3 distribution was restricted to the basolateral domain of the RPE both in the periphery (A) and perifovea (D). In the periphery of donor 1 (B) MCT3 distribution was not altered while donor 2 displayed significant decrease in the expression of MCT3 in RPE cells (C). In contrast, in the perifovea of donor 1 (E) MCT3 was distributed in both the apical and basolateral membranes of RPE cells (arrows). Bar = 40µm.

The authors thank Dr. Nancy J. Philp, Thomas Jefferson Univ., Philadelphia, PA, for providing the MCT3 antibody.

Autofluoresence of Donor Eyes

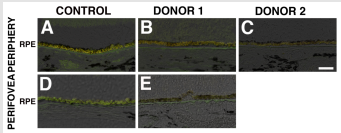

Figure 7. Significantly decreased autofluorescent material in the RPE of *VMD2* donor eyes. Representative epifluorescence photomicrographs of cryosections obtained from the donors and an age-similar control. Sections were observed using the green channel (FITC filter: excitation 490nm/ emission 519nm) and red (TRITC filter: excitation 550/emission 570nm). Autofluorescence was overlaid on differential interference contrast (DIC) images. Autofluorescent granules are present in the control RPE both in the periphery (A) and perifovea (D). In the periphery, the RPE from both donor 1 (B) and 2 (C) displayed significantly decreased autofluorescent granules when compared to the control RPE (A). In addition, RPE from the donor 1 (E) displayed significantly decreased autofluorescent granules in the perifovea when compared to the control RPE. Bar = 40µm.

Conclusions

The retina of Donor 1 (Asn29His *VMD2* mutation) showed:

- A macular lesion by Fundus/ SLO imaging
- Periphery: Edema of interphotoreceptor matrix, distinct GCL, INL, ONL, and RPE (with some thinning of RPE in places) and distinct choroid. Rod labeling was found throughout the complete cell. Cone labeling with red/green opsin was present.
- Perifovea: Fibrovascular scar between Bruch's membrane and the retina. This area had a thinned RPE and no photoreceptors. Prominent inner layers of retina were present. Labeled rod photoreceptors were disorganized with displaced expression persisting in rod nuclei. There was a significant decrease of cones labeled in the perifovea and cones were absent near the fibrovascular scar.

The retina of Donor 2 (Ile201Thr*VMD2* mutation) showed:

- No pathology by Fundus/SLO imaging.
- Periphery: Distinct GCL, INL, ONL, RPE and choroid. Drusen was observed in this eye. Rod labeling was restricted to the outer segment with reduction in the signal. Cone labeling with red/ green opsin was the same as in Donor 1.
- Perifovea: Prominent lamina, and thinned, yet robust, RPE and normal choroid. Labeled rod photoreceptors were disorganized with displaced expression persisting in rod nuclei. No cones evident.

NIH National Eye Institute

Foundation Fighting Blindness

Research to Prevent Blindness

RETINAL HISTOPATHOLOGY IN EYES FROM A PATIENT WITH DIGENIC USHER SYNDROME CAUSED BY MUTATIONS IN *USH2A* AND *GPR98*

Meghan J. Marino[1], Vera L. Bonilha[1], Mary E. Rayborn[1], Brent A. Bell[1], William J. Kimberling[2], Elias I. Traboulsi[1], Stephanie A. Hagstrom[1] and Joe G. Hollyfield[1]

Program #6331

[1]Cole Eye Institute, Department of Ophthalmology, CCLCM, Cleveland, OH; [2] Department of Ophthalmology and Visual Sciences, University of Iowa, Iowa City, IA

Cleveland Clinic

Abstract

Purpose: To define the histopathological features in donor eyes from a patient with Usher syndrome type 2 caused by mutations in *USH2A* and *GPR98*.

Methods: Eyes were obtained from a 60 year-old female and were fixed within 25 hours from death. Globes were evaluated with macroscopic, SLO and OCT imaging. Perifoveal and peripheral retina were processed for electron microscopy and immunocytochemistry using cell-specific antibodies. Three age- similar (61, 65, and 70 year old) normal eyes were used as controls. DNA was obtained from blood samples of the donor and analyzed using the OtoSCOPE® platform that includes 66 of the most common hearing loss genes. Segregation analysis was performed by testing this donor's affected son and unaffected daughter's samples for the two mutations identified in the donor.

Results: DNA analysis of the donor identified a heterozygous p.Gly2109Ser mutation in *USH2A* and a heterozygous p.Gln4989Stop mutation in *GPR98*. The donor's affected son also carried these two mutations. Her unaffected daughter did not carry either. AF-SLO was unable to delineate the macular lutea pigment and showed some mild degeneration around the optic disk. OCT showed areas around the fovea and optic disk with a thin photoreceptor layer. The peripheral retina was still intact, but lacked structural features (i.e. an ellipsoid band). In the periphery, histology showed distinct GCL and INL, but the ONL was reduced to 3-5 nuclear rows. In addition, several patchy areas of photoreceptor loss were noted. Prominent GCL and INL were present in the perifoveal retina, but the ONL retained only scattered nuclei. The RPE was thin but the choriocapillaris was present and robust. No cone opsin or cone arrestin labeled cells were observed in the macula, but a few highly disorganized cone-specific cells were present in the periphery. No rhodopsin-positive cells were observed in the macula, but were evident in the peripheral retina.

Conclusions: The histopathology of the retina in a patient with Usher syndrome due to digenic *USH2A* and *GPR98* mutations displayed a highly degenerated perifoveal retina with preservation of some peripheral cone and rod photoreceptors. To our knowledge, digenic Usher syndrome has not been previously described due to molecular interactions between the *USH2A* and *GPR98* genes.

Support: The Foundation Fighting Blindness, Research to Prevent Blindness, Wolf Family Foundation, National Eye Institute, and Llura and Gordon Gund Foundation

Pedigree

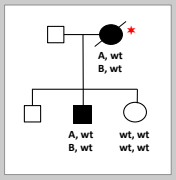

Legend

A: p.Gly2109Ser in *USH2A*
B: p.Gln4989Stop in *GPR98*
wt: wild type allele
*** : eye donor**

Figure 1: Pedigree of Eye Donor's Family. The affected eye donor and her affected son were both heterozygous for the *USH2A* and *GPR98* mutations.

Fundus & SLO Images of Donor Eyes

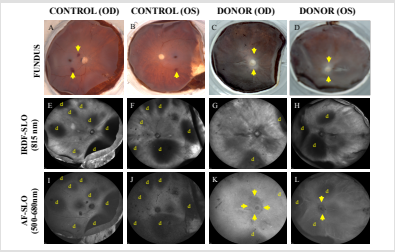

Figure 2: *Ex vivo* imaging of donor and age-similar control eyes. Macroscopic fundus and SLO images were collected using an AxioCam MRC5 camera and video zoom lens (Zeiss) and a model HRA2 SLO (Heidelberg Engineering), respectively. All eyes showed areas of artifact (detached retina; d) due to fixation and processing. All imaging modalities indicated that control eyes (A-B, E-F, I-J) are free of retinal pathology with exception of 3 small spots of hemorrhage (A, B-arrows). Macula lutea are present with AF-SLO in controls, indicating a normal retina (I,J). Images from the donor eyes are also relatively free of any profound pathological changes with the exception of atrophy surrounding the optic disk. Fundus (C,D) and AF-SLO (K,L) modes show hyper-reflective and hypofluorescent areas which indicate mild degeneration, respectively (arrows). Both donor eyes (OD-faint; OS-clearly still present) show a macula lutea ring around the fovea.

OCT Images of Donor Eyes

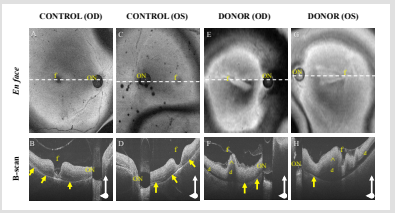

Figure 3: *Ex Vivo* imaging of the donor (E-H) and age-similar control eyes (A-D) using OCT. Spectral Domain-OCT images were collected using the Model SDOIS system (Bioptigen, Inc.) with ~7x7mm field of view. Control eyes had intact retinas that (1) were still congruent with the RPE-choroid complex, (2) contained normal appearing laminar morphology, and (3) showed evidence of a well-defined photoreceptor layer (B, D-dark space above arrows). In contrast, retinal images from donor eyes (F, H) lacked a well-defined photoreceptor layer, suggestive of degeneration, relative to controls (F, H – minimal dark space above arrows with exception of detachments). Regions of retinal detachment (d) and elevated retina (^) were also observed. These artifacts can likely be attributed to the tissue being in a compromised state (i.e. diseased) as well as from the post-mortem stresses of enucleation, fixation and processing. *En face* view has a 1mm ruby sphere over the optic nerve disk for scale calibration (ON), fovea (f), and dashed lines in *en face* images indicate B-scan location. B-scan scale bar is 0.5mm.

Histology of Donor Eyes

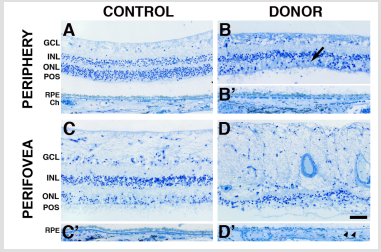

Figure 4: Degeneration in the retina of donor eyes with *USH2A* and *GPR98* mutations. Representative photomicrographs from toluidine blue stained plastic sections (1µm) of both the donor retinas and an age-similar control are shown for comparison. Morphology of the control retina in the periphery (A) and perifovea (C, C') displayed typical characteristics including structural lamina consisting of retinal cells. In the periphery, histology of the donor retina showed distinct GCL and INL, but the ONL was reduced to 3-5 nuclear rows. In addition, several patchy areas of photoreceptor loss were noted (B, arrow) and the RPE was thinner (B') than in the control. Prominent GCL and INL were present in the perifoveal retina, but the ONL retained only scattered nuclei (D). The RPE was thin and absent in some areas but the choriocapillaris was present and robust (D', arrowheads). GCL= ganglion cell layer; INL= inner nuclear layer; ONL= outer nuclear layer; POS= photoreceptor outer segments; RPE= retinal pigment epithelium. Bars =50µm.

Immunocytochemistry of Donor Eyes

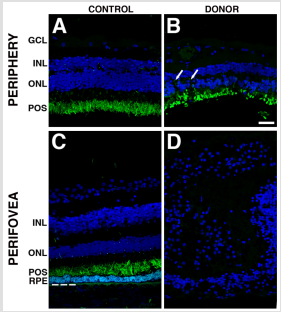

Figure 5: Significant decrease in rods in the perifovea of donor eyes with *USH2A* and *GPR98* mutations. Representative photomicrographs of cryosections collected from the age-similar control and the affected donor. Sections are shown labeled with antibodies specific to rhodopsin (Alexa488, green) while cell nuclei were labeled with TO-PRO-3 (blue). In the control retina, rhodopsin was restricted to the rod outer segments both in the periphery (A) and perifovea (C). In the periphery of the affected donor (B) rhodopsin was also distributed to the photoreceptor inner segments and synapses (arrows). No rhodopsin-labeled cells were detected in the perifovea (D). Bruch's membrane is indicated by a hashed white line. GCL= ganglion cell layer; INL= inner nuclear layer; ONL= outer nuclear layer; POS = photoreceptor outer segments. Bar = 40µm.

Immunocytochemistry of Donor Eyes

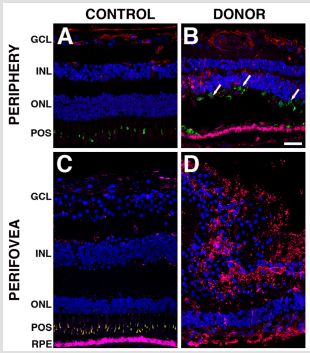

Figure 6: Significant reduction in the cones in the perifovea of donor eyes with *USH2A* and *GPR98* mutations. Representative photomicrographs of cryosections obtained from the donor and an age-similar control. Sections were labeled with antibodies specific to red/green cone opsin (Alexa488, green) and GFAP (Alexa594, red) while cell nuclei have been labeled with TO-PRO-3 (blue). In the control retina, red/green cone opsin distribution was restricted to the cone outer segments both in the periphery (A) and perifovea (C). Few cones were still present in the periphery of the donor retinas but red/green cone opsin was distributed to the photoreceptor inner segments (B, arrows). In contrast, no red/green opsin-labeled cells were present in the perifovea of the donor (D). The Muller cells had undergone reactive gliosis throughout the retina and their hypertrophic processes were GFAP positive in the periphery (B) and perifovea (D) of the affected donor when compared to the control retina (A, B). GCL= ganglion cell layer; INL= inner nuclear layer; ONL= outer nuclear layer; POS = photoreceptor outer segments. Bar = 40µm.

Conclusions

An eye donor affected with digenic Usher syndrome due to *USH2A* and *GPR98* mutations showed the following:

- Overall, a more severely degenerated perifoveal retina compared to the peripheral retina
- Atrophy around the optic disc
- Absence of a well-defined photoreceptor layer
- ONL degeneration with localized loss of photoreceptors in the periphery
- Total absence of rods in the perifovea
- Positive GFAP staining indicates the Muller cells had gone through gliosis in response to the retinal degenerative disease

NIH National Eye Institute

Supported by: Research to Prevent Blindness

Foundation Fighting Blindness

Program #6338

RETINAL HISTOPATHOLOGY IN EYES FROM A CARRIER OF XLRP WITH AN *RP2* MUTATION

Cleveland Clinic

Gayle J.T. Pauer[1], Vera L. Bonilha[1], Mary E. Rayborn[1], Brent A. Bell[1], Meghan J. Marino[1], John R. Heckenlively[2], Elias I. Traboulsi[1], Stephanie A. Hagstrom[1] and Joe G. Hollyfield[1]

[1]Cole Eye Institute, Department of Ophthalmology, CCLCM, Cleveland, OH; [2]Department of Ophthalmology and Visual Sciences, University of Michigan, Ann Arbor, MI.

Abstract

Purpose: To describe the histopathological features of donor eyes from a carrier of X-linked retinitis pigmentosa (XLRP) with an *RP2* mutation.

Methods: Eyes were obtained from a 90 year-old and fixed within 25 hours postmortem. Globes were evaluated with macroscopy, SLO and OCT imaging. Perifoveal and peripheral retina were processed for electron microscopy and immunocytochemistry using cell-specific antibodies. Three age-similar normal eyes were used as controls. Genetic testing was performed on the family using sequence analysis. The donor was reported to have a macular dystrophy late in life. Therefore, her DNA was also genotyped for the high risk AMD SNPs rs1061170 (*CFH),* rs10490924 *(ARMS2),* rs11200638 *(HTRA1),* and rs2230199 *(C3),* using TaqMan SNP genotyping assays.

Results: Genetic analysis identified a heterozygous 2 bp insertion in the *RP2* gene, c.77insCA. She was heterozygous at the *CFH* Y402H and *C3* R80G sites and homozygous for the non-risk alleles at the A69S *ARMS2* and promoter *HTRA1* sites. The fovea and optic nerve could be clearly identified by all imaging modalities. IR and red free-SLO identified hyper-reflective lesions adjacent to the macula and optic disk. OCT identified these lesions as retinal deposits, extending from the RPE to the OPL. Histology of the peripheral retina showed a distinct GCL, INL, and ONL. Patchy areas of photoreceptor loss associated with gliosis were noted in the retinal periphery. Prominent GCL and INL were present in the perifoveal retina in addition to gliosis associated with a fibrovascular scar. A serous detachment was present near the fovea, containing material stained with toluidine blue, except proximal to the RPE where blister-like projections were visible along the apical surface. Patchy, highly disorganized cells labeled with cone opsin and cone arrestin antibodies were present in the perifovea; however, cone-specific labeled cells appeared normal in the periphery. A few disorganized cells labeled with rhodopsin antibodies were detected in the perifovea but were more abundant and rod-shaped in the periphery.

Conclusions: The histopathological features identified in this donor, including the loss of photoreceptors in the peripheral retina, indicate the retinal degeneration is likely due to XLRP. Although the genetic screening suggests a low risk of developing AMD, the fibrovascular scar indicated a previous hemorrhage followed by fibrosis consistent with wet AMD.

Pedigree

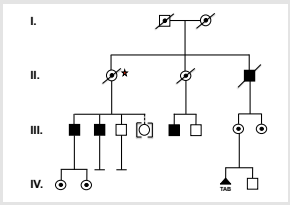

Figure 1. Pedigree of family with X-linked retinitis pigmentosa (XLRP) due to an *RP2* mutation. Genetic analysis of the family identified a heterozygous 2 bp insertion in the *RP2* gene, c.77insCA (Mears et al, 1999 AJHG 64:897-900).
★ = eye donor

Fundus & SLO Images of Donor Eye

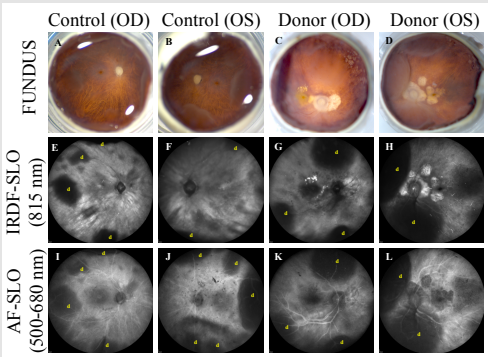

Figure 2. *Ex vivo* imaging of donor and age-similar control eyes. Macroscopic fundus and SLO images were collected using an AxioCam MRC5 camera and video zoom lens (Zeiss) and a model HRA2 SLO (Heidelberg Engineering), respectively. All eyes showed areas of artifact (detached retina; d) due to fixation and processing. All imaging modalities indicated that control eyes (A-B, E-F, I-J) are free of retinal pathology. In contrast, images from the donor eye identified atrophy (fundus and IR-SLO - white, hyporeflective areas; AF-SLO - dark hyporeflective areas) in multiple regions including the macula, perimacula and areas surrounding the optic nerve. Imaging with different modalities provided additional information in regards to the retinal pathology as both pronounced and subtle differences between the right and left eyes could be observed between fundus and SLO. Postmortem imaging using these three modalities revealed that the pathology observed by fundus imaging is not identical in both eyes. This may suggest different states of disease progression in various locations of the retina, or in right vs. left eye of the donor.

OCT Images of Donor Eye

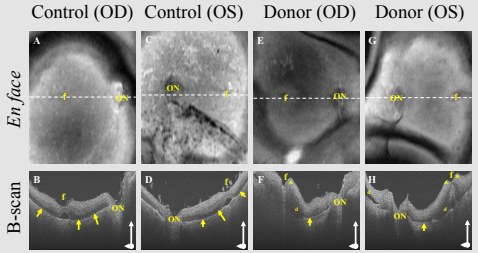

Figure 3. *Ex Vivo* imaging of the donor (E-H) and age-similar control eyes (A-D) using OCT. Spectral Domain-OCT images were collected using the Model SDOIS system (Bioptigen, Inc.) with ~7x7 mm field of view. Control eyes had intact retinas that (1) were still adherent and congruent with the RPE-choroid complex, (2) contained normal appearing laminar morphology, and (3) showed evidence of a well-defined photoreceptor layer (B, D - dark space above arrows). In contrast, retinal images from donor eyes (F, H) lacked a well-defined photoreceptor layer relative to controls (F, H – minimal dark space above arrows). Regions of retinal detachment (d) and elevated retina (^) were also observed. Dashed lines in *En face* image indicates B-scan location; fovea (f), optic nerve (ON), B-scan scale bar is 0.5mm.

Histology of Donor Eye

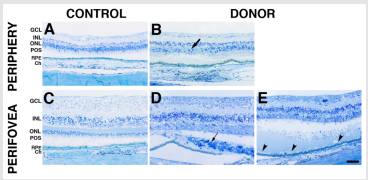

Figure 4. Degeneration in the retina of donor eyes with an *RP2* mutation. Representative photomicrographs from toluidine blue stained plastic sections (1µm) of both the donor retinas and an age-similar control are shown for comparison. Morphology of control retina in the periphery (A) and perifovea (C) displayed typical characteristics including structural lamina consisting of retinal cells. Histology of the donor retina revealed a distinct GCL, INL, and ONL. Patchy areas of photoreceptor loss associated with gliosis (B, thick arrow) were also noted in this region. Prominent GCL and INL were present in the perifoveal retina of the donor in addition to gliosis associated with a fibrovascular scar (D, thin arrow). A serous detachment was present near the fovea, containing material stained with toluidine blue, except proximal to the RPE where blister-like projections were visible along the apical surface (E, arrowheads). GCL = ganglion cell layer; INL = inner nuclear layer; ONL = outer nuclear layer; POS = photoreceptor outer segments; RPE = retinal pigment epithelium; Ch = choroid. Bars =50µm.

Immunocytochemistry of Donor Eye

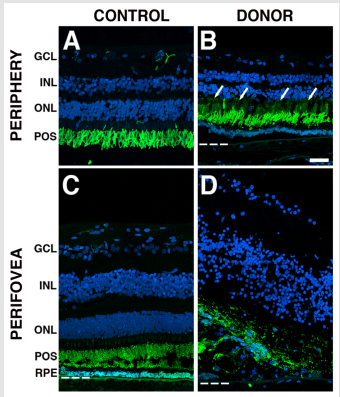

Figure 5. Significant decrease in rods in the perifovea of donor eyes with an *RP2* mutation. Representative photomicrographs of cryosections collected from the age-similar control and the donor. Sections are shown labeled with antibodies specific to rhodopsin (Alexa488, green) while cell nuclei were labeled with TO-PRO-3 (blue). In the control retina rhodopsin was restricted to the rod outer segments both in the periphery (A) and perifovea (C). In the periphery of the donor (B) rhodopsin was also distributed to the photoreceptor inner segments (arrows). In the perifovea several very disorganized rhodopsin-labeled cells were detected in the edge of the serous detachment present near the fovea (D). Bruch's membrane is indicated by hashed white line. GCL = ganglion cell layer; INL = inner nuclear layer; ONL = outer nuclear layer; POS = photoreceptor outer segments; RPE = retinal pigment epithelium . Bar = 40µm.

Immunocytochemistry of Donor Eye

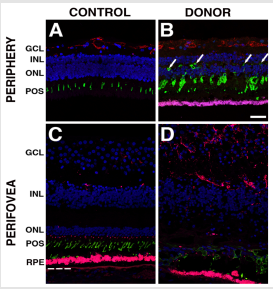

Figure 6. Significant reduction in the cones in the perifovea of donor eyes with an *RP2* mutation. Representative photomicrographs of cryosections obtained from the donor and an age-similar control. Sections were labeled with antibodies specific to red/green cone opsin (Alexa488, green) and GFAP (Alexa594, red) while cell nuclei have been labeled with TO-PRO-3 (blue). In the control retina, red/green cone opsin distribution was restricted to the cone outer segments both in the periphery (A) and perifovea (C). Cones were still present in the periphery of the donor retinas but red/green cone opsin was distributed along the entire plasma membrane of this cone type (B, arrows). In contrast, few highly disorganized red/green opsin-labeled cells were present in the edge of the serous detachment near the fovea (D). The Muller cells had undergone reactive gliosis throughout the retina and their hypertrophic processes were GFAP positive in the perifovea (D) of the donor but not in the control retina (A, C). Bruch's membrane is indicated by hashed white line. GCL = ganglion cell layer; INL = inner nuclear layer; ONL = outer nuclear layer; POS = photoreceptor outer segments; RPE = retinal pigment epithelium. Bar = 40µm.

Conclusions

A Carrier of XLRP with an *RP2* mutation showed:

- Atrophy in the macula, perimacula and area surrounding the optic nerve
- Imaging of both eyes was not identical; this may be due to X-inactivation
- Lack of a well defined photoreceptor layer
- Patchy photoreceptor loss associated with gliosis
- A fibrovascular scar associated with gliosis
- Serous detachment near the fovea
- Rhodopsin-labeled inner segments in the periphery
- Red/green cone opsin distributed along the entire plasma membrane
- Muller cells have undergone reactive gliosis throughout the retina

NIH National Eye Institute

Supported by Research to Prevent Blindness

Foundation Fighting Blindness

Program No. 2402
Board #C0052

RETINAL HISTOPATHOLOGY IN EYES FROM A PATIENT WITH CONE DYSTROPHY

Meghan J. Marino[1], Vera L. Bonilha[1], Mary E. Rayborn[1], Brent A. Bell[1], Elias I. Traboulsi[1], Stephanie A. Hagstrom[1], and Joe G. Hollyfield[1]

[1]Cole Eye Institute, Department of Ophthalmology, Cleveland Clinic Lerner College of Medicine, Cleveland, OH

NIH National Eye Institute
SUPPORTED BY RPB Research to Prevent Blindness
Cleveland Clinic Cole Eye Institute
FOUNDATION FIGHTING BLINDNESS

Abstract

Purpose: To define the retinal histopathology in donor eyes from a patient with a cone dystrophy of unknown genetic origin.
Methods: Eyes were from a 54 year-old female, fixed within 13 hours postmortem. Globes were evaluated with macroscopic, SLO and OCT imaging. Perifoveal and peripheral regions were processed for electron microscopy and immunocytochemistry using cell-specific antibodies. Two age-matched normal eyes were used as controls. DNA was obtained from blood samples of the donor and analyzed for 26 cone dystrophy genes by next generation sequencing.
Results: Fundus macroscopy and SLO showed an abnormal ring encompassing the macula and centered on the fovea. OCT showed retinal thinning in this region. Histology confirmed the presence of this lesion, which measured ~5.5mm in diameter. There was an abrupt transition at the periphery of the lesion. Outside the lesion several rows of nuclei were present in the ONL, but within the lesion, only occasional patches of stubby cones projected from the outer limiting membrane.Immunocytochemistry revealed patches of cone arrestin labeled cells in the lesion but this labeling was reduced in the periphery. Co-labeling with cone opsin antibodies was not observed in these cells. Rhodopsin-positive cells were rarely observed in the central lesion, but were prominent throughout the rest of the retina. DNA analysis failed to identify a mutation in any of the genes analyzed (*ABCA4, ADAM9, AIPL1, BEST1, c8ORF37, CACNA1F, CACNA2D4, CDHR1, CERKL, CNGB3, CNNM4, CRX, GUCA1A, GUCY2D, KCNV2, PDE6C, PDE6H, PITPNM3, PROM1, PRPH2/RDS, RAX2, RDH5, RIMS1, RPGRIP1, SEMA4A,* and *UNC119*). Molecular analysis of additional retinal dystrophy genes is currently pending.
Conclusions: The histopathology of the retina in a patient with a cone dystrophy of unknown genetic etiology displayed a central lesion characterized by degenerated cones and the absence of rod photoreceptors.

OCT Images of Donor Eyes

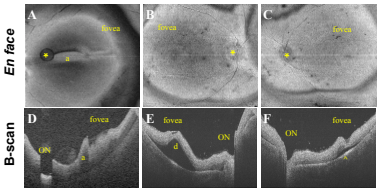

Figure 2. ***Ex Vivo*** **OCT imaging of the donor (B,C,E, F) and an age-similar control eye (A,D).** The control eye (A, D) had an intact retina that (1) was still adherent and congruent with the RPE-choroid complex, (2) showed evidence of a photoreceptor layer (D - dark space above arrows), and (3) showed a fixation artifact due to ON-fovea traction from tissue shrinking/swelling (A, D – lowercase "a"). Asterisk indicates the location of a 1mm ruby sphere positioned over the ON as a scale reference (A). In contrast, the B-scan images from the donor (E-F) showed a thinned retina and lacked a well-defined photoreceptor layer compared to the control eye. Regions of retinal detachment (d) and elevated retina (^) were also observed as a result of fixation and processing. Broken lines in *en face* image indicates B-scan location, optic nerve (ON), B-scan scale bar is 0.5mm (F).

Immunohistochemistry of Donor Eyes

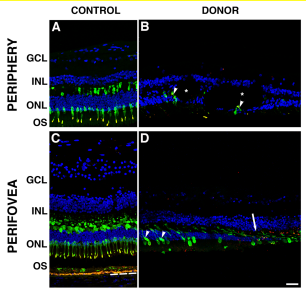

Figure 4. Significant decrease in rods in the perifovea of donor eyes with a cone dystrophy of unknown genetic origin. Sections are labeled with antibodies specific to rhodopsin (Alexa488, green). Nuclei are labeled with TO-PRO-3 (blue). In control retina, rhodopsin is restricted to the rods outer segment in both periphery (A) and perifovea (C). In the periphery of the donor retina (B), rhodopsin is distributed through the whole photoreceptor cells body, with the exception of the cystoid-like spaces (*). In the perifovea rhodopsin labeling is absent from the area where the ONL was reduced to one row of nuclei (arrow) but is prominent in the retina outside this central lesion, where it is also distributed through the whole cell body. Bruch's membrane is indicated by hashed white line. Bar = 40μm.

Immunohistochemistry of Donor Eyes

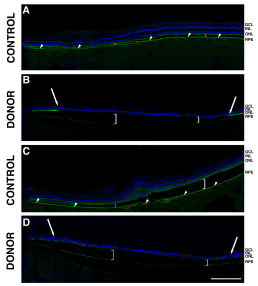

Figure 6. Significant decrease in photoreceptors in the foveal lesion: Sections are labeled with antibodies specific to rhodopsin (A, B, Alexa488, green), to cone opsin (C, D, Alexa488, green) and cell nuclei are labeled with TO-PRO-3 (blue). In the control perifovea rhodopsin is regularly distributed to the rods outer segment (A). In the donor (B) rhodopsin is absent from area in the perifovea (arrows). The control perifovea displays high density of cone opsin-labeled cells (C). The donor perifovea shows significant reduction in cone opsin labeling in the perifovea (arrows). The RPE in the control retina displays increased autofluorescence (arrowheads). In both samples the retina is detached from the RPE (brackets). Bar = 1mm.

Immunohistochemistry of Donor Eyes

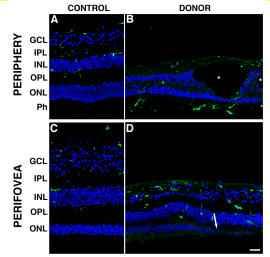

Figure 8. Significant increase in the presence of reactive Muller cells. Sections are labeled with antibodies to Calbindin (Alexa488, green) and GFAP (Alexa594, red) and cell nuclei are labeled with TO-PRO-3 (blue). In the control retina Calbindin labeling is present in the amacrine, bipolar and cones both in the periphery (A) and in the perifovea (C). In the periphery of the donor retina Calbindin-positive cells are concentrated in the OPL (B). In the perifovea of the donor (D) Calbindin labeling showed several disorganized stubby cones (arrow). In the retina peripheral to this central lesion, cones with synaptic terminals are labeled by Calbindin. Calbindin-positive cells are also abnormally present in the ONL. The Muller cells have undergone some reactive gliosis in the GCL of control retina in both periphery (A) and perifovea (C). In the periphery of the donor (B) GFAP-positive labeling is observed throughout the retina, including the inside edges of the of the cystoid-like spaces (*). In the perifovea of the donor, GFAP reactivity is increased in the OPL in the area where the ONL is reduced to one row of nuclei (D, arrow). Bar = 40μm.

Fundus & SLO Images of Donor Eyes

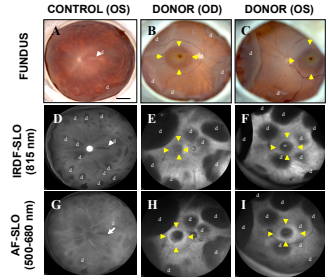

Figure 1. ***Ex vivo*** **fundus and SLO imaging of donors and an age-similar control eye.** All eyes showed a fixation/processing artifact (detached retina; d). The control eye had a fixation-induced detachment due to traction between the optic nerve and fovea (D, G; d+arrow). The control eye (A, D, G) was free of retinal pathology but a macula lutea, typically observed in normal eyes, was noticeably absent (G). Both donor eyes showed biannular features (yellow arrows) involving the macula and perimacular regions that bore some resemblance to a bull's eye maculopathy. These binannular rings were easily noticeable by visible light fundus macroscopy (B-C) and AF-SLO (H-I), but not by IRDF-SLO (E-F), where it appeared more as a single, isolated annulus. The ring observed by IR-SLO in the donor's left eye (OS) was more prominent than in the right eye (OD). In contrast, OD and OS observations using fundus and AF-SLO were similar showing a dual annulus containing both hypo- and hyper-reflectance/autofluorescence regions, respectively.

Histology of Donor Eyes

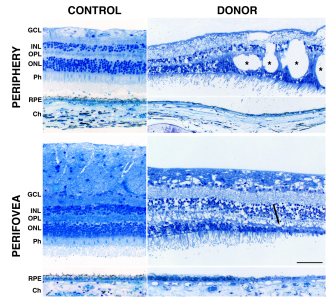

Figure 3. Representative photomicrographs from toluidine blue stained plastic sections (1μm). Structure of control retina in periphery (A) and perifovea (C) display normal retinal lamination. Histology of the donor retina show a distinct GCL, INL, and ONL in the periphery (B). Moreover, the periphery is characterized by the presence of cystoid degeneration with vacuole-like spaces (*) in the inner and outer plexiform layer. The RPE is reduced in thickness. In the perifovea (D) distinct GCL and INL are present; however, the ONL is reduced to one row of nuclei at the edges of the foveal lesion (arrow). Patches of stubby cone inner segments protrude from the outer limiting membrane (arrowheads). Bars = 50μm.

Immunohistochemistry of Donor Eyes

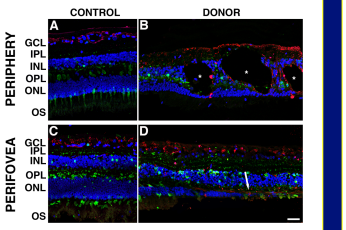

Figure 5. Significant reduction in cones: Photomicrographs of retinal cryosections from donor and control eyes. Sections are labeled with antibodies specific to cone arrestin (Alexa488, green) and red/green cone opsin (Alexa594, red) with cell nuclei labeled with TO-PRO-3 (blue). In control retina red/green cone opsin distribution is restricted to the cone outer segments both in the periphery (A) and perifovea (C). Synaptic terminals are visible in control sample in both areas. Cones are still present in the periphery of the donor retinas (B) and red/green cone opsin is distributed along the entire plasma membrane of this cone type (arrowheads). In the perifovea, several disorganized stubby cones not expressing red/green opsin are present in the area where the ONL is reduced to one row of nuclei (D, arrow). In the retina beyond this central lesion, cones with synaptic terminals are visible and red/green cone opsin is distributed along the entire plasma membrane of this cone type (arrowheads). Bruch's membrane is indicated by hashed white line. Bar = 40μm.

Immunohistochemistry of Donor Eyes

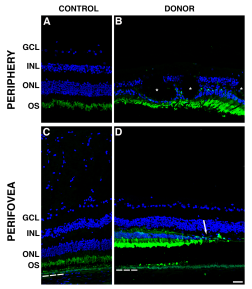

Figure 7. Enhanced expression of Iba-1 (marker for microglia): Photomicrographs of retinal cryosections obtained from donor and control. Sections are labeled with antibodies specific to Iba-1 (Alexa488, green) and cell nuclei are labeled with TO-PRO-3 (blue). In the control retina, stained cells with highly branched processes are observed mostly in the GCL IPL, INL and OPL both in the periphery (A) and perifovea (C). However, in the periphery of the donor retina (B) the shape of Iba-1 labeled cells is shrunken and irregular. A significant increase in Iba-1 labeled cells is observed in the photoreceptor layer. In the perifovea of the donor retinas (C) the shape of Iba-1 labeled cells is shrunken and irregular. Shrunken and irregular Iba-1 positive cells are also visible in the perifovea (D, arrow). (*) cyst-like spaces in the periphery; Bar = 40μm.

Clinical Summary of Donor

Last Eye Exam at age 54 years (data extracted from redacted medical records):

- **Visual Acuity:** 20/50 OD and 20/40 OS **IOP:** 17 OD and 19 OS
- **Anterior Segment:** normal OU
- **Dilated Fundus Exam:**
  - **Nerve** – no disc pallor or edema OU
  - **Vitreous** – clear OU
  - **Retinal vessels** – normal OU
  - **Macula** – no hemorrhage or subretinal fluid. Significant for Bull's eye RPE changes OU
  - **Periphery** – no holes or tears
- **Fluorescein Angiography Findings OU** – normal AV transit and choroidal filling. Late leakage consistent with NVD. Transmission defects consistent with RPE changes
- **Medical History** – hypertension and acid reflux, otherwise noncontributory
- **Family History** – AMD (cone dystrophy) in sister and brother .

Conclusions

- **The post-mortem analysis in this donor's retinas supports the clinical diagnosis of cone dystrophy.**
- **The retinas had a central lesion characterized by degenerated cones and an absence of rod photoreceptors. This correlated to the medical record description of Bull's eye RPE changes in the macula.**
- **The underlying genetic etiology in this patient remains unknown. There were no detectable mutations in 26 cone/cone-rod dystrophy associated genes – suggesting the possible involvement of a novel cone dystrophy gene or a mutation(s) in a gene described as causing a rod-dystrophy that is causing a unique phenotype.**

Abbreviations: GCL= ganglion cell layer; INL= inner nuclear layer; IPL = inner plexiform layer; OPL= outer plexiform layer; ONL= outer nuclear layer; Ph= photoreceptors; RPE= retinal pigment epithelium; Ch= choroid; OS= photoreceptor outer segments.

RETINAL ANALYSIS OF A FEMALE SYMPTOMATIC CARRIER OF CHOROIDEREMIA.

M.Rayborn[1], V.L. Bonilha[1], Y. Li[1], J.G.Hollyfield[1], P.J. Francis[2], K.M. Trzupek[2], and R.G. Weleber[2].

1-Cole Eye Institute, Cleveland Clinic, Cleveland, OH, 2- Casey Eye Institute, Oregon Health and Science University, Portland, OR.

Abstract

Purpose: To define the morphology and distribution of photoreceptor markers in a donor eye from a female symptomatic carrier of choroideremia with an X linked choroideremia. This donor was a member of a family in which multiple female carriers have macular dysfunction. **Methods:** A multi-generation family with X-linked choroideremia was evaluated over two decades with dilated fundus examination, photography, visual field testing and electroretinography. A family history was obtained, and molecular testing was performed. The donor died at age 91 and eyes were fixed in 4% paraformaldehyde and 0.5% glutaraldehyde in phosphate buffer. Paraffin tissue sections from 3 different areas of the eye were studied by indirect immunofluorescence, using well-characterized monoclonal antibodies to the cone and rod specific markers. Also, representative samples were processed for electron microscopy analysis. **Results:** At age 77, fundus examination revealed a reticular pigmentary retinopathy throughout the mid and far periphery; the ERG was normal. Within 10 years, she developed night blindness and significant central vision impairment. Molecular testing in the family revealed the heterozygous splice site mutation 1413+1 G>A in CHM. Postmortem morphological analysis of the donor revealed RPE thinning and pigment clumping typical for choroideremia, as well as photoreceptor degeneration in some areas and basal laminar deposits. In addition, a great number of drusen was observed in the donor's fovea. Labeling of the sections with the cone cytoplasmic marker revealed no differences when compared to the control eye. However, labeling with cone opsin antibodies revealed that cones were drastically affected. Blue opsin was almost completely absent in the affected retina. Moreover, red/green opsins were distributed along the entire plasma membrane of cones with this pigment type in all observed areas. Also, rhodopsin was also distributed along the entire rod plasma membrane in all the observed areas. **Conclusions:** Morphological changes typical of choroideremia were observed in the RPE and photoreceptors of the carrier donor. However, the histological data obtained suggests that the clinical manifestation of this donor seems to be related to abnormal distribution of both cone opsins and rhodopsin.

Supported in part by NIH grant EY015638, a Research Center Grant from The Foundation Fighting Blindness and Research to Prevent Blindness.

Introduction

Choroideremia is a rare X-linked recessive retinal degeneration characterized by progressive atrophy of the photoreceptors, the RPE, and choroid in affected men, resulting in severe loss of vision. Typically, females carries are mosaics due to lyonization (random inactivation of one X chromosome in each cell early in fetal development) (Lyon., 1961).

Choroideremia is caused by mutations in the REP-1 gene that encodes component A of Rab geranylgeranyl-transferase, referred to as Rab escort protein (REP-1) (Seabra et al., 1993; Seabra et al., 1995; van den Hurk et al., 1997). However, it is not known how the mutation in this protein leads to the degeneration of the choroid, RPE and retina.

Female carriers usually show fundus changes, including patchy depigmentation of the RPE and coarse pigmentary granularity in the periphery, but can retain good visual function throughout life.The severity of retinal disease in carriers is variable and depends on the proportion of cells expressing the mutant X chromosome. Female carriers are generally unaffected, although affected females have been described in the literature.

Male patients with choroideremia show complete loss of the choroid and of all the outer retina, displaying a thin line of atrophic inner retina lying against the sclera (Ghosh and McCulloch, 1980; Cameron et al., 1987; Rodrigues et al., 1984). The complete atrophy of the retina and choroid in male patients precludes identification of the primary defect in these structures. However, the milder changes in female patients allow an understanding of the mechanisms involved in this pathological process. In the present study we analyzed the morphology and distribution of photoreceptor markers in a donor eye from a female symptomatic carrier of X linked choroideremia.

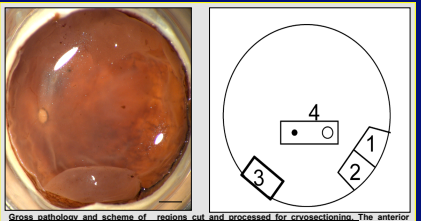

Gross pathology and scheme of regions cut and processed for cryosectioning. The anterior segment has been removed and the retina is viewed *en face*. Bar = 0.5cm.

Figure 1

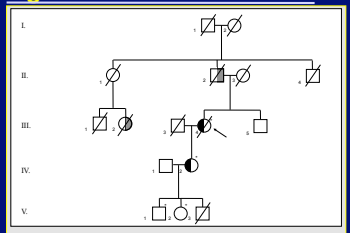

Pedigree of a family with an X-linked choroideremia showing the symptomatic carrier member (III.4) on whom the postmortem analysis was performed.
* Molecularly confirmed to carry 1413+1 G>A in *CHM*
II-2: By report, totally blind by early 50's
III-2: By report, legally blind in adulthood
III-4: Propositus. Night blindness & central vision loss late in life (>75yo)
IV-2: Night blindness & significant central vision loss in 50's. Abnormal rod & cone responses on ERG
V-1: Salt and pepper retinopathy; asymptomatic at 34 years old
V-2: Mottling of inferior RPE; asymptomatic at 33 years old

Figure 2

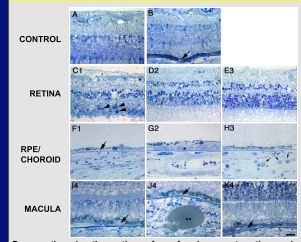

Degeneration in the retina of a female symptomatic carrier of choroideremia. Human 1µm plastic sections of both a matched control and an affected choroideremia stained with toluidine blue. (A, B) Morphology of control retina in the periphery (A) and macular region of the eye (B). (C1, D2, E3) The retina of the affected donor displayed different degrees of photoreceptor degeneration in each of the regions observed. In C1 some pigmented cells are seen invading the degenerating retina (arrowheads). (F1, G2, H3). RPE of the affected donor displayed typical thinning,pigment clumping, basal laminar deposits. In G2 extensive accumulation of amorphos material underneath the RPE layer is observed (*) while in H3 the presence of inflammatory cells (small arrows) is observed in the choroid. (I4, J4, K4) Different areas of the affected donor displaying deposition of drusen under the RPE (large arrows), RPE thinning and pigment clumping, photoreceptor degeneration and the presence of giant lipophilic drops in the choroid (**). Bar= 200µm.

Figure 3

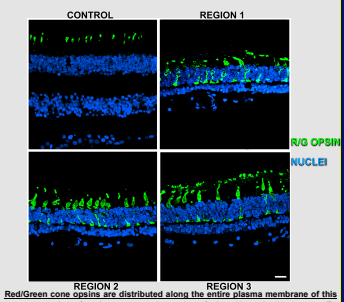

Red/Green cone opsins are distributed along the entire plasma membrane of this cone type in a female symptomatic carrier of choroideremia. Human paraffin sections of both a matched control and affected choroideremia donor were labeled with antibodies specific to red/green cone opsins (Alexa488, green) while cell nuclei were labeled with TO-PRO-3 (blue). Sections were analyzed using a Leica laser scanning confocal microscope (TCS-SP2, Leica, Exton, PA). A series of 1 µm xy (en face) sections were collected. Each individual xy image of the retinas stained represents a three-dimensional projection of the entire section (sum of all images in the stack). Microscopic panels were composed using AdobePhotoshop 5.5. Comparison of the samples showed that red/green cone opsins are distributed along the entire plasma membrane of this cone type, from the tip of the outer segment to the synaptic base in all the observed regions of the affected eye. Bar = 40µm.

Summary

- Histopathological analysis of the choroideremia affected retina revealed the presence of different degrees of degeneration in the several areas analyzed:
  - The retina displayed areas of severe degeneration, with no photoreceptor outer segments, photoreceptors nuclei atrophy, and atrophy of the inner retina. On the other hand, other areas displayed close to normal retina.
  - The RPE displayed severe atrophy, thinning, pigment clumping and sub-epithelial debris deposition in all the areas observed.
  - The choroid displayed light signs of degeneration.
- Labeling of the affected retina with a cone cytoplasmic marker did not reveal any significant cell body difference from the control sample (data not shown).
- Red/green opsins are distributed along the entire plasma membrane of this cone type, from the tip of the outer segment to the synaptic base.
- Blue opsin expression is almost completely absent from the affected retina. Very few cones could be observed still expressing blue opsin in all the 3 different areas analyzed; in these cone cells blue opsin was detected both in their inner and outer segments.
- Rhodopsin was also found to be distributed along the entire plasma membrane of the rods, from the tip of the outer segment to the synaptic base.
- Ultrastructural analysis of the affected macula revealed the absence of RPE apical microvilli and basal infoldings. Instead, RPE's basal surface and choroid displayed the presence of banded fibers composed of clumps of wide-spacing collagen. Bruch's membrane was filled with vesicular structures, some smooth and others like bristle-coated vesicles.

Figure 4

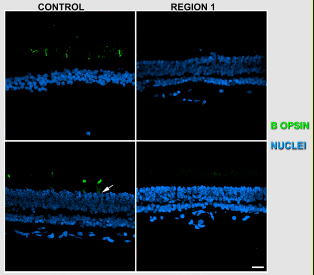

Blue cone opsins are significantly decreased in this cone type in a female symptomatic carrier of choroideremia. Human paraffin sections of both a matched control and affected choroideremia donor were labeled with antibodies specific to blue cone opsins (Alexa488, green) while cell nuclei were labeled with TO-PRO-3 (blue). Sections were analyzed using a Leica laser scanning confocal microscope (TCS-SP2, Leica, Exton, PA). A series of 1 µm xy (en face) sections were collected. Each individual xy image of the retinas stained represents a three-dimensional projection of the entire section (sum of all images in the stack). Microscopic panels were composed using AdobePhotoshop 5.5. Comparison of the samples showed that blue cone opsins are significantly decreased in all the observed regions of the affected eye. Region 2 display a few cones that still express blue opsin but it is distributed throughout the inner and outer segments of the cones (arrow). Bar = 40µm.

Figure 5

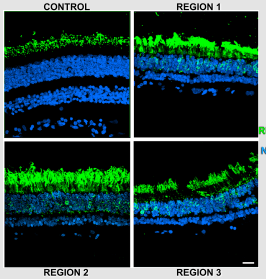

Rhodopsin is distributed along the entire plasma membrane of the rods in a female symptomatic carrier of choroideremia. Human paraffin sections of both a matched control and affected choroideremia donor were labeled with antibodies specific to rhodopsin (Alexa488, green) while cell nuclei were labeled with TO-PRO-3 (blue). Sections were analyzed using a Leica laser scanning confocal microscope (TCS-SP2, Leica, Exton, PA). A series of 1 µm xy (en face) sections were collected. Each individual xy image of the retinas stained represents a three-dimensional projection of the entire section (sum of all images in the stack). Microscopic panels were composed using AdobePhotoshop 5.5. Comparison of the samples showed that rhodopsin is distributed along the entire plasma membrane of rods, from the tip of the outer segment to the synaptic base in all the observed regions of the affected eye. Bar = 40µm.

Figure 6

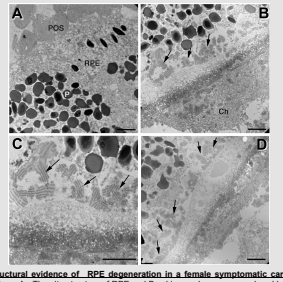

Ultrastructural evidence of RPE degeneration in a female symptomatic carrier of choroideremia. The ultrastructure of RPE and Bruch's membrane was analyzed by TEM. Observation at low magnification showed photoreceptor outer segments (POS) lying on top of a collapsed RPE apical surface. Moreover, the cytoplasm is filled with small vacuoles and pigments (P) (A). Observation of RPE's basal surface revealed absence of basal infoldings and the presence of banded fibers composed of clumps of wide-spacing collagen (arrows, B, C, D). The choroid (Ch), Bruch's membrane and the space between the RPE basal membrane was filled with vesicular structures, some smooth and others like bristle-coated vesicles (B, C). Higher magnification of this area is shown in C. Beneath drusen Bruch's membrane contains residual bodies, vesicular material and filaments (D). Electron micrographs were taken on a Tecnai 20, 200 kv digital electron microscope using a Gatan image filter. Panels were composed using AdobePhotoshop 5.5. Bars: A, B, D = 2µm and C = 1µm.

References

- Cameron, J.G., Fine, B.S. and Shapiro, I. (1987) Ophthalmol, 94: 187-96.
- Ghosh, M. and McCulloch, J.C. (1980) Can J Ophthalmol, 15: 147-53.
- Lyon., 1961
-Seabra, M.C., Brown, M.S., Goldstein, J.L. (1993;) Science, 259: 377-81.
-Seabra, M.C., Ho, Y.K., and Anant, J.S. (1995) J Biol Chem, 270: 24420-7.
-Rodrigues, M.M., Ballintine, E.S., Wiggert, B.N., (1984) Ophthalmol, 91: 873-883.
-van den Hurk, J.A.J.M., Schwartz, M., van Bokhoven, H., (1997) Human Mutation, 9: 110-7.

ACKNOWLEDGMENTS

We thank Dr. Peter MacLeish (Morehouse School of Medicine, Atlanta, GA) for providing us with the antibody to cone cytoplasmic marker (7G6), Dr. R. Molday (University of British Columbia, Vancouver, Canada) for providing us with the antibody to rhodopsin (B630N).

SUPPORTED BY
Research to Prevent Blindness
Foundation Fighting Blindness

Program # 6444

RETINAL HISTOPATHOLOGY FROM A PATIENT WITH AUTOSOMAL RECESSIVE RETINITIS PIGMENTOSA CAUSED BY *EYS* MUTATIONS.

M. J. Marino[1], V. L. Bonilha[1], M. E. Rayborn[1], B. A. Bell[1], G. J. Pauer[1], C. D. Beight[1], J. Chiang[2], E. I. Traboulsi[1], S. A. Hagstrom[1], and J. G. Hollyfield[1].

1- The Cole Eye Institute, Cleveland Clinic Lerner College of Medicine, Cleveland, OH; 2- Casey Eye Institute Molecular Lab, Portland, OR.

Cleveland Clinic

Supported by Research to Prevent Blindness

Foundation Fighting Blindness

Abstract

Purpose: To evaluate the histopathology in donor eyes from a patient with autosomal recessive retinitis pigmentosa (arRP) caused by *EYS* mutations.

Methods: Eyes were obtained from a 72 year-old female who died from pancreatic cancer. Eyes were fixed in 4% paraformaldehyde and 0.5% glutaraldehyde in PBS within 6 hours postmortem. Globes were evaluated with macroscopic, SLO and OCT imaging. Macula and peripheral regions were processed for electron microscopy and immunocytochemistry. An age-matched normal eye and the eye donated by donor's asymptomatic mother were used as controls. DNA was obtained from blood samples of the donor, her affected brother and sister, and two unaffected sisters. Direct genomic sequencing of the 19 arRP genes was performed.

Results: DNA analysis of the affected brother revealed the novel *EYS* gene mutations, IVS11+1G>A and Q874X. Imaging revealed peripheral bone spicules and RPE atrophy immediately surrounding the optic nerve and macula. SLO showed demarcated, circular patches of hypofluorescence in the perimacula region of both eyes, suggesting focal loss of RPE as choroidal vasculature could be visualized. Histology revealed a highly degenerate retina with little evidence of stratified nuclear layers in all peripheral areas studied. In contrast, the macula and perimacula region contained well organized ganglion cell and inner nuclear layer with only a few nuclei remaining in the outer nuclear layer. The RPE was thin in the macula and absent in the far periphery. An amorphous material was present between the degenerate retina and the RPE in the macula. Rhodopsin labeled rods were absent except in the far periphery. Cones labeled with opsin and arrestin antibodies were present in the macula, but were mostly absent from the periphery. Cone synapses and outer segments were not observed. Calbindin D labeled second order neurons were unevenly distributed in the periphery.

Conclusions: Advanced retinal degenerative changes with near-total absence of rods and preservation of macular cones characterize the retinal histopathology of and arRP patient due to *EYS* mutations.

Introduction

Mutations in 34 different genes cause autosomal recessive RP (https://sph.uth.tmc.edu/retnet/). Together these account for approximately 50% of the arRP cases. Recently, the *eyes shut homolog (EYS)* gene was identified at the RP25 locus (Abd et al., 2008; Collin et al., 2008). Mutations in the *EYS* gene account for approximately 5% of arRP cases (Littink et al., 2010).

Human *EYS* protein is localized in the photoreceptor outer segments (Abd et al., 2008). However, the function of the protein in the retina is still unknown. Here we report for the first time, the distribution of photoreceptors and other retinal cells in an adult donor carrying two novel *EYS* gene mutations.

(1) Pedigree of Family Studied

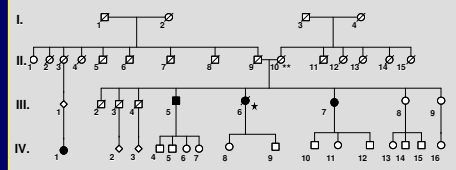

Pedigree of family with autosomal recessive RP due to a *EYS* mutations. Slashed symbols reflect deceased family members. Affected family members are shown in black and unaffected family members are shown in white. DNA analysis was carried out in all three affected members (III-5, III-6, and III-7), in their two unaffected living sisters (III-8 and III-9), and in their mother (II-10); *EYS* mutation was initially identified in III-5. The postmortem analysis in this study was done on unaffected carrier member II-10 (**) and affected member III-6 (★).

(2) Fundus Images of Donor Eye

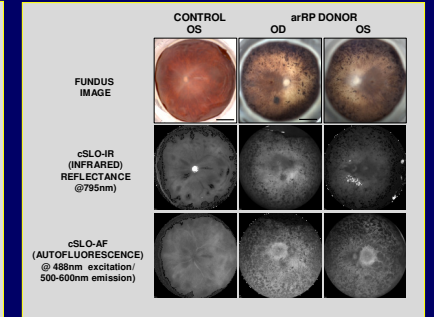

***In situ* imaging of whole *EYS* arRP donor and age-matched control eyes.** SLO and macroscopic fundus images were collected by using a model HRA2 confocal scanning laser ophthalmoscope (Heidelberg Engineering, Inc.) and Zeiss AxioCam MRC5 camera equipped with a macro video lens, respectively. Prior to imaging the cornea and lens were removed leaving only the posterior pole. Remaining eye cups were filled with PBS to eliminate specular reflections and improve contrast and image quality. To accomplish SLO imaging the entire instrument was rotated 90° so that the scan direction is perpendicular to the table surface for optimal imaging of the PBS filled eye cups. All imaging modalities revealed bone spicules in peripheral regions. SLO-IR showed demarcated, circular patches of hypofluorescence in the perimacula region of both eyes, suggesting focal loss of RPE as choroidal vasculature could be visualized. SLO-AF imaging revealed strong autofluorescence (AF) signal around the optic nerve that was devoid of any structural detail compared to the control which clearly showed retinal vasculature. Scale bars in fundus image = 0.5 cm.

(3) OCT Imaging of Donor Eye

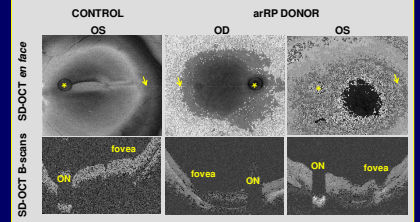

In situ imaging of the *EYS* arRP donor eyes using SD-OCT. Spectral Domain Optical Coherence Tomography images were collected using the SD-OCT system (Bioptigen, Inc.) with a 5x5mm field of view. The eye was placed in the holder and positioned directly below the SD-OCT objective. The fovea and optic nerve could be clearly identified. SD-OCT B-scans revealed structural differences in the retina that suggested disorganization of the affected retina, absence of a photoreceptor layer when compared to the control eye. Arrows point to the in-depth, B-scan plane shown in the OCT images; (*) 1mm ruby sphere positioned on top of the ON to serve as reference. SD-OCT *en face* view displayed several bone spicules around the fovea and ON in the retina of the *EYS* arRP donor eye. A retina fold between the optic nerve and the macula could be observed in the control eye.

(4) Histology of Donor Eye

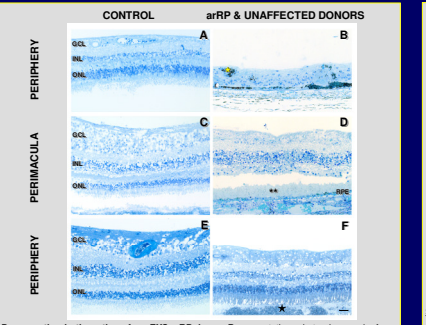

Degeneration in the retina of an *EYS* arRP donor. Representative photomicrographs from toluidine blue stained plastic sections (1µm) of both the arRP donor (B, D), matched controls (A, C), the unaffected mother of the donor (F) and an older (88 y.o.) age-matched control (E) retinas. Morphology of control retina in the periphery (A) and perimacular (C) region displayed typical characteristics including structural lamina consisting of retinal cells. The arRP donor retina in the periphery (B) became atrophic with disorganization of the lamina and cellular layers, gliosis, and presence of intraretinal bone spicules, usually associated with blood vessels (*). In contrast, a prominent inner and outer nuclear layer was present in the perimacular region (D). A few photoreceptor nuclei were still detectable in the perimacular (D) area. An amorphous material was present between the degenerate retina and the RPE in the perimacula (**). The RPE was reduced from normal thickness in the perimacula and thin and discontinuous in the periphery. The unaffected mother of the arRP donor displayed significant decrease in the nuclei in the inner and outer nuclei layers. In addition, this retina displayed myelin artifact in subretinal space (★). GCL= ganglion cell layer; INL= inner nuclear layer; ONL= outer nuclear layer; RPE= retinal pigment epithelium. Bars = 50µm.

(5) Immunocytochemistry

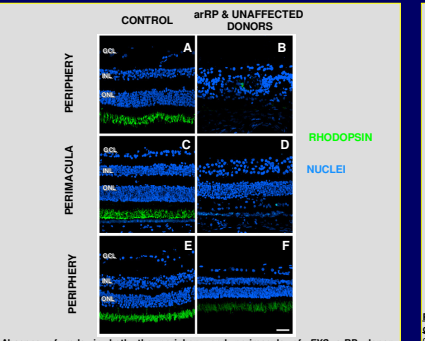

Absence of rods in both the periphery and perimacula of *EYS* arRP donor. Representative photomicrographs of cryosections collected from the matched control (A, C), the arRP donor (B, D), the unaffected mother of the donor (F) and an older age-matched control (E). Sections are shown labeled with antibodies specific to N-terminal domain of rhodopsin (Alexa488, green) while cell nuclei were labeled with TO-PRO-3 (blue). Sections were imaged using a Leica laser scanning confocal microscope (TCS-SP2, Leica, Exton, PA). A series of 1 µm xy (*en face*) sections were collected. Each individual xy retinal image represents a three-dimensional projection of the entire section (sum of all images in the stack). Comparison of the samples showed that rhodopsin expression was absent in both the periphery (B) and perimacula (D) of the arRP donor retina. Control samples (A, C, E) and the unaffected mother (F) displayed rhodopsin distribution restricted to the rods outer segments. However, the unaffected mother displayed significant decrease in the nuclei in the inner and outer nuclei layers. Bar = 40µm.

(6) Immunocytochemistry

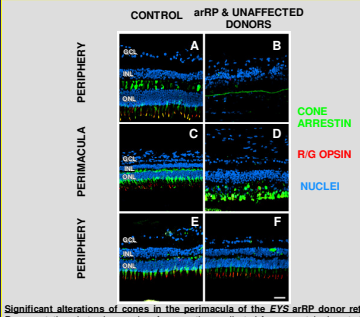

Significant alterations of cones in the perimacula of the *EYS* arRP donor retina. Representative photomicrographs of cryosections collected from a matched control (A, C), the arRP donor (B, D), the unaffected mother of the donor (F) and an older age-matched control (E). Sections are shown labeled with antibodies specific to cone arrestin (Alexa488, green) and red/green opsin (Alexa594, red) while cell nuclei were labeled with TO-PRO-3 (blue). Images were obtained using the same methodology previously aforementioned in Figure 5. Cone arrestin was distributed along the entire plasma membrane of this cone type, from the tip of the outer segment to the synaptic base while the red/green opsin was restricted to the cone outer segments in the control retina both in the periphery (A) and perimacula (C), in the unaffected donor mother (F) and the older matched control (E). These samples also displayed red/green opsin restricted to the outer segments. Cones were mostly absent from the periphery of the arRP donor retina (B). In contrast, cones were present in the macular region of the arRP donor (D), but they were clearly disorganized and morphologically different than controls. In addition, synaptic terminals were not visualized as well. The unaffected mother (F) displayed significant decrease in the nuclei in the inner and outer nuclei layers but otherwise appeared similar to controls. Bar = 40µm.

(7) Immunocytochemistry

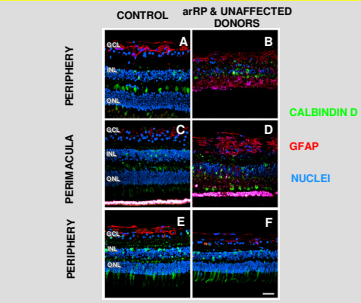

Presence of amacrine, bipolar and Müller cells which have undergone reactive gliosis in *EYS* arRP donor eyes. Representative photomicrographs of cryosections collected from the matched control (A, C), the arRP donor (B, D), the unaffected mother of the donor (F) and an older age-matched control (E). Sections were labeled with antibodies specific to calbindin D-28K (Alexa488, green) and GFAP (Alexa594, red) while cell nuclei were labeled with TO-PRO-3 (blue). Sections were analyzed using a Leica laser scanning confocal microscope. Images were obtained using the same methodology previously aforementioned in Figure 5. Comparison of the samples revealed that calbindin labeling in the control retina was present in the amacrine, bipolar and photoreceptor cells, whereas GFAP was restricted to only astrocytes within both the periphery (A) and perimacula (C). The older control (E) and unaffected mother of the arRP donor (F) also displayed similar distribution of both markers. However, in the periphery (B) and perimacula (D) of the arRP donor, calbindin positive cells were observed scattered throughout the entire retina. The Müller cells had undergone reactive gliosis throughout the retina, and their hypertrophic processes were GFAP positive in both arRP retinas. Bar = 40µm.

Conclusions

The retina of an adult arRP donor with two novel *EYS* mutations displays:

- atrophic retina with disorganization of the cellular layers, gliosis, and presence of intraretinal bone spicules in the periphery;
- reduced thickness of the RPE in the perimacula and thin and discontinuous RPE in the periphery;
- absence of rods in the perimacula and periphery;
- significant decrease of cones in the periphery;
- presence of disorganized, morphologically different cones in the perimacula;
- distribution of calbindin D-28k positive cells throughout the whole retina;
- Müller cells which have undergone reactive gliosis throughout the retina, and their hypertrophied processes were GFAP positive.

The retina of the unaffected mother of the arRP donor displays:

- typical characteristics including structural lamina consisting of retinal cells;
- significant decrease in the nuclei in the inner and outer nuclei layers;
- myelin artifact in subretinal space;
- similar to control distribution of rhodopsin and red/green cone opsin proteins (restricted to the outer segments);
- similar to control distribution of calbindin D-28K positive cells and GFAP labeling.

References

- Abd El-Aziz MM, Barragan I, O'Driscoll CA, et al. *Nat Genet.* 2008; 40: 1285-1287.
- Collin RW, Littink KW, Klevering BJ, et al., *Am J Hum Genet.* 2008; 83: 594-603.
- https://sph.uth.tmc.edu/retnet
- Littink KW, van den Born LI, Koenekoop RK, et al. *Ophthalmology.* 2010; 117: 2026-2033.

Acknowledgements

We thank Dr. Peter MacLeish (Morehouse School of Medicine, Atlanta, GA) for providing us with the antibody to cone arrestin (7G6).

Support

The Foundation Fighting Blindness
Research to Prevent Blindness
Wolf Family Foundation
National Eye Institute

PHOTORECEPTOR ANALYSIS IN THE RETINA OF A DONOR WITH GOLDMANN-FAVRE SYNDROME.

Cleveland Clinic

M.E. Rayborn[1], V.L. Bonilha[1], G.A. Fishman[2], and J.G.Hollyfield[1].

1-The Cole Eye Institute, Cleveland Clinic, Cleveland, OH, 2- Department of Ophthalmology and Visual Sciences, University of Illinois, Chicago, IL.

Abstract

Purpose: Patients with Goldmann-Favre syndrome carry mutations in the *NR2E3* gene. This gene codes for a photoreceptor-specific nuclear receptor. The present study aimed to analyze the distribution of rods, cones, and the red/green and blue opsins in the eyes of a donor with Goldmann-Favre syndrome. The patient was 88 years-old at the time of his death. His clinical phenotype, including an early history of night blindness, peripheral retinoschisis and midperipheral plumping of pigment were characteristic of the Goldmann-Favre syndrome. He was found to have a homozygous splice site mutation in the *NR2E3* gene. **Methods:** The affected eye was fixed in 4% paraformaldehyde and 0.5% glutaraldehyde in phosphate buffer. A perimacular area was cut and processed for transmission electron microscopy (TEM). Alternatively, cryostat tissue sections of the macula and periphery were studied by indirect immunofluorescence, using well-characterized monoclonal antibodies to the rhodopsin (mAb B630N), cone cytoplasm (mAb 7G6) and polyclonal antibodies to either red/green (AB5405) and blue (AB5407) opsins. The affected donor eye was compared to a matched normal eye. **Results:** The retina was highly disorganized with indistinct layers. Bone spicule pigment was observed both in the perimacular and periphery of the eye. The RPE layer was discontinuous in some regions of the perimacula. Large (>1mm) spherical electrondense melanosomes were observed in the RPE and choroid by TEM. Rods were virtually absent in the affected retina. Cones were present in the macula, but were mostly absent from the retinal periphery. In addition, rosettes of cones were observed in the perimacular area. Both red/green and blue opsins were distributed along the entire cellular expanse of the cone photoreceptors in the affected eye, but were restricted to the cone outer segments in the control retina. Cone synapses were not observed. **Conclusions:** The histological data obtained from an elderly male patient with Goldmann-Favre syndrome showed an absence of rods and abnormal distribution of red/green and blue cone opsins.

Supported in part by NIH grant EY015638, a Research Center Grant from The Foundation Fighting Blindness and Research to Prevent Blindness.

Introduction

The Goldmann-Favre syndrome was described from two separate reports in 1957 (Goldmann, 1957) and 1958 (Favre, 1958) describing a teenage brother and sister, respectively, with a distinctive vitreoretinal degenerative disorder. The Goldmann-Favre syndrome is a rare autosomal recessive vitreoretinal degeneration characterized by night blindness, pigmentary degeneration, macular and peripheral retinoschisis, posterior subcapsular cataract, markedly abnormal or nondetectable electrograms, and degenerative vitreous changes, such as liquefaction, strands, or bands. Since the original description, other cases have been reported confirming that this is a clinically recognizable disease. However, it has been shown that the clinical features vary among pedigrees.

Later on, it was proposed that the Goldmann-Favre syndrome is a type of enhanced S cone syndrome since in both retinal dysfunctions the patients display hypersensitivity to blue light and their electroretinograms have greater amplitudes to short-wavelength (eg, blue) light flashes than to long-wavelength (eg, orange) light flashes (Jacobson et al., 1991).

The Goldmann-Favre syndrome is caused by loss-of-function mutations in the *NR2E3* gene (also known as *PNR*), which encodes a retinal nuclear receptor recently discovered to be a ligand-dependent transcription factor (Kobayashi et al., 1999). Reported results suggest that *NR2E3* controls photoreceptor differentiattion (Haider et al., 2000; Cheng et al., 2006). However, it is not known how the mutation in this protein leads to the degeneration of the choroid, RPE and retina.

In the present study we analyzed the morphology of the retina and the distribution of photoreceptor markers in a donor eye from a male donor affected by Goldmann-Favre syndrome.

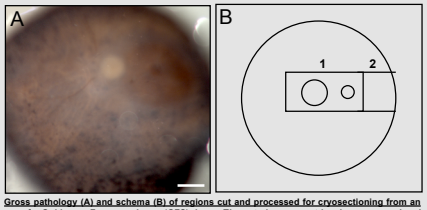

Gross pathology (A) and schema (B) of regions cut and processed for cryosectioning from an eye of a Goldmann-Favre syndrome (GFS) donor. The anterior segment has been removed and the retina is viewed *en face*; characteristic pigmentary changes can be observed. Region 1= perimacular area; region 2= periphery. Bar = 0.5cm.

Figure 1

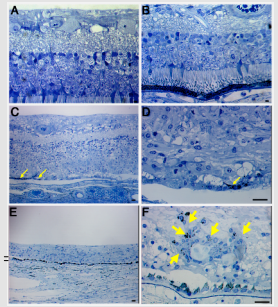

Degeneration in the retina of a Goldmann-Favre syndrome affected donor. Human 1μm plastic sections of both a matched control (A, B) and the affected GFS (C-F) retinas stained with toluidine blue. (A, B) Morphology of control retina in the perimacular region of the eye. (C-F) The retina of the affected GFS donor displayed different degrees of retinal degeneration. Observation at low magnification of both perimacula (C) and periphery tissue (E) demonstrated sparse inner and outer nuclear layers with stunted photoreceptor inner and outer segments. A thin, restricted area of pigmented RPE cells was observed in the perimacular retina (C, small arrows) while a continuous layer of pigmented RPE cells was observed in the periphery (E) of the affected donor. High magnification observation of the affected retina in the periphery (F) but not in the perimacula (D) revealed the presence of several bone spicule pigments (large arrows). Bar= 200μm.

Figure 2

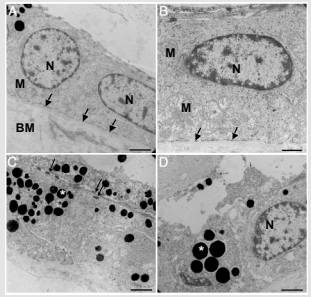

Ultrastructural evidence of RPE degeneration in a GFS affected donor. The ultrastructure of perimacula tissue was analyzed by TEM. Observation at both low (A) and high (B) magnification showed a collapsed RPE apical surface mostly deprived of apical microvilli; no photoreceptor outer segments are observed on top of the RPE apical surface. Moreover, observation of RPE's basal surface revealed absence of basal infoldings (large arrows); Bruch's membrane was very disorganized (A). Some areas displayed multi layers of pigmented cells (C, D). The presence of desmosomes (C, small arrows) was noticed between adjacent cells. The cytoplasm of RPE and choroid cells was filled with abnormally large (>1mm) spherical electrondense melanosomes (C, D, *). Electron micrographs were taken on a Tecnai 20, 200 kv digital electron microscope using a Gatan image filter. Panels were composed using AdobePhotoshop 5.5. N= nucleus; M= mitochondria; BM= Bruch's membrane. Bars: A, C, D = 2μm and B =1μm.

Figure 3

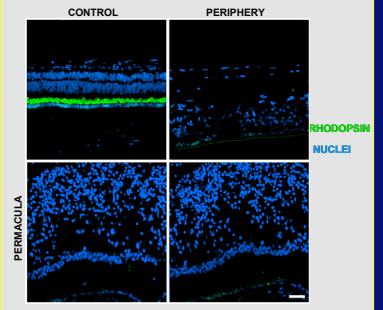

Absence of rhodopsin in the rods in a GFS affected donor. Human cryosections of both a matched control and affected GFS donor were labeled with antibodies specific to rhodopsin (Alexa488, green) while cell nuclei were labeled with TO-PRO-3 (blue). Sections were analyzed using a Leica laser scanning confocal microscope (TCS-SP2, Leica, Exton, PA). A series of 1 μm xy (en face) sections were collected. Each individual xy image of the retinas stained represents a three-dimensional projection of the entire section (sum of all images in the stack). Microscopic panels were composed using AdobePhotoshop 5.5. Comparison of the samples showed that rhodopsin was absent in the affected retina in all the regions observed. Bar = 40μm.

Figure 4

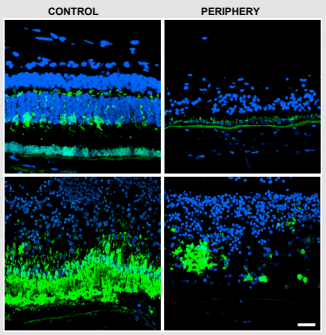

Significant absence of cones in the periphery together with the presence of rosettes of cones in the perimacula of a GFS affected donor. Human cryosections of both a matched control and a GFS affected donor were labeled with antibodies specific to cone cytoplasm (7G6) (Alexa488, green) while cell nuclei were labeled with TO-PRO-3 (blue). Sections were analyzed using a Leica laser scanning confocal microscope (TCS-SP2, Leica, Exton, PA). A series of 1 μm xy (en face) sections were collected. Each individual xy image of the retinas stained represents a three-dimensional projection of the entire section (sum of all images in the stack). Microscopic panels were composed using AdobePhotoshop 5.5. Comparison of the samples showed that 7G6 was almost absent in the periphery while in the perimacula it was distributed in rosettes. Bar = 40μm.

Figure 5

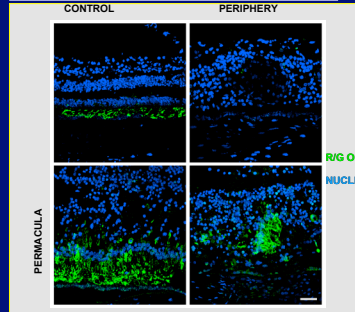

Red/green cone opsin is distributed along the entire plasma membrae of this cone type in a GFS affected donor. Human cryosections of both a matched control and affected GFS donor were labeled with antibodies specific to red/green cone opsins (Alexa488, green) while cell nuclei were labeled with TO-PRO-3 (blue). Sections were analyzed using a Leica laser scanning confocal microscope (TCS-SP2, Leica, Exton, PA). A series of 1 μm xy (en face) sections were collected. Each individual xy image of the retinas stained represents a three-dimensional projection of the entire section (sum of all images in the stack). Microscopic panels were composed using AdobePhotoshop 5.5. Comparison of the samples showed that red/green cone opsins were distributed along the entire plasma membrane of this cone type, from the tip of the outer segment to the synaptic base; the abnormal distribution was also observed in rosettes in the perimacula. On the other hand, red/green opsins were mostly absent in the periphery of the affected retina. Bar = 40μm.

Figure 6

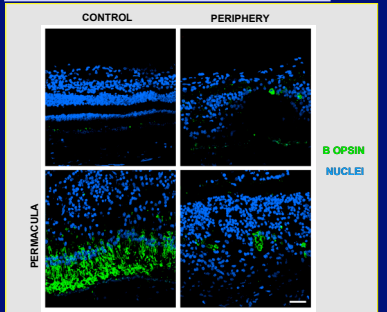

Blue cone opsin is significantly increased and distributed along the entire plasma membrane of this cone type in a GFS affected donor. Human cryosections of both a matched control and affected GFS donor were labeled with antibodies specific to blue cone opsins (Alexa488, green) while cell nuclei were labeled with TO-PRO-3 (blue). Sections were analyzed using a Leica laser scanning confocal microscope (TCS-SP2, Leica, Exton, PA). A series of 1 μm xy (en face) sections were collected. Each individual xy image of the retinas stained represents a three-dimensional projection of the entire section (sum of all images in the stack). Microscopic panels were composed using AdobePhotoshop 5.5. Comparison of the samples showed that blue cone opsins were significantly increased in all the observed regions of the affected eye, where blue cone opsins were distributed along the entire plasma membrane of this cone type, from the tip of the outer segment to the synaptic base; the abnormal distribution was also observed in rosettes in the perimacula. Bar = 40μm.

Summary

- Histopathological analysis of the GFS affected retina revealed the presence of different degrees of degeneration in both areas analyzed:
  -sparse inner and outer nuclear layers with stunted photoreceptor inner and outer segments were observed; high magnification observation of the affected retina in the periphery but not in the perimacula revealed the presence of several bone spicule pigments.
  -a thin, restricted area of pigmented RPE cells was observed in the perimacular retina while a continuous layer of pigmented RPE cells was observed in the periphery.
- Ultrastructural observation of the perimacular area revealed a collapsed RPE apical surface mostly deprived of apical microvilli and basal infoldings; no photoreceptor outer segments are observed on top of the RPE apical surface. Moreover, Bruch's membrane was very disorganized. Some areas displayed multi layers of pigmented cells. The presence of desmosomes was noticed between adjacent cells. The cytoplasm of RPE and choroid cells was filled with abnormally large (>1mm) spherical electrondense melanosomes
- Rhodopsin was mostly absent in the affected retina.
- Labeling with a cone cytoplasmic marker revealed significant absence of cones in the periphery together with the presence of rosettes of cones in the perimacula of the affected donor.
- Red/green opsins are distributed along the entire plasma membrane of this cone type, from the tip of the outer segment to the synaptic base. This distribution is also observed in the rosettes.
- Blue opsin expression is significantly increased in the affected retina. Blue opsin was also distributed along the entire plama membrane of this cone type.

References

-Cheng, H, Aleman, T.S., Cideciyan A.V., Khanna, R., Jacobson, S.G. and Swaroop, A. (2006) Hum Mol Gen, 15: 2588-2602.
- Favre, M. (1958) Ophthalmologica, 135: 604-9.
- Goldmann, H, (1957) Bull Mec Soc Fr Ophthalmol, 70: 265.
- Haider, N.B., Jabobson, S.G., Cideciyan, AV., Swiderski, R., Streb, L.M., Searby, C., Beck, G., Hockey, R., Hanna, D.B., Gorman, S., Duhl, D., Carmi, R., Bennet, J., Weleber, R.G., Fishman, G.A., Wright, A.F., Stone, E.M. and Sheffield, V.C. (2000) Nat Gen, 24: 127-31.
- Jacobson, S.G., Roman, A.J., Roman, M.I., Gass, J.D. and Parker, J.A. (1991) Am J Ophthalmol, 111: 446-53.
- Kobayashi, M., Takezawa, S., Hara, K., Yu, R.T., Umesono, Y., Agata, K., Taniwaki, M., Yasuda, K. and Umesono, K. (1999) Proc Natl Acad Sci, 96: 4814-9.

ACKNOWLEDGMENTS

We thank Dr. Peter MacLeish (Morehouse School of Medicine, Atlanta, GA) for providing us with the antibody to cone cytoplasmic marker (7G6), Dr. R. Molday (University of British Columbia, Vancouver, Canada) for providing us with the antibody to rhodopsin (B630N).

SUPPORTED BY Research to Prevent Blindness

Foundation Fighting Blindness

RETINAL HISTOPATHOLOGY IN THE EYES FROM PATIENTS WITH LEBER CONGENITAL AMAUROSIS

Program # 1824

M. E. Rayborn[1]*, V. L. Bonilha[1], Brent A. Bell[1], Y. Li[1] and J. G. Hollyfield[1].

Cleveland Clinic

1-The Cole Eye Institute, Cleveland Clinic Lerner College of Medicine, Cleveland, OH

* rayborm@ccf.org

Abstract

Purpose: To evaluate the histopathology in donor eyes from patients with LCA.

Methods: Eyes were obtained from a 3 year-old male who died from undiagnosed genetic abnormalities through the donor program of the FFB. The eyes were fixed in 4% paraformaldehyde and 0.5% glutaraldehyde in phosphate buffer within 11 hours postmortem. Eyes were analyzed through the use of visible macroscopic fundus photography (VMF), confocal scanning laser ophthalmoscope (cSLO) and spectral-domain optical coherence tomography (SD-OCT). After that, small areas from the fundus macula and periphery were processed for electron microscopy and indirect immunofluorescence, using specific antibodies to retinal proteins such as rhodopsin, cone arrestin and opsins, RPE65 among others. The content of autofluorescent material was analyzed in epifluorescence. The donor eye was compared to a matched normal eye (3 y.o) and to additional eyes from another young donor with LCA (11 y.o. female).

Results: VMF, cSLO and SD-OCT images of LCA eyes revealed atypical retinas as compared to the control. With all three imaging modalities, the LCA eyes lacked distinct morphological detail typically observed using these techniques even in postmortem eyes. VMF images of the LCA eye revealed a "photonegative effect" This effect is punctuated by a hypopigmented macula relative to a hyperpigmented, dark retinal background. cSLO infrared (IR) imaging identified the optic disk and the hypopigmented macula region seen by VMF. Some evidence of vasculature could be seen around the optic disk with this modality albeit much less pronounced than in the control eye. cSLO autofluorescence (AF) imaging revealed some weak AF signal that was largely devoid of any structural detail compared to the control which clearly showed retinal vasculature and lipofuscin AF background. SD-OCT revealed structural differences in the retina that suggested disorganization of the affected retina, absence of a photoreceptor layer, and degeneration of the choroid in the macular area. Retinal vessels appear to be absent or atrophic in the retina even around the optic nerve. Histologic findings revealed highly disorganized photoreceptor layer in the macula and periphery. The RPE layer displayed thinning in some regions of the periphery and decreased pigmentation in most areas. In addition, pigmented cells were also observed within the retina. Rods were virtually absent in the affected retina. Cones were present in the macula, but were mostly absent from the retinal periphery. Cone synapses were not observed. Autofluorescent material was greatly reduced in the RPE in all areas studied.

Conclusions: The 3 y.o. patient with LCA showed an absence of rods and cones in the periphery. In the macula, a few cone photoreceptors were still present, albeit highly disorganized.

Supported by The Foundation Fighting Blindness Histopathology Grant; Research Center Grants from The Foundation Fighting Blindness; Research to Prevent Blindness Unrestricted Grants; and the National Eye Institute (NIH).

Introduction

Leber Congenital Amaurosis (LCA) comprises a group of genetic disorders in which vision loss or dysfunction occurs early in life, often from birth. The extent of vision defects varies from patient to patient, but are usually quite severe. Currently mutations have been identified in 14 different genes in LCA patients and each is a recessive disorder (Cremers et al., 2002; den Hollander et al., 2008).

Review of the literature identified thirteen pathological specimens that most likely represent LCA (reviewed in Koenekoop et al., 2004; den Hollander et al., 2008). All globes but one were obtained from adults, and likely underwent extensive secondary retinal changes from retinal remodeling and re -wiring.

Analysis of the retinal histology of the reported LCA eyes suggests three possible disease categories (Koenekoop, 2004; den Hollander et al., 2008). Degenerations or abiotrophy (Aubineau, 1903; Sorsby and Williams, 1960; Kroll and Kuwabara, 1964; Francois and Hanssens, 1969; Flanders et al., 1984; Sullivan et al., 1994; Porto et al., 2002) are characterized by extensive atrophy, dropout, and/or gliosis of the photoreceptor, inner retinal layer, and RPE layer; they may also represent aplasias or dysfunctions with a consequent, superimposed degeneration. Aplasias are characterized by the complete absence of the photoreceptor layer or the presence of a very unusual looking, primitive cuboidal cells in this layer (Vrabec, 1951; Babel, 1962; Gillespie, 1966). The biochemical dysfunction (dysplasia) category of disease is characterized by intact entire retina or most of it, including the inner layer, the photoreceptor layer, and the RPE (Horsten, 1960; Babel, 1962 and Milam et al, 2003).

Figure 1

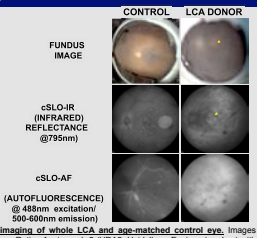

***In situ* imaging of whole LCA and age-matched control eye.** Images were collected by a cSLO Heidelberg Retina Angiograph 2 (HRA2, Heidelberg Engineering, Inc.) with a 55º objective and a Zeiss AxioCam MRC5 camera equipped with a Zoom 7000 Navitar macro video lens. The cSLO housing was positioned so that the lens is directed down onto the aqueous surface for optimal imaging of the fundus. Fundus image of the LCA eye revealed a "photonegative effect" in the macula. This effect is punctuated by a hypopigmented macula relative to a hyperpigmented, dark retinal background. Confocal scanning laser ophthalmoscope (cSLO) -IR imaging identified the optic disk and the hypopigmented macula identified by fundus image (arrow). cSLO -AF imaging revealed some weak AF signal that was devoid of any structural detail compared to the control which clearly showed retinal vasculature and lipofuscin AF background.

Figure 2

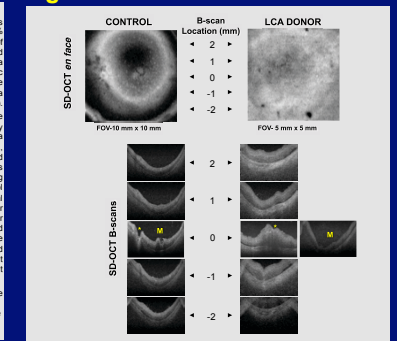

In situ imaging of LCA donor eye using SD-OCT. Spectral Domain Optical Coherence Tomography images were collected using the SD-OCT system (Bioptigen, Inc.) with a 50º field of view. The eye was placed in the holder and positioned directly below the SD-OCT objective. SD-OCT B-scans revealed structural differences in the retina that suggested disorganization of the affected retina, absence of a photoreceptor layer, and degeneration of the choroid in the macular area (M) when compared to the control eye. Retinal vessels appear to be absent or atrophic in the retina even around the optic nerve (*). SD-OCT *en face* view displayed remarkable lack of structural features in the retina of the LCA eye.

Figure 3

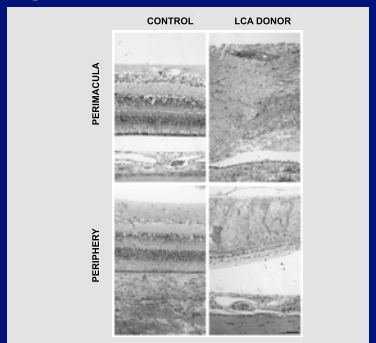

Degeneration in the retina of an LCA donor. Gross pathology of regions cut and processed from an eye of a 3 y.o. LCA donor. Human 1µm plastic sections of both a matched control and LCA donor retinas stained with toluidine blue are shown. Morphology of control retina in the perimacular and periphery region displayed characteristic layers of retinal cells. The retina of the LCA donor displayed edema both in the perimacula and periphery. In addition, ganglion cell layer and inner nuclei layer were not observed in both regions. A few photoreceptor nuclei are still detectable, however inner and outer nuclear layers were not observed. A thin, continuous area of pigmented RPE cells was observed in the perimacula but not in some areas of the periphery. Bars =100µm.

Figure 4

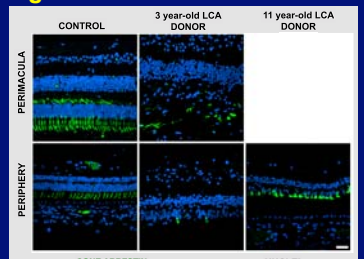

Significant alterations in the cones both in the perimacula and in the periphery of LCA donors. Human cryosections of both a matched control and affected LCA donors were labeled with antibodies specific to cone arrestin (Alexa488, green) while cell nuclei were labeled with TO-PRO-3 (blue). Sections were analyzed using a Leica laser scanning confocal microscope (TCS-SP2, Leica, Exton, PA). A series of 1 µm xy (*en face*) sections were collected. Each individual xy retinal image represents a three-dimensional projection of the entire section (sum of all images in the stack). Comparison of the samples showed that cone arrestin was distributed along the entire plasma membrane of this cone type, from the tip of the outer segment to the synaptic base in the control retina. Cones were present in the macula of the 3 y.o. LCA donor but they were sparse and had lost their vertical orientation, synapses were not visualized. In addition, cones were mostly absent from the periphery of the 3 y.o. LCA donor retina. On the other hand, cones were still present in the retina of the 11 y.o. LCA donor. However, these cones were deprived of outer segments. Bar = 40µm.

Figure 5

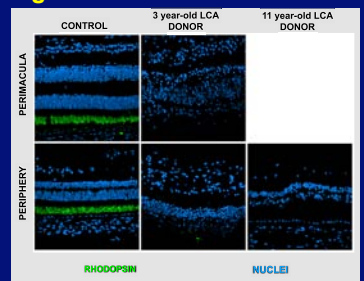

Significant decrease in rods both in the perimacula and in the periphery of LCA donor. Human cryosections of both a matched control and affected LCA donors were labeled with antibodies specific to rhodopdin (Alexa488, green) while cell nuclei were labeled with TO-PRO-3 (blue). Sections were analyzed using a Leica laser scanning confocal microscope (TCS-SP2, Leica, Exton, PA). A series of 1 µm xy (*en face*) sections were collected. Each individual xy retinal image represents a three-dimensional projection of the entire section (sum of all images in the stack). Comparison of the samples showed that rhodopsin expression is significantly decreased in all the observed regions of the 3 y.o. LCA donor retina. In addition, rods were also not detected in the retina of the 11 y.o. LCA donor. Bar = 40µm.

Figure 6

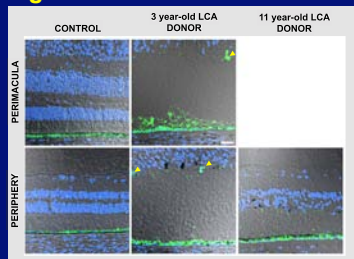

Presence of RPE cells expressing RPE65 in the eyes from LCA donors. Human cryosections of both a matched control and affected LCA donors were labeled with antibodies specific to RPE65 (Alexa488, green) while cell nuclei were labeled with TO -PRO-3 (blue). Sections were analyzed using a Leica laser scanning confocal microscope (TCS-SP2, Leica, Exton, PA). A series of 1 µm xy (*en face*) sections were collected. Each individual xy retinal image represents a three-dimensional projection of the entire section (sum of all images in the stack). Immunofluorescence images were imposed on differential interference contrast images to provide additional information about the retinal tissue.Comparison of the samples showed a continuous layer of cells expressing RPE65 in the perimacula and periphery of the control retina and in the retinas of both LCA donors. However, in several areas of both perimacula and periphery of the 3 y.o. LCA donor, several layers of RPE65 positive cells were observed in the retina with some cells also present in the retina (arrows). In the periphery of the 11 y.o. LCA donor retina no cells were detected expressing RPE65. A few pigmented cells (not labeled with RPE65 antibody) were also observed in the retina of both LCA donors. Bar = 40µm.

Figure 7

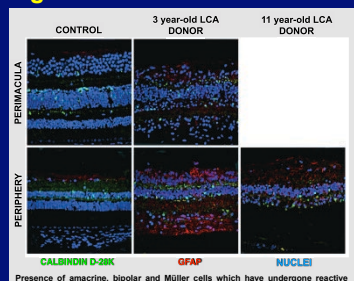

Presence of amacrine, bipolar and Müller cells which have undergone reactive gliosis in the eyes from LCA donors. Human cryosections of both a matched control and affected LCA donors were labeled with antibodies specific to calbindin D-28K (Alexa488, green) and GFAP (Alexa594, red) while cell nuclei were labeled with TO -PRO-3 (blue). Sections were analyzed using a Leica laser scanning confocal microscope (TCS-SP2, Leica, Exton, PA). A series of 1 µm xy (*en face*) sections were collected. Each individual xy retinal image represents a three-dimensional projection of the entire section (sum of all images in the stack). Comparison of the samples showed that in the normal retina calbindin positive cells were present in the amacrine and bipolar cells while GFAP was restricted to the astrocytes. However, in perimacula and periphery of the 3 y.o. LCA donor, calbindin positive cells were observed in the whole retina. In the periphery of the 11 y.o. LCA donor retina scattered cone bipolar cells and amacrine cells were positive for calbindin. The Müller cells had undergone reactive gliosis throughout the retina, and their hypertrophied processes were GFAP positive in both LCA retinas. Bar = 40µm.

SUMMARY:

The retina of a 3 year-old donor with LCA displays:

- disorganization of the retinal layers and presence of edema in the retina;
- degeneration in the retina;
- presence of disorganized cones in the perimacula;
- significant decrease of cones in the periphery;
- near-absence of rods in the perimacula and periphery;
- presence of a continuous layer of RPE cells expressing RPE65;
- presence of RPE65 positive cells in the retina;
- presence of calbindin D-28k positive cells in the whole retina;
- Müller cells which have undergone reactive gliosis throughout the retina, and their hypertrophied processes were GFAP positive.

REFERENCES:

- Cremers FP, van den Hurk JA, den Hollander AI. *Hum Mol Genet.* 2002; 11: 1169-1176.
- den Hollander AI, Roepman R, Koenekoop RK, Cremers FP. *Prog Retin Eye Res.* 2008; 27: 391-419.
- Koenekoop RK. *Surv Ophthalmol.* 2004; 49: 379-398.
- Aubineau M. *Ann Oculist.* 1903; 129: 432-439.
- Sorsby A, Williams CE. *Br Med J.* 1960; 1: 293-297.
- Kroll AJ, Kuwabara T. *Arch Ophthalmol.* 1964; 71: 683-690.
- Francois J, Hanssens M. *Ann Oculist.* 1969; 202: 127-155.
- Flanders M, Lapointe ML, Brownstein S, Little JM. *Can J Ophthalmol.* 1984; 19: 310-314.
- Sullivan TJ, Heathcote JG, Brazel SM, Musarella MA. *Aust N Z J Ophthalmol.* 1994; 22: 25-31.
- Porto FB, Perrault I, Hicks D, et al. *J Gene Med.* 2002; 4: 390-396.
- Vrabec F. *Ophthalmologica.* 1951; 122: 65-75.
- Babel J. *Ophthalmologica.* 1962; 145: 399-402.
- Gillespie FD. *Am J Ophthalmol.* 1966; 61: 874-880.
- Horsten GP, Winkelman JE. *Arch Ophthalmol.* 1960; 63: 232-242.
- Milam AH, Barakat MR, Gupta N, et al. *Ophthalmology.* 2003; 110: 549-558.

ACKNOWLEDGMENTS:

We thank Dr. Peter MacLeish (Morehouse School of Medicine, Atlanta, GA) for providing us with the antibody to cone arrestin (7G6), Dr. Paul Hargrave (University of Florda, Gainesville, FL) for providing us with the antibody to rhodopsin (B630N) and Dr. Rosalie Crouch (University of South Carolina, Charleston, SC) for providing us with the RPE65 antibody (PETLET).

SUPPORTED BY

Research to Prevent Blindness

Foundation Fighting Blindness

RETINAL HISTOPATHOLOGY IN EYES FROM A PATIENT WITH AUTOSOMAL DOMINANT RETINITIS PIGMENTOSA CAUSED BY THE Pro23His RHODOPSIN MUTATION

Program #6443

M. E. Rayborn, V. L. Bonilha, B. A. Bell, M. J. Marino, G. J. Pauer, C. D. Beight, E. I. Traboulsi, S. A. Hagstrom, and J. G. Hollyfield

The Cole Eye Institute, Cleveland Clinic Lerner College of Medicine, Cleveland, OH

Cleveland Clinic

Supported by Research to Prevent Blindness

Foundation Fighting Blindness

Abstract

Purpose: To evaluate the histopathology in donor eyes from a patient with autosomal dominant retinitis pigmentosa (adRP) caused by a Pro23His rhodopsin mutation.

Methods: Eyes were obtained from a 72 year-old male who died from a stroke secondary to subdural hematoma. Eyes were fixed in 4% paraformaldehyde and 0.5% glutaraldehyde in PBS within 17.5 hours postmortem. Globes were evaluated with macroscopic, SLO and OCT imaging. Macula and peripheral regions were processed for electron microscopy and immunocytochemistry. Three age-matched normal eyes were used as controls. DNA was obtained from blood and buccal samples of the donor, his affected daughter and son. Direct genomic sequencing of the entire rhodopsin coding region and flanking intronic sequences was performed.

Results: DNA analysis of the donor and affected family members revealed a rhodopsin Pro23His mutation. All imaging modalities revealed peripheral areas of heavy bone spicules. The area surrounding the optic nerve showed evidence of RPE atrophy as choroidal vasculature could be visualized. The fovea and optic nerve could be clearly identified with OCT. Histology revealed a highly degenerate retina with little evidence of stratified nuclear layers in all peripheral areas studied. In contrast, a prominent outer nuclear layer was present in the perifoveal region. The RPE was reduced from normal thickness in the macula and thin and discontinuous in the far periphery. Bone spicule pigmentation was extensive, and present throughout the degenerate retina in the periphery, usually associated with blood vessels. Cones labeled with opsin and arrestin antibodies were present in the macula, but were mostly absent from the periphery. Cone synapses and outer segments were not observed. A few highly disorganized, rhodopsin labeled rods were detected in the macula but were absent in the periphery. Calbindin labeled second order neurons were unevenly distributed in the periphery.

Conclusions: The histopathology of the retina in a patient with advanced Pro23His rhodopsin mutation displayed highly degenerate peripheral retina and preservation of some cone and rod photoreceptors in the macula.

Introduction

Between 15 and 35% of all cases of RP follow an autosomal dominant inheritance pattern (adRP). Currently mutations have been identified in 23 different genes in ADRP patients according to RetNet. The most common rhodopsin mutation in North America is Pro23His, which is found in about one third of patients with rhodopsin mutations.

Previous studies of ocular observation of affected patients suggested clinical heterogeneity even in related patients with this same point mutation in the rhodopsin gene (Berson et al., 1991; Aleman et al., 2008).

A few previous studies reported analysis of the retinal histology of eyes with Pro23His mutation. A common finding in those studies was variable histological findings in the retina with a final common pathway leading to photoreceptor cell death (Kolb & Gouras, 1974; To et al., 2002; To et al., 2004). Here we analyzed and reported for the first time the distribution of photoreceptors and other retinal cells in an adult Pro23His RP donor.

(1) Pedigree of Donor Family Studied

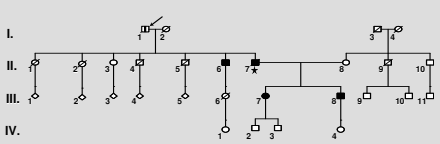

Pedigree of family with autosomal dominant RP due to a Pro23His Rhodopsin mutation. Slashed symbols reflect deceased family members. Affected family members are shown in black and unaffected family members are shown in white. DNA analysis was carried out in donor and his two affected children; Pro23His rhodopsin mutation was initially identified in donor II-7(★) followed by confirmation of the mutation in his two affected children. The postmortem analysis in this study was done on member II-7 (★). Interview with family members suggested that I-1 (arrow) may also have been affected.

(2) Fundus Images of Donor Eye

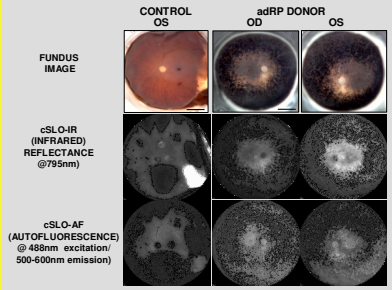

***In situ* imaging of whole Pro23His Rhodopsin adRP donor and age-matched control eyes.** SLO and macroscopic fundus images were collected by using a model HRA2 confocal scanning laser ophthalmoscope (Heidelberg Engineering, Inc.) and Zeiss AxioCam MRC5 camera equipped with a macro video lens, respectively. Prior to imaging the cornea and lens were removed leaving only the posterior pole. Remaining eye cups were filled with PBS to eliminate specular reflections and improve contrast and image quality. To accomplish SLO imaging the entire instrument was rotated 90º so that the scan is perpendicular to the table surface for optimal imaging of the PBS filled eye cups. All imaging modalities revealed peripheral areas of heavy bone spicules. SLO-IR imaging identified the optic disk and the hypopigmented macula identified by fundus image (arrow). SLO-AF imaging revealed some weak autofluorescence (AF) signal that was devoid of any structural detail compared to the control which clearly showed retinal vasculature and lipofuscin AF background. The area surrounding the optic nerve showed evidence of RPE atrophy as choroidal vasculature could be visualized. Scale bars in fundus image = 0.5 cm.

(3) OCT Images of Donor Eye

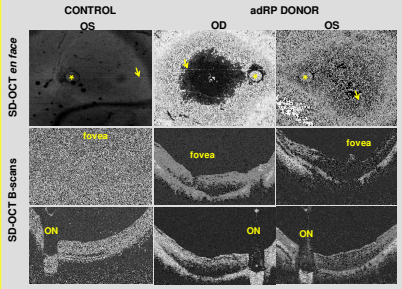

In situ imaging of the Pro23His Rhodopsin adRP donor eyes using SD-OCT. Spectral Domain Optical Coherence Tomography images were collected using the SD-OCT system (Bioptigen, Inc.) with a 5x5mm field of view. The eye was placed in the holder and positioned directly below the SD-OCT objective. The fovea and optic nerve could be clearly identified. SD-OCT B-scans revealed structural differences in the retina that suggested disorganization of the affected retina, absence of a photoreceptor layer when compared to the control eye. Arrows point to the in-depth, B-scan plane shown in the OCT images; (*) 1mm ruby sphere positioned on top of the ON to serve as reference. SD-OCT *en face* view displayed several bone spicules around the fovea and ON in the retina of the Pro23His rhodopsin RP donor eye.

(4) Histology of Donor Eye

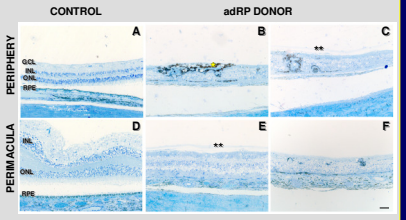

Degeneration in the retina of a Pro23His Rhodopsin adRP donor. Representative photomicrographs from Toluidine blue stained plastic sections (1µm) of both the adRP donor retinas and a matched control are shown for comparison. Morphology of control retina in the periphery (A) and perimacular (D) region displayed typical characteristics including structural lamina consisting of retinal cells. The adRP donor retina in the periphery (B) and far periphery (C) became atrophic with disorganization of the lamina and cellular layers, gliosis, and presence of intraretinal bone spicules, usually associated with blood vessels (*). In contrast, a prominent inner and outer nuclear layer was present in the permacular region (E). In addition, a few photoreceptor nuclei were still detectable both in the perimacular (E) and adjacent (F) areas. Both the perimacular (E) and far periphery (C) retina of the ADRP contained a prominent pre-retina (epiretinal) compartment composed of several layers of fibroblast-like cells that were separated from the retina by a connective tissue-like matrix (**). The RPE was reduced from normal thickness in the macula and thin and discontinuous in the far periphery. GCL= ganglion cell layer; INL= inner nuclear layer; ONL= outer nuclear layer; RPE= retinal pigment epithelium. Bars =50µm.

(5) Immunocytochemistry

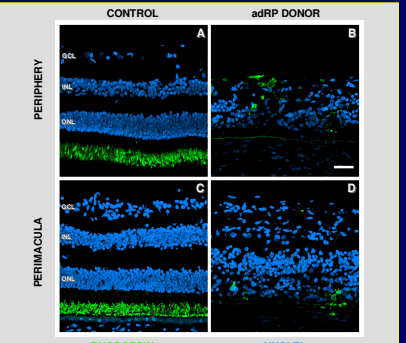

Significant decrease in rods both in the periphery and in the perimacula of Pro23His Rhodopsin adRP donor. Representative photomicrographs of cryosections collected from the matched control (A, C) and the adRP donor (B, D). Sections are shown labeled with antibodies specific to N-terminal domain of rhodopsin (Alexa488, green) while cell nuclei were labeled with TO-PRO-3 (blue). Sections were imaged using a Leica laser scanning confocal microscope (TCS-SP2; Leica, Exton, PA). A series of 1 µm *xy* (*en face*) sections were collected. Each individual xy retinal image represents a three-dimensional projection of the entire section (sum of all images in the stack). Comparison of the samples showed that rhodopsin expression is significantly decreased both in the periphery (B) and perimacula (D) of the RP donor retina. Bar = 40µm.

(6) Immunocytochemistry

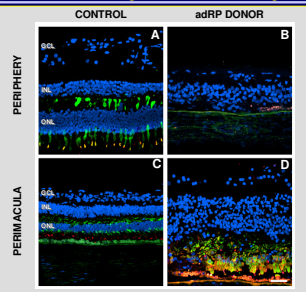

Significant alterations in the cones in the perimacula of a Pro23His Rhodopsin adRP donor retina. Representative photomicrographs of cryosections obtained from the adRP donor and a matched control. Sections were labeled with antibodies specific to cone arrestin (Alexa488, green) and red/green cone opsin (Alexa594, red) while cell nuclei have been labeled with TO-PRO-3 (b lue). Sections were analyzed using a Leica laser scanning confocal microscope. Images were obtained using the same methodology previously aforementioned in Figure 5. Comparison of the samples showed that cone arrestin was distributed along the entire plasma membrane of this cone type, from the tip of the outer segment to the synaptic base while the red/green opsin was restricted to the cone outer segments in the control retina both in the periphery (A) and perimacula (C). Cones were mostly absent from the periphery of the ADRP donor retina (B). In contrast, cones were present but highly disorganized in the macular region of the adRP donor (D), but synaptic terminals were not visualized. Bar = 40µm.

(7) Immunocytochemistry

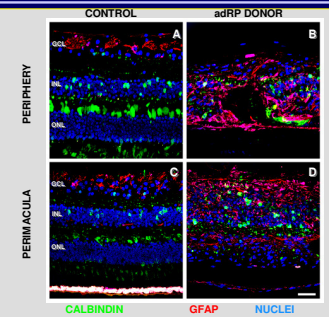

Presence of amacrine, bipolar and Müller cells which have undergone reactive gliosis in the eyes from a Pro23His Rhodopsin adRP donor. Representative photomicrographs of cryosections obtained from the adRP donor and a matched control. Sections were labeled with antibodies specific to calbindin D-28K (Alexa488, green) and GFAP (Alexa594, red) while cell nuclei were labeled with TO-PRO-3 (blue). Sections were analyzed using a Leica laser scanning confocal microscope. Images were obtained using the same methodology previously aforementioned in Figure 5. Comparison of the samples showed that calbindin labeling in the control retina was present in the amacrine, bipolar and photoreceptor cells, whereas GFAP was restricted to only astrocytes within both the periphery (A) and perimacula (C). However, in the periphery (B) and perimacula (D) of the ADRP donor, calbindin positive cells were observed scattered throughout the entire retina. The Müller cells had undergone reactive gliosis throughout the retina, and their hypertrophic processes were GFAP positive in both adRP retinas. Bar = 40µm.

Conclusions

The retina of a Pro23His Rhodopsin adRP donor retina displays:

- atrophic retina with disorganization of the cellular layers, gliosis, and presence of intraretinal bone spicules in the periphery and far periphery;
- reduced thickness of the RPE in the perimacula and thin and discontinuous RPE in the far periphery;
- prominent inner and outer nuclear layer in the perifoveal region;
- near-absence of rods both in the periphery and in the perimacula;
- presence of disorganized cones in the perimacula;
- absence of cones in the periphery;
- distribution of calbindin D-28k positive cells throughout the whole retina;
- Müller cells which have undergone reactive gliosis throughout the retina, and their hypertrophied processes were GFAP positive.

References

- Aleman TS, Cideciyan AV, Sumaroka A, et al. *Invest Ophthalmol Vis Sci.* 2008; 49: 1580-1590.
- Berson EL, Rosner B, Sandberg MA, et al . *Arch Ophthalmol.* 1991; 109: 92-101.
- Kolb H & Gouras P. *Invest Ophthalmol Vis Sci.* 1974; 13: 487-498.
- To K, Adamian M, Dryja TP, et al. *Am J Ophthalmol.* 2002; 134: 290-293.
- To K, Adamian M & Berson EL. *Am J Ophthalmol.* 2004; 137: 946-948.

Acknowledgements

We thank Dr. Peter MacLeish (Morehouse School of Medicine, Atlanta, GA) for providing us with the antibody to cone arrestin (7G6).

Support

The Foundation Fighting Blindness
Research to Prevent Blindness
Wolf Family Foundation
National Eye Institute

RETINAL DEIMINATION AND PAD2 LEVELS IN RETINAS FROM DONORS WITH AGE-RELATED MACULAR DEGENERATION (AMD) .

Y. Li[1], V.L. Bonilha[1], K.G. Shadrach[1], and J.G.Hollyfield[1].

1-The Cole Eye Institute, Cleveland Clinic, Cleveland, OH.

Cleveland Clinic

Abstract

Purpose: Posttranslational modifications (PTMs) to proteins are fundamental events in the regulation of cellular processes. Proteins may also undergo hundreds of PTM that can be interpreted as manifestations of protein aging. Protein deimination is a PTM that is carried out by peptidyl arginine deiminases (PADs) and involves conversion of protein bound arginine into citrulline. PAD2 is the main PAD expressed in the retina. Elevated levels of PAD2 and protein deimination have been found in a number of human neurological diseases, with or without ocular manifestation. Moreover, we have recently shown that PAD2 and protein deimination decreases with aging in the retinas of an animal model. To better understand the pathogenesis of age-related macular degeneration (AMD) we studied protein deimination and PAD2 levels in AMD and age matched control retinas.

Methods: The eyes from control and AMD donors were fixed in 4% paraformaldehyde and 0.5% glutaraldehyde in phosphate buffer. RPE and retina from donor eyes were subjected to immunohistochemical detection and western blots using antibodies to PAD2 and deiminated residues.

Results: The ganglion cell layer, inner plexiform layer, inner nuclear layer and photoreceptor nuclei were labeled by both PAD2 and citrulline antibodies. Changes in the localization of deiminated residues and PAD2 were noticed due to the remodeling of the retinal cell layers in AMD retinas. Immunodetection of both PAD2 and citrulline residues was not analyzed in the RPE layer due to the high autofluorescence levels in this layer. On the other hand, no significant changes in the levels of deimination and PAD2 levels were observed between the AMD and control neural retina lysates.

Conclusions: Our observations show similar levels of protein deimination and PAD2 in AMD retinas, contrary to the previously described elevated levels in other age-related neurological diseases. This observation may be a consequence of the degenerative nature of the disease that leads to substantial cell loss in the retina.

Supported in part by NIH grant EY015638, a Research Center Grant from The Foundation Fighting Blindness and Research to Prevent Blindness.

Introduction

The posttranslational modifications (PTMs) of proteins enable nature to incorporate more information on proteins and generate more diversity in protein molecules. Posttranslational modification has been shown to regulate several of the cellular processes. Protein deimination is a posttranslational modification that is carried out by peptidyl arginine deiminases (PADs) (Vossenaar *et al.* 2003). Mammalian cells posses five protein deiminases, PAD1-4 and 6 (Vossenaar *et al.* 2003). PAD4 is a nuclear enzyme, all other PADs are cytosolic entities (Vossenaar *et al.* 2003). Elevated levels of PAD2 and protein deimination has been found in rheumatoid arthritis (Scofield 2004), and in a number of human neurological diseases, with or without ocular manifestation, for example in multiple sclerosis (MS) (Moscarello *et al.* 2002), autoimmune encephalomyelitis (Nicholas *et al.* 2005), Alzheimer's (Maruyama *et al.* 2005; Louw *et al.* 2007), amyotrophic lateral sclerosis (Chou *et al.* 1996) and glaucoma (Bhattacharya *et al.* 2006a; Bhattacharya *et al.* 2006b). In contrast to these observations, we have recently presented evidence of reduced levels of deimination in the retina, the optic nerve as well as a systemic reduction in older F344BN rats compared to young. In addition, reduced protein and mRNA levels and activity were also found for PAD2 in the retina and the optic nerve of older rats compared with those from the young rats. Our data suggested that the increased deimination and PAD2 expression, reported in age-related neurodegenerative ocular diseases, is probably associated with the disease process rather than aging (Bhattacharya et al., 2008).

To better understand the pathogenesis of AMD we studied protein deimination and PAD2 levels in AMD and age matched control retinas.

Figure 1

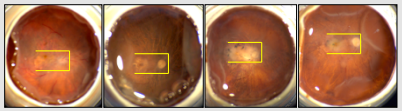

FFB#739	FFB#716	FFB#722	FFB#711
- 90 y.o.;	- 80 y.o.;	- 90 y.o.;	- 83 y.o.;
- Anonymous (caucasian female);	- Anonymous (caucasian female);	-Anonymous (caucasian male);	-Anonymous (caucasian female);
- 8.5 hrs PMI	- 35.5 hrs PMI	- 22 hrs PMI	- 13 hrs PMI

= Region cut and processed for IHC

Gross pathology of some of the eyes studied with AMD. The anterior segment has been removed and the retina is viewed *en face*. Note the presence of geographic atrophy and exudate in the areas selected for histological analysis.

Figure 2

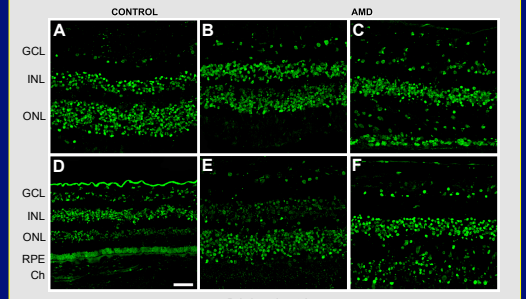

Similar levels of protein deimination in the retinas of AMD donors. Human cryosections of both matched controls and several AMD donors were labeled with antibodies specific to citrulline and a secondary Alexa 488 antibody. (Alexa488, green). Sections were analyzed using a Leica laser scanning confocal microscope (TCS-SP2, Leica, Exton, PA). A series of 1 μm xy (en face) sections were collected. Each individual xy image of the retinas stained represents a three-dimensional projection of the entire section (sum of all images in the stack). Microscopic panels were composed using AdobePhotoshop CS3. Immunohistochemistry of cryosections showed that the deiminated proteins were detected in the ganglion cell layer (GCL), inner nuclear layer (INL), outer nuclear layer (ONL) and choroid (Ch) in control (A, D) retinas. A disorganized distribution of deiminated proteins was visible in the degenerated areas of the retinas of AMD donors (B, C, E, F). The levels of deiminated proteins observed in AMD retinas were similar to the levels observed in control retinas (A, D). RPE= Retinal pigment epithelium; Bar = 40μm.

Figure 3

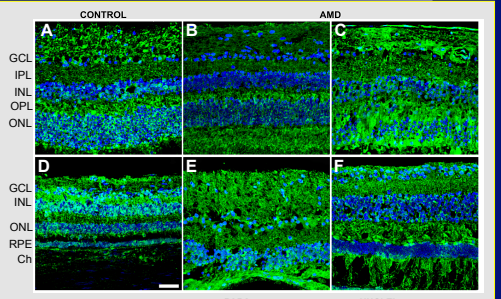

Similar levels of PAD2 in the retinas of AMD donors. Human cryosections of both matched controls and several AMD donors were labeled with antibodies specific to PAD2 and a secondary Alexa 488 antibody. (Alexa488, green). Sections were analyzed using a Leica laser scanning confocal microscope (TCS-SP2, Leica, Exton, PA). A series of 1 μm xy (en face) sections were collected. Each individual xy image of the retinas stained represents a three-dimensional projection of the entire section (sum of all images in the stack). Microscopic panels were composed using AdobePhotoshop CS3. Immunolocalization of PAD2 was present in several retinal layers of both control (A, D) and AMD retinas (B, C, E, F). Interestingly, PAD2 was frequently localized to the nuclei of cells in the ganglion cell layer (GCL) and the inner nuclear layer (INL). Immunohistochemistry of cryosections showed that the retina of AMD donors (B, C, E, F) showed similar levels of deiminated proteins when compared to the control retinas (A, D). PAD2 was detected in all retinal layers. Inner Plexiform layer (IPL), outer nuclear layer (ONL), outer plexiform layer (OPL), retinal pigment epithelium (RPE), and choroid (Ch); Bar = 40μm.

Summary

- Histopathological analysis of the retinas from AMD donors revealed the presence of deiminated proteins were detected in the ganglion cell layer (GCL), inner nuclear layer (INL), outer nuclear layer (ONL) and choroid (Ch). Additional deiminated proteins were visible in the degenerated, disorganized the retina of AMD donors;
- Similar levels of deiminated proteins were observed in cryosections of control and AMD retinas;
- Immunolocalization of PAD2 was present in several retinal layers of both control and AMD retinas. Interestingly, PAD2 was frequently localized to the nuclei of cells in the ganglion cell layer (GCL) and the inner nuclear layer (INL);
- Similar levels of PAD2 were observed in cryosections of control and AMD retinas;
- Presence of deiminated proteins was similar in RPE and retinal lysates from AMD donors;
- Presence of PAD2 was similar in RPE and retinal lysates from AMD donors.

Figure 4

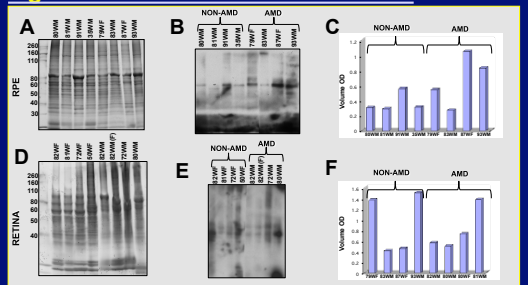

Presence of protein deimination is similar in retinas and RPE lysates from AMD donors. RPE (A-C) and retinal (D-F) lysates from several human donors previously diagnosed with AMD and control samples were harvested, lysed in RIPA buffer (150mM NaCl, 25mM Tris, pH 7.4, 2mM EDTA, 1% Triton X-100, 1% deoxycholate, 0.1% SDS) supplemented with 1mM PMSF, protease and phosphatase cocktail inhibitors (SIGMA). 40μg of protein of each sample was separated on a 10-20% SDS gel, transferred to PVDF membranes and probed with antibodies specific to semenogelin followed by ECF detection of immunoreactivity (B and E). The gels were stained with Coomassie blue after partial transfer to PVDF membranes to serve as a reference for the load homogeneity of the samples (A and D). The age, ethnical background and gender of the donors is indicated on top of each lane. Membranes were exposed to film, films were scanned and figures were composed in Adobe Photoshop CS3. In C and F, a rectangular area was drawn around the most intense band signal and used as a template to measure the signal intensity in each band using the volume analysis report macro from Quantity One 4.2.3. Plotted signals represent intensity for each band subtracted from the background signal.

Figure 5

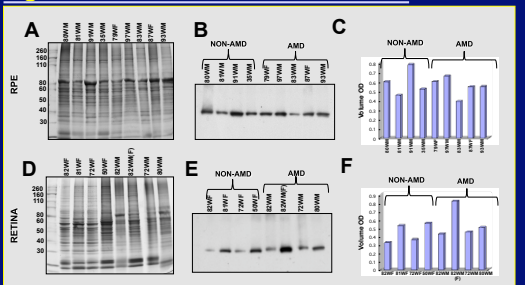

Presence of PAD2 is similar in retinas and RPE lysates from AMD donors. RPE (A-C) and retinal (D-F) lysates from several human donors previously diagnosed with AMD and control samples were harvested, lysed in RIPA buffer (150mM NaCl, 25mM Tris, pH 7.4, 2mM EDTA, 1% Triton X-100, 1% deoxycholate, 0.1% SDS) supplemented with 1mM PMSF, protease and phosphatase cocktail inhibitors (SIGMA). 40μg of protein of each sample was separated on a 10-20% SDS gel, transferred to PVDF membranes and probed with antibodies specific to PAD2 followed by ECF detection of immunoreactivity (B and E). The gels were stained with Coomassie blue after partial transfer to PVDF membranes to serve as a reference for the load homogeneity of the samples (A and D). The age, ethnical background and gender of the donors is indicated on top of each lane. Membranes were exposed to film, films were scanned and figures were composed in Adobe Photoshop CS3. In C and F, a rectangular area was drawn around the PAD2 band signal and used as a template to measure the signal intensity in each band using the volume analysis report macro from Quantity One 4.2.3. Plotted signals represent intensity for each band subtracted from the background signal.

References

- Bhattacharya SK, Bhat MB and Takahara H. (2006a) *Curr. Eye Res.* **31**, 1063-1071.
-Bhattacharya SK, Crabb JS, Bonilha VL, Gu X, Takahara H and Crabb JW. (2006b) *Invest. Ophthalmol. Vis. Sci.* **47**, 2508-2514.
- Bhattacharya SK, Sincrope B, Rayborn ME, Hollyfield JG and Bonilha VL (2008) *Aging Cell.* **7**, 1397-1405.
-Chou SM, Wang HS and Taniguchi A. (2006) *J Neurol Sci.* **139 Suppl**, 16-26.
-Louw C, Gordon A, Johnston N, Moliatt C, Bradley G and Whiteley CG. (2007) *J Enzyme Inhib Med Chem.* **22**, 121-126.
-Maruyama N, Ishigami A and Kondo Y. (2005) *Rinsho Byori.* **53**, 728-734.
- Moscarello MA, Pritzker L, Mastronardi FG and Wood DD. (2002) *J Neurochem.* **81**, 335-343.
- Nicholas AP, Sambandam T, Echols JD and Barnum SR. (2005) *J Comp Neurol.* **486**, 254-266.
- Scofield RH. (2004) *Lancet.* **363**, 1544-1546.
- Vossenaar ER, Zendman AJ, van Venrooij WJ and Pruijn GJ. (2003) *Bioessays.* **25**, 1106-1118.

ACKNOWLEDGMENTS
We thank Dr. Hidenari Takahara (Ibaraki, Japan) for providing us with the antibody to PAD2.

SUPPORTED BY
Research to Prevent Blindness

Foundation Fighting Blindness

POSTMORTEM ANALYSIS OF CONE OPSINS IN A PATIENT WITH AN AUTOSOMAL DOMINANT CONE DYSTROPHY.

S. Grover[2], V.L. Bonilha[1], G.A. Fishman[2], and J.G.Hollyfield [1]

[1]-The Cole Eye Institute, The Cleveland Clinic Foundation, Cleveland, OH and

[2]-Department of Ophthalmology and Visual Sciences, University of Illinois, Chicago, IL.

ABSTRACT

Purpose: The present study aimed to analyze the distribution of the red/green and blue opsins in the cones from an eye of a patient with an autosomal dominant cone dystrophy.

Methods: Eyes were fixed in 4% paraformaldehyde and 0.5% glutaraldehyde in phosphate buffer. Cryosections were studied by indirect immunofluorescence, using well-characterized monoclonal antibodies to the cone cytoplasm (mAb 7G6) and polyclonal antibodies to either red/green (UW-16 and p4924A) and blue (p108B) opsins. The affected donor eye was compared to a postmortem compatible normal eye.

Results: The patient's vision was corrected to 20/200 in each eye when last seen 3 years before his death at age 85. Visual field testing showing normal peripheral boundaries and central scotomas. ERG testing showed normal rod function while the cone b-wave amplitude was reduced 40% below the lower limit of normal. Fundus exam showed only isolated drusen within the macula. The normal-appearing fovea was a common feature in all affected family members. Blue opsin was restricted to the outer segments of blue cones in the affected retina. In contrast, red/green opsins were distributed along the entire plasma membrane of cones with this pigment type. The cone pedicles appeared larger than normal.

Conclusions: The histological data obtained suggest that the clinical manifestation of this dystrophy is related to an abnormal distribution of the red/green opsin. Additionally, changes in the cone pedicles may be correlated with the abnormal cone ERG in this patient.

Supported by The Foundation Fighting Blindness, and The Grant Healthcare Foundation.

INTRODUCTION

The cone dystrophies are characterized by bilateral visual loss, colour vision abnormalities, central scotoma, variable degrees of nystagmus and photophobia, together with electrophysiological or psychophysical evidence of abnormal cone function. Cone dystrophies can show autosomal dominant, autosomal recessive, and X-linked recessive inheritance. There is clinical as well as genetic heterogeneity. Here we report the histological findings resulting from the analysis of both eyes of a member of a family with an autosomal dominant cone dystrophy.

FIGURE 1

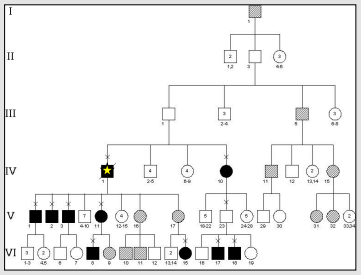

Pedigree of the family with autosomal dominant cone dystrophy showing the affected member (IV-1, ☆ on whom the postmortem analysis was performed.

FIGURE 2

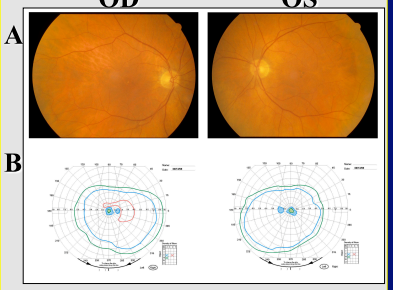

A-Fundus photograph of both the right (OD) and left (OS) eyes of family member IV-1, showing normal-looking disc, vessels and macula with isolated drusen in the foveal area.

B- Goldmann visual field of the right (OD) and left (OS) eyes of family member IV-1, showing central scotomas to targets III4e and II4e with normal-looking peripheral isopters. Right eye (OD) shows an additional central scotoma to a target II2e.

FIGURE 3

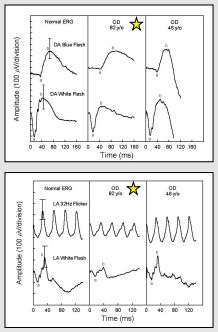

Full-field, dark (A) and light (B)-adapted electroretinogram (ERG) from the right eye of family member IV-1 (☆) (middle column).

A- Shows normal b-wave amplitudes as compared to normal eyes (left column). Also shown, the ERG from the right eye of one of his affected sons (family member V-2), with normal amplitudes (right column).

B- Shows reduced amplitudes as compared to normal eyes (left column). Also shown, the ERG from the right eye of one of his affected sons (family member V-2), showing normal amplitudes (right column).

FIGURE 4

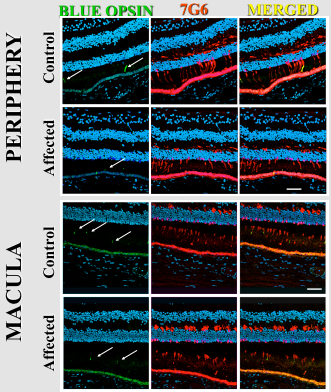

Blue cone opsin is restricted to outer segments of the cones in the affected retina. Human cryosections of both the matched control and affected family member (IV-1☆) were labeled with antibodies specific to blue cone opsin (Alexa488, green) and the cone cytoplasm marker 7G6 (Alexa594, red). Cell nuclei were labeled with TO-PRO-3 (blue). Sections were analyzed using a Leica laser scanning confocal microscope (TCS-SP2, Leica, Exton, PA). A series of 1 µm *xy* (*en face*) sections were collected. Each individual *xy* image of the retinas stained represents a three-dimensional projection of the entire cryosection (sum of all images in the stack). Microscopic panels were composed using AdobePhotoshop 5.5. Comparison of the samples showed that blue cone opsin is restricted to the outer segments of the cones in both normal and affected eye (arrows). Bar = 40µm.

FIGURE 5

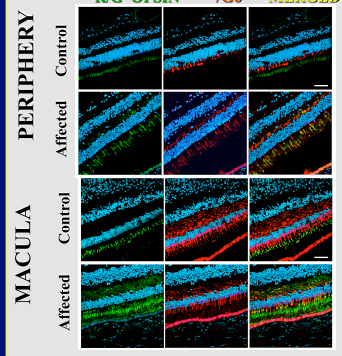

Red/Green cone opsins are distributed along the entire plasma membrane of this cone type in the affected retina. Human cryosections of both the matched control and affected family member (IV-1, ☆) were labeled with antibodies specific to red/green cone opsins (Alexa488, green) and the cone cytoplasm marker 7G6 (Alexa594, red). Cell nuclei were labeled with TO-PRO-3 (blue). Sections were analyzed using a Leica laser scanning confocal microscope (TCS-SP2, Leica, Exton, PA). A series of 1 µm *xy* (*en face*) sections were collected. Each individual *xy* image of the retinas stained represents a three-dimensional projection of the entire cryosection (sum of all images in the stack). Microscopic panels were composed using AdobePhotoshop 5.5. Comparison of the samples showed that red/green cone opsins are distributed along the entire plasma membrane of this cone type, from the tip of the outer segment to the synaptic base in the affected eye. Bar = 40µm.

FIGURE 7

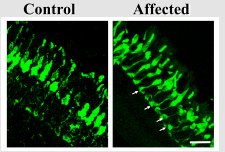

Abnormally enlarged pedicles in the cones of the affected retina. Human cryosections of both the matched control and affected family member (IV-1☆) were labeled with an antibody specific to the cone cytoplasm marker 7G6 (Alexa488, green). Sections were analyzed using a Leica laser scanning confocal microscope (TCS-SP2, Leica, Exton, PA). A series of 1 µm *xy* (*en face*) sections were collected. Each individual *xy* image of the retinas stained represents a three-dimensional projection of the entire cryosection (sum of all images in the stack). Microscopic panels were composed using AdobePhotoshop 5.5. Comparison of the samples showed that the cone pedicles (arrows) are markedly enlarged compared to those in the normal retina. Bar= 20µm.

FIGURE 6

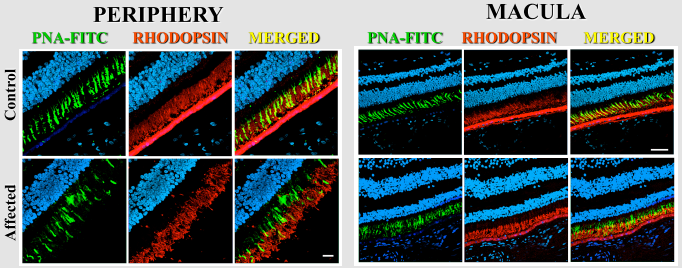

Rod distribution is normal in the affected retina. Human cryosections of both the matched control and affected family member (IV-1,☆) were labeled with the cone interphotoreceptor matrix (IPM) marker PNA (FITC, green) and an antibody specific to rhodopsin (Alexa594, red). Cell nuclei were labeled with TO-PRO-3 (blue). Sections were analyzed using a Leica laser scanning confocal microscope (TCS-SP2, Leica, Exton, PA). A series of 1 µm *xy* (*en face*) sections were collected. Each individual *xy* image of the retinas stained represents a three-dimensional projection of the entire cryosection (sum of all images in the stack). Microscopic panels were composed using AdobePhotoshop 5.5. Comparison of the samples showed that the cone IPM displayed a heterogeneous distribution both in the macula and the periphery. In contrast, rhodopsin staining was not different from the control eye. Bar in the periphery panel = 20µm; bar in the macula panel = 40 µm.

SUMMARY

- Blue opsin is restricted to the outer segments of blue cones in the affected retina.
- Red/green opsins are distributed along the entire plasma membrane of this cone type, from the tip of the outer segment to the synaptic base.
- The cone IPM displayed a heterogeneous distribution.
- The cone pedicles appeared larger than normal, both in the macula and the periphery.
- Rhodopsin staining was not different from the control eye.
- The distribution of the studied markers is similar both in the macula and in the periphery of the affected retina.

ACKNOWLEDGMENTS

We thank Dr. Peter MacLeish (Morehouse School of Medicine, Atlanta, GA) for providing us with the antibody to cone cytoplasmic marker (7G6), Dr. P. Hargrave (University of Florida, Gainesville, FL) for providing us with the antibody to rhodopsin (B630N) and Dr. John C. Saari (University of Washington, Seattle, WA) for providing us with the antibody to red/green cone opsins (UW-16).The anti blue (p4924A) and red/green (p108B) cone opsin antibodies were prepared by the late Dr. C. Lerea.

HISTOPATHOLOGY OF THE RETINA IN AN EYE DONATION FROM A PATIENT WITH AN RPE65 MUTATION

M. E. Rayborn[1], V. L. Bonilha[1], Y. Li[1], G. H. Grossman[1], J. G.Hollyfield[1] and E. L. Berson[2].

Cleveland Clinic

1-The Cole Eye Institute, Cleveland Clinic Lerner College of Medicine, Cleveland, OH; 2-The Berman-Gund Laboratory, Harvard Medical School, MEEI, Boston, MA.

Abstract

Purpose: RPE65 is an enzyme exclusively expressed in the retinal pigment epithelium (RPE) that converts trans retinol to the 11-cis form. Mutations in this gene are found in some recessive forms of Leber congenital amaurosis. We evaluated the histopathology of a donor eye from a patient with a homozygous missense change Ala132Thr in the RPE65 gene.

Methods: Autopsy eyes were obtained from a 56 year old woman who died from metastatic breast cancer. The eyes were fixed in 4% paraformaldehyde and 0.5% glutaraldehyde in phosphate buffer within 13.5 hours postmortem. Small areas from the fundus periphery were processed for electron microscopy and indirect immunofluorescence, using monoclonal antibodies to rhodopsin (mAb B630N) and cone arrestin (mAb 7G6). The content of autofluorescent material was analyzed. The affected donor eye was compared to a matched normal eye.

Results: The patient had night deficiency and decreased side vision since childhood. At age 51 she had hand motions OD and 20/200 OS, a central island of vision with far peripheral crescents OU, and peripheral bone spicule pigmentation OU. Cone ERGs were barely detectable. Histologic findings revealed a highly disorganized retina with indistinct layers in each quadrant. The RPE layer displayed thinning in some regions of the periphery. Rods were virtually absent in the affected retina. Cones were present in the macula, but were mostly absent from the retinal periphery. Cone synapses were not observed. Autofluorescent material was greatly reduced in the RPE in all areas studied.

Conclusions: This patient with an RPE65 mutation showed an absence of rods and cones in the periphery. In the macula, cone photoreceptors were present, albeit highly disorganized. The lack of autofluorescent material in the RPE suggested that these cells had not been functional in the photoreceptor outer segment renewal process for an extended period of time.

Supported by The Foundation Fighting Blindness Histopathology Grant; Research Center Grant from The Foundation Fighting Blindness; Research to Prevent Blindness Unrestricted Grants; and an NIH infrastructure grant (EY015638).

Introduction

The retinal pigment epithelium-specific 65 kDa protein is expressed by the RPE and is involved in the conversion of all-trans retinol to 11-cis retinal during phototransduction, which is then used in visual pigment regeneration in photoreceptor cells. There are two forms of this protein, a soluble form called sRPE65, and a palmitoylated, membrane-bound form known as mRPE65. Targeted disruption of the mouse *Rpe65* gene leads to absence of 11-*cis* retinal in the photoreceptor outer segments together with 11-*cis* retinyl esters absence and all-*trans* retinyl esters accumulation in the RPE further supporting the hypothesis that the RPE65 protein is essential for the isomerization of all-*trans* retinyl esters (Redmond et al., 1998).

Mutations in the *RPE65* gene cause diseases that involve impaired vision from birth and typically progress to blindness in the third decade of life (Gu et al., 1997; Marlhens et al., 1997; Morimura et al., 1998; Lorenz et al., 2000; Paunescu et al., 2005). This donor had a homozygous mutation Ala132Thr in this gene. She had a clinically affected brother who also showed this mutation homozygously and a clinically unaffected sister who is heterozygous for this mutation (Morimura, et al., 98). Unlike most patients with RPE65 mutations she retained some vision into her early fifties.

Like many genetic diseases, this condition is presently incurable. Although the retinal dystrophies caused by defects in RPE65 are severe, features of the disorder such as useful visual function in childhood and photoreceptor-cell death late in the disease process suggest that it may respond to gene-replacement therapy. Over 60 different pathogenic mutations of RPE65 are known and these affect all 14 exons of the gene and its boundaries. Severity and age of onset of disease are related to the particular type of mutation and the residue/site affected (Redmond, 2009).

In the present study we analyzed the morphology of the retina and the distribution of photoreceptor markers in a donor eye from a female affected by an RPE65 mutation. To our knowledge this is the first report to analyze the retinal morphology and the distribution of photoreceptor markers in a donor eye from a patient with a homozygous mutation in the *RPE65* gene.

Figure 1

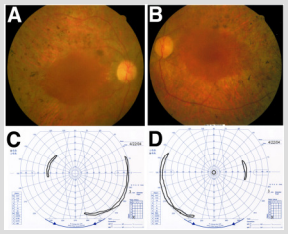

At the time of the most recent examination at age 51, this RPE65 patient had hand motion vision O.D. and 20/200 O.S. Fundus photograph of both the right (A) and left (B) eyes, showing normal disc, granular macula, attenuated retinal vessels, and bone spicule pigmentation around the mid-periphery O.U. A small central macular hole could be visualized O.D (only with the ophthalmoscope). Slit lamp examination revealed central posterior subcapsular cataracts O.U. Goldmann visual field testing with a V-4e white test light showed only thin peripheral islands O.U., no detectable central field O.D. (C), and only a 4º central field diameter O.S. (D). Dark adaptation testing showed a final threshold elevated 3.5 log units above normal. Computer-averaged narrow bandpassed, full-field, 30-Hz cone ERGs were only 0.50 µV O.D. and 0.67 µV O.S. (lower normal = 50.0 µV).

Figure 2

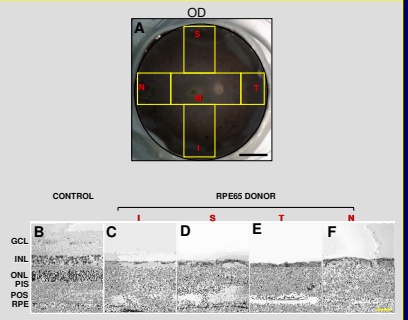

Degeneration in the retina of an RPE65 donor. Gross pathology and schema (A) of regions cut and processed from an eye of a 56 y.o. Ala132Thr RPE65 donor. The anterior segment has been removed and the retina is viewed *en face*; characteristic pigmentary changes can be observed. Human 1µm plastic sections of both a matched control (B) and the RPE65 mutant retinas stained with toluidine blue (C-F). Morphology of control retina in the perimacular region of the eye. (B-E) The retina of the RPE65 mutant donor displayed different degrees of retinal degeneration in all quadrants observed. Low magnification observation of the RPE65 mutant retina demonstrated sparse inner and outer nuclear layers with stunted photoreceptor inner and outer segments. A thin, continuous area of pigmented RPE cells was also observed. Quadrants: I= inferior; S= superior; T= temporal; N= nasal. Bars: A= 0.5 cm; B-F= 200µm.

Figure 3

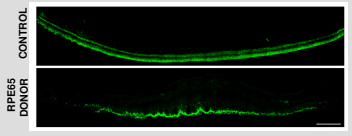

Presence of disorganized cones in the macular region of an RPE65 donor. Human cryosections of both a matched control and affected RPE65 donor were labeled with antibodies specific to cone arrestin (Alexa488, green). Sections were analyzed using an Olympus microscope (BX-61, Tokyo, Japan). Each image represents a montage of a series of photomicrographs collected throughout the whole tissue piece. In the mutant donor eye cones were still present in the perimacula but they were highly disorganized and synapses were absent. Bar = 500µm.

Figure 4

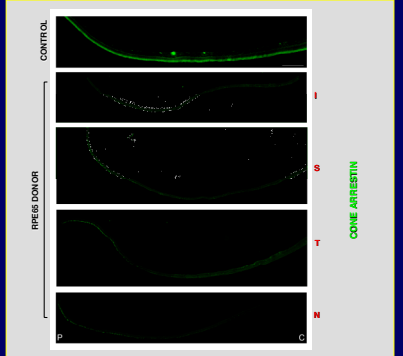

Significant reduction in the cones in the periphery of an RPE65 donor. Human cryosections of both a matched control and affected RPE65 donor were labeled with antibodies specific to cone arrestin (Alexa488, green). Sections were analyzed using an Olympus microscope (BX-61, Tokyo, Japan). Each image represents a montage of a series of photomicrographs collected throughout the whole tissue piece. Comparison of the samples showed that cones were mostly absent in the affected retina in all the regions observed. P= periphery; C= central. Quadrants: I= inferior; S= superior; T= temporal; N= nasal. Bar = 500µm.

Figure 5

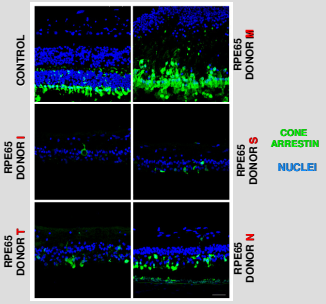

Disorganized morphology of the cones remaining in the retina of an RPE65 donor. Human cryosections of both a matched control and RPE65 donor were labeled with antibodies specific to cone arrestin (Alexa488, green) while cell nuclei were labeled with TO-PRO-3 (blue). Sections were analyzed using a Leica laser scanning confocal microscope (TCS-SP2, Leica, Exton, PA). A series of 1 µm xy (en face) sections were collected. Each individual xy retinal image represents a three-dimensional projection of the entire section (sum of all images in the stack). Comparison of the samples showed that cone arrestin was distributed along the entire plasma membrane of this cone type, from the tip of the outer segment to the synaptic base in the control retina. Cones were present in the macula of the RPE65 donor but synapses were not visualized. On the other hand, cones were mostly absent in the periphery of the RPE65 mutant retina. Quadrants: M= macula; I= inferior; S= superior; T= temporal; N= nasal. Bar = 40µm.

Figure 6

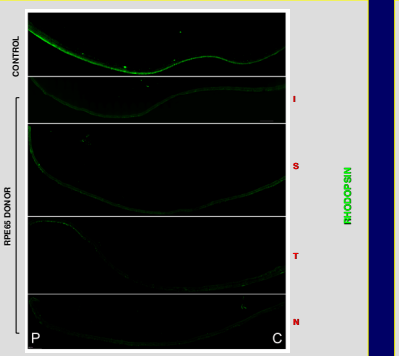

Absence of rhodopsin in the rods in the periphery of an RPE65 donor. Human cryosections of both a matched control and affected RPE65 donor were labeled with antibodies specific to rhodopsin (Alexa488, green). Sections were analyzed using an Olympus microscope (BX-61, Tokyo, Japan). Each image represents a montage of a series of photomicrographs collected throughout the whole tissue piece. Comparison of the samples showed that rhodopsin was mostly absent in the affected retina in all the regions observed. A few rods were still observed in the far periphery of the temporal region of the RPE65 mutant retina. P= periphery; C= central. Quadrants: I= inferior; S= superior; T= temporal; N= nasal. Bar = 500µm.

Figure 7

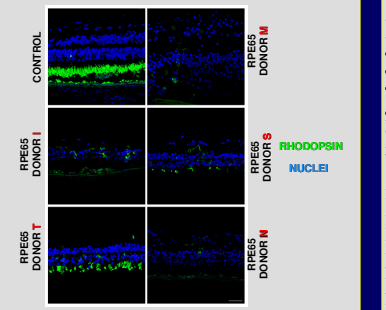

Disorganized morphology of the rods remaining in the retina of an RPE65 donor. Human cryosections of both a matched control and RPE65 donor were labeled with antibodies specific to rhodopsins (Alexa488, green) while cell nuclei were labeled with TO-PRO-3 (blue). Sections were analyzed using a Leica laser scanning confocal microscope (TCS-SP2, Leica, Exton, PA). A series of 1 µm xy (en face) sections were collected. Each individual xy retinal image represents a three-dimensional projection of the entire section (sum of all images in the stack). Comparison of the samples showed that rods were significantly decreased in all the observed regions, with the remaining rods expanding horizontally into the RPE5 mutant retina. Quadrants: M= macula; I= inferior; S= superior; T= temporal; N= nasal. Bar = 40µm.

Figure 8

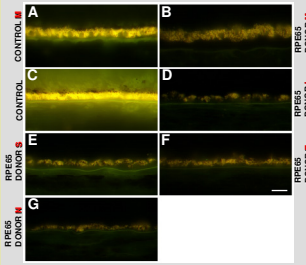

Significant decrease in the accumulation of autofluorescent material in the RPE of an RPE65 donor. Human cryosections of both a matched control (A, C) and affected RPE65 donor (B, D, E, F, G) were observed on epifluorescence in the green channel (FITC filter: excitation 495nm/emission 519nm). RPE from the RPE65 mutant retina displayed significantly decreased autofluorescent granules when compared to an age-matched control RPE. Quadrants: M= macula; I= inferior; S= superior; T= temporal; N= nasal. Bar = 200µm.

SUMMARY:

The retina of a donor with an Ala132Thr RPE65 mutation displays:

- degeneration in the retina;
- presence of disorganized cones in the macula;
- significant decrease of cones in the periphery;
- near-absence of rods in the periphery;
- significant decrease in the accumulation of autofluorescent material in the RPE in the macula and periphery;
- the patient's constricted fields with temporal islands, and her reduced full-field cone ERGs are consistent with the observation of cone photoreceptors only in the macula and far periphery;
- the elevated final dark adaptation threshold of 3.5 log units is consistent with near-absence of rods and compromise of remaining cones.

REFERENCES:

- Gu, S.M., Thomson, D.A., Srikumari, C.R., et al.,. (1997) Nat Gen, 17: 194-7.
- Lorenz, B., Gyurus, P., Preising, M., et al., (2000) Invest Ophthalmol Vis Sci, 41: 2735-42.
- Marlhens, F., Bareil, C., Griffoin, J.M., et al., (1997) Nat Gen, 17: 139-41.
- Morimura, H., Fishman, G.A., Grover, S.A., Fulton, A.B., Berson, E.L., and Dryja, T. P. (1998) Proc Natl Acad Sci USA, 95: 3088-93.
- Paunescu, K., Wabbels, B., Preising, M.N., and Lorenz, B. (2005) Graefes Arch Clin Exp Ophthalmol , 243: 417-26.
- Redmond, T.M., Yu S., Lee E., et al., (1998) Nat Gen, 20: 344-51.
- Redmond, T.M. (2009) Exp Eye Res, 88:846-7.

ACKNOWLEDGMENTS:

We thank Dr. Peter MacLeish (Morehouse School of Medicine, Atlanta, GA) for providing us with the antibody to cone arrestin (7G6), Dr. Paul Hargrave (University of Florida, Gainesville, FL) for providing us with the antibody to rhodopsin (B630N).

SUPPORTED BY Research to Prevent Blindness

Foundation Fighting Blindness

CHARACTERIZATION OF SEMENOGELIN PROTEINS IN THE HUMAN RETINAS OF AMD DONORS

M.Rayborn[1], V.L. Bonilha[1], K. Shadrach[1], Åke Lundwall[2], J. Malm[2], and J.G.Hollyfield.[1]

1-The Cole Eye Institute, Cleveland Clinic Foundation, Cleveland, OH, 2- Department of Laboratory Medicine, Lund University, Malmö, Sweden .

Abstract

Purpose: Semenogelin I (SgI) and II (SgII) are the major structural protein components of semen coagulum. Their function is not fully understood, but several activities have been ascribed to semenogelin or semenogelin-derived peptides, e.g. inhibition of sperm motility and capacitation, activation of sperm hyaluronidase and antibacterial properties. Recently, we reported the presence and localization of both SgI and SgII in the RPE, neural retina (choroid, photoreceptors, inner nuclear layer and ganglion cell layer) and vitreous of human donors not diagnosed with any eye disease. In the present study, we further analyzed the expression of these proteins in the retinal cells of AMD eyes *in vivo*.

Methods: Cryo and paraffin sections of human retina were processed for both immunofluorescence and DAB reaction with an antibody that recognizes both forms of semenogelin proteins. The presence of both proteins was analyzed in retina and RPE total lysates.

Results: Both proteins were detected by western blot in human RPE. However, the intensity of expression was significantly lower in the AMD eyes. In AMD eyes immune reaction was detected only in the tips of the photoreceptor outer segments.

Conclusions: Semenogelin I and II are expressed in the normal human retina and in the retina of AMD donor eyes. The expression of semenogelins in the AMD eyes is substantially lower than that observed in the normal retina. A recent report indicates that both SgI and SgII bind zinc. Earlier clinical trial data found a significant decrease in the progression of AMD in individuals supplemented with antioxidants and zinc. Our observations that Sgs are localized to photoreceptors and the RPE, the two cellular targets in AMD, may point to a function related to the ability of these cells to sequester zinc for protection against AMD.

Supported in part by NIH grants EY06603, EY14240, EY015638, a Research Center Grant from The Foundation Fighting Blindness and funds from the Cleveland Clinic Foundation.

Introduction

Semenogelin I and II are secreted from the glandular epithelium of the seminal vesicles and the epithelium of the epididymis (Bjartell et I., 1996). Semenogelin I (SgI) is a non-glycosylated protein with a molecular mass of 50KDa (Lilja et al., 1989). Semenogelin II (SgII) has a molecular mass of 63KDa (Lilja and Lundwall, 1992). It has a potential site for N-linked glycosylation and around half of the molecules in seminal plasma are glycosylated, yielding two molecular species with an apparent mass difference of 5KDa (Lilja and Laurell, 1985). Studies have indicated a role of semenogelin molecules related to capacitation and motility of sperm (Robert and Gagnon, 1996, de Lamirande et al., 2001).

Recently, semenogelin proteins expression was characterized in non-genital tissues like trachea, bronchi, skeletal muscle cells, and cells in the central nervous system (Lundwall et al., 2002), suggesting additional yet unknown functions for these molecules. Moreover, we have just described the expression and distribution of both semenogelin proteins in the posterior part of the eye of several donors (Bonilha et al., 2006). These findings have not been substantiated by independent studies and it is therefore still unclear whether the semenogelin proteins have any function beside their role as structural components of the seminal coagulum. However, the high Zn^{2+}-binding capacity of both SgI and SgII (Jonsson et al., 2005), as recently demonstrated, could suggest that semenogelin molecules might function as important regulators of extracellular Zn^{2+} homeostasis.

Earlier clinical trial data found a significant decrease in the progression of age-related macular degeneration (AMD) in individuals supplemented with antioxidants and zinc (Clemons et al., 2005; Schmidt-Erfurth, 2005). The cellular targets in AMD are the RPE and macular photoreceptors (Penfold et al., 2001). Our observations that semenogelins are localized to photoreceptors and the RPE may point to a function related to the ability of these cells to sequester zinc for protection against AMD. In this regard, we decided to define the distribution of semenogelin proteins in the eyes from donors with diagnosed AMD.

Figure 1

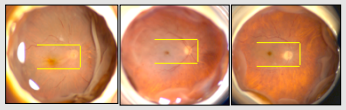

FFB#704	FFB#774	FFB#714
- 93 y.o.;	- 70 y.o.;	- 82 y.o.;
- Anonymous (caucasian female);	- Anonymous (caucasian female);	- Anonymous (caucasian female);
- 8.5 hrs PMI	- 10 hrs PMI	- 6.5 hrs PMI

= Region cut and processed for IHC

Gross pathology of some of the eyes studied with AMD. The anterior segment has been removed and the retina is viewed *en face*. Note the presence of drusen in the area selected for histology.

Figure 2

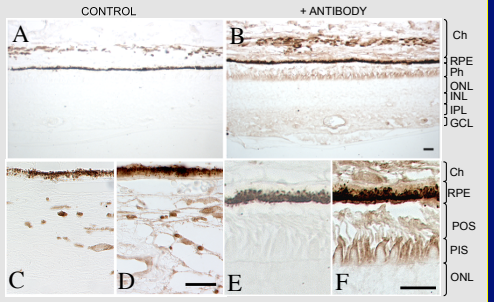

Presence of semenogelin in photoreceptors, RPE, choroid, inner nuclear layer, and ganglion cell layer of the control human retina. 5 µm paraffin sections of human donors were probed with semenogelin I antibody in 5% BSA, PBS and 0.3% Triton-X100 overnight at 4°C. The controls (A, C, E) omitted the antibodies. Sections were washed, incubated with secondary antibody, conjugated to biotin for 1h at RT, washed, and incubated with avidin in PBS for 30 min, then developed with DAB for 2 minutes. The sections were examined with a Zeiss Axiophot light microscope and the images were digitized using a Hamamatsu CCD camera. Comparison of the samples showed that semenogelin I antibody displays stronger reaction with the photoreceptors inner (PIS) and outer segments (POS), choroid (Ch), retinal pigment epithelium (RPE), cells in the inner plexiform layer (IPL), and the ganglion cell layer (GCL). Figure panels were composed using Adobe Photoshop 5.5. ONL = Outer Nuclear Layer, INL = Inner Nuclear Layer. Bar = 200µm.

Figure 3

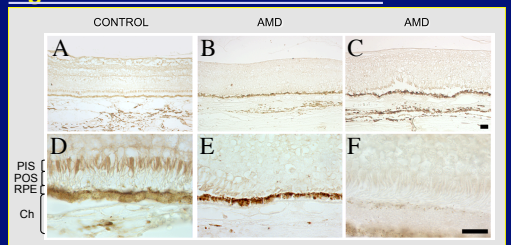

Semenogelin protein localization is remarkably decreased in the retinas of AMD donors. 5µm paraffin sections of human donors previously diagnosed with AMD (B, C, E, F) and control eyes (A, D) were probed with semenogelin I antibody in 5% BSA, PBS and 0.3% Triton-X100 overnight at 4°C. Sections were washed, incubated with secondary antibody, conjugated to biotin for 1h at RT, washed, and incubated with avidin in PBS for 30 min, then developed with DAB for 2 minutes. The controls (not shown) were omitted the antibodies and did not display any labeling. The sections were examined with a Zeiss Axiophot light microscope and the images were digitized using a Hamamatsu CCD camera. Comparison of the AMD samples showed that semenogelin I staining is significantly reduced in all layers of the retina when compared to the control eyes. Specifically, reduced labeling was observed in the photoreceptors and RPE cells. Notice that semenogelin localization in AMD photoreceptors was either completely extinguished (B, F) or confined to the photoreceptor outer segments (C, E). Microscopic panels were composed using AdobePhotoshop 5.5. Bar = 200µm.

Figure 4

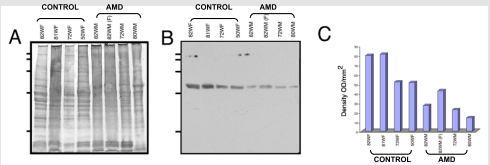

Semenogelin I expression is remarkably decreased in the retinas of AMD donors. Retinas from several human donors previously diagnosed with AMD and control samples were harvested, lysed in RIPA buffer (150mM NaCl, 25mM Tris, pH 7.4, 2mM EDTA, 1% Triton X-100, 1% deoxycholate, 0.1% SDS) supplemented with 1mM PMSF, protease and phosphatase cocktail inhibitors (SIGMA). 40µg of protein of each sample was separated on a 10-20% SDS gel,transferred to PVDF membranes and probed with antibodies specific to semenogelin followed by ECF detection of immunoreactivity (B). The gels were stained with Coomassie blue after partial transfer to PVDF membranes to serve as a reference for the load homogeneity of the samples (A). The age, ethnical background and gender of the donors is indicated on top of each lane. Membranes were exposed to film, films were scanned and figures were composed in Adobe Photoshop 5.5. In C, a rectangular area was drawn around the most intense band signal and used as a template to measure the signal intensity in each band using the volume analysis report macro from Quantity One 4.2.3. Plotted signals represent intensity for each band subtracted from the background signal. (F) in sample 82WM denotes the fovea of that donor.

Figure 5

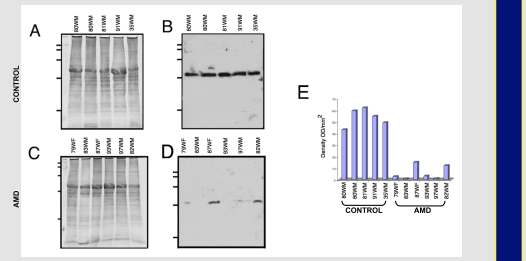

Presence of Semenogelin I is significantly decreased in RPE lysates from AMD donors. RPE lysates from several human donors previously diagnosed with AMD and control samples were harvested, lysed in RIPA buffer (150mM NaCl, 25mM Tris, pH 7.4, 2mM EDTA, 1% Triton X-100, 1% deoxycholate, 0.1% SDS) supplemented with 1mM PMSF, protease and phosphatase cocktail inhibitors (SIGMA). 40µg of protein of each sample was separated on a 10-20% SDS gel, transferred to PVDF membranes and probed with antibodies specific to semenogelin followed by ECF detection of immunoreactivity (B and D). The gels were stained with Coomassie blue after partial transfer to PVDF membranes to serve as a reference for the load homogeneity of the samples (A and C). The age, ethnical background and gender of the donors is indicated on top of each lane. Membranes were exposed to film, films were scanned and figures were composed in Adobe Photoshop 5.5. In E, a rectangular area was drawn around the most intense band signal and used as a template to measure the signal intensity in each band using the volume analysis report macro from Quantity One 4.2.3. Plotted signals represent intensity for each band subtracted from the background signal.

Summary

- Semenogelin molecules are expressed in the eye, in the vitreous and in several cell types of the retina.
- In control samples semenogelin molecules are expressed by the RPE, the photoreceptors (both cones and rods), the ganglion cells and cells in the inner nuclear/outer plexiform layer.
- In AMD tissue semenogelin molecules distribution in retinal sections is greatly decreased. In some donors a weak localization in the tips of the photoreceptor outer segments was still observed, but in the majority of the AMD samples photoreceptor and RPE localization of semenogelin molecules was completely lost.
- Presence of semenogelin I is significantly decreased in retinal lysates from AMD donors.
- Presence of semenogelin I is significantly decreased in RPE lysates from AMD donors.

References

- Bjartell, A., Malm, J., Möller, C., Gunnarsson, M., Lundawall, Å, & Lilja, H. (1996) *J. Androl.*, **17:** 17-26.
- Bonilha, V.L., Rayborn, M. E.,Shadrach, K., Lundwall, Å, Malm, J., Bhattacharya, S. K., Crabb, J. W., Hollyfield, JG. (2006) *Exp. Eye Res.*'in press".
- Clemons, T. E., Milton, R. C., Klein, R., Seddon, J. M. and Ferris, F. L., 3rd. (2005) *Ophthalmology,* **112:** 533-539.
- de Lamirande, E., Yoshida, K., Yoshiike, T.M., Iwamoto, T., & Gagnon, C. (2001) *J. Androl.*, **22:** 672-679.
- Jonsson, M., Linse, S., Frohm, B., Lundwall, A. and Malm, J. (2005) *Biochem J.*, **387:** 447-453.
- Lilja, H. and Laurell, C.-B. (1985) *Scand. J. Clin. Lab. Invest.*, **45:** 635-641.
- Lilja, H. Abrahamsson, P.A., and Lundwall, A. (1989) *J. Biol. Chem,* **264:** 1894-1900.
- Lilja, H., and Lundwall, A. (1992) *Proc.Natl Acad. Sci. USA*, **89:** 4559-4563.
- Lundwall, A. Bjartell, A., Olsson, A. Y., & Malm, J. (2002).*Mol. Hum. Rep.*, **8:** 805-810.
- Malm, J, Hellman, H., Laurell, C.B. & Lilja, H. (1996) *Eur. J. Biochem.*, **238:** 48-53.
- Penfold, P. L., Madigan, M. C., Gillies, M. C. and Provis, J. M. (2001) *Prog Retin Eye Res.*, **20:** 385-414.
- Robert, M., & Gagnon, C. (1996). *Biol. Reprod.*, **55:** 813-821.
- Schmidt-Erfurth, U.(2005) *Dev Ophthalmol.*, **38:** 120-147.